

# Supporting Information

for

## Synthesis and properties of 1,2,3-diazapnictol-5-yl substituted ferrocenes.

Pavel Kozáček,<sup>a</sup> Libor Dostál,<sup>a</sup> Martin Hejda,<sup>a</sup> Tomáš Mikysek,<sup>b</sup> Aleš Růžička,<sup>a</sup> and Milan Erben<sup>a,\*</sup>

<sup>a</sup> Department of General and Inorganic Chemistry, University of Pardubice, Studentská 573, CZ 532 10 Pardubice, Czech Republic.

<sup>b</sup> Department of Analytical Chemistry, University of Pardubice, Studentská 573, CZ 532 10 Pardubice, Czech Republic.

\* e-mail: [milan.erben@upce.cz](mailto:milan.erben@upce.cz)

### Table of Contents

Infrared, Raman and NMR spectra of prepared compounds	S2
Crystallographic and refinement data for <b>1a</b> , <b>2a</b> - <b>2c</b> , <b>3c</b> , <b>4a</b> , <b>5a</b> , <b>8</b> , <b>9</b> and <b>10</b>	S33
Molecular structure and hydrogen-bonding scheme for <b>1a</b>	S35
Molecular structure of <b>3c</b>	S36
Molecular structure and hydrogen-bonding scheme for <b>4a</b> (two polymorphs)	S37
Hydrogen-bonding scheme for <b>2a</b>	S39
Hydrogen-bonding scheme for <b>2b</b>	S40
Hydrogen-bonding scheme for <b>2c</b>	S41
Partial packing scheme for <b>8</b> showing dipole-dipole interactions	S42
Hydrogen-bonding scheme for <b>9</b>	S43
Scheme of the C–H···π interactions in crystalline <b>9</b>	S44
Cyclic voltammograms of <b>2a</b> , <b>2b</b> , <b>5a</b> , <b>8 – 13</b> and <b>2H-5Bu<sup>t</sup>-dap</b>	S45
References	S50

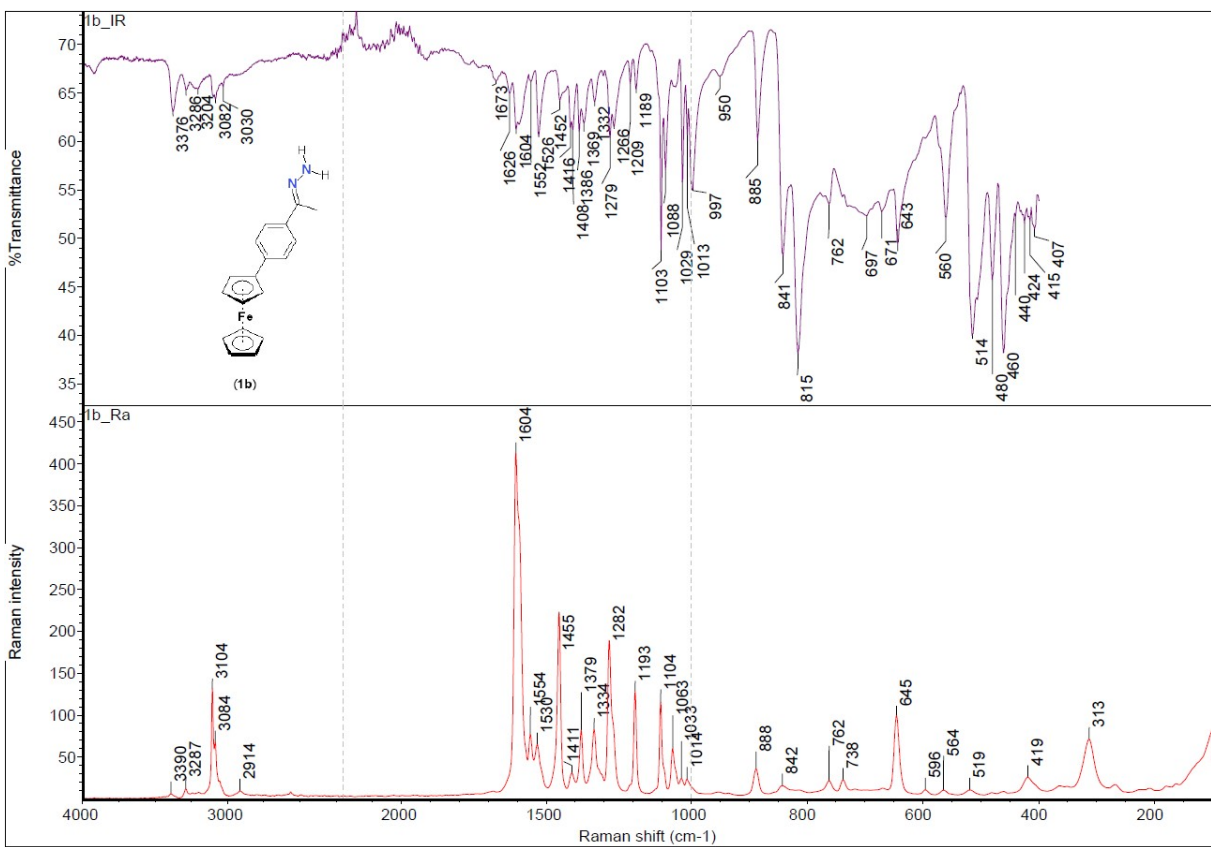


**Figure S1.** Infrared (top) and Raman (bottom) spectra of **1b** measured in the solid state.

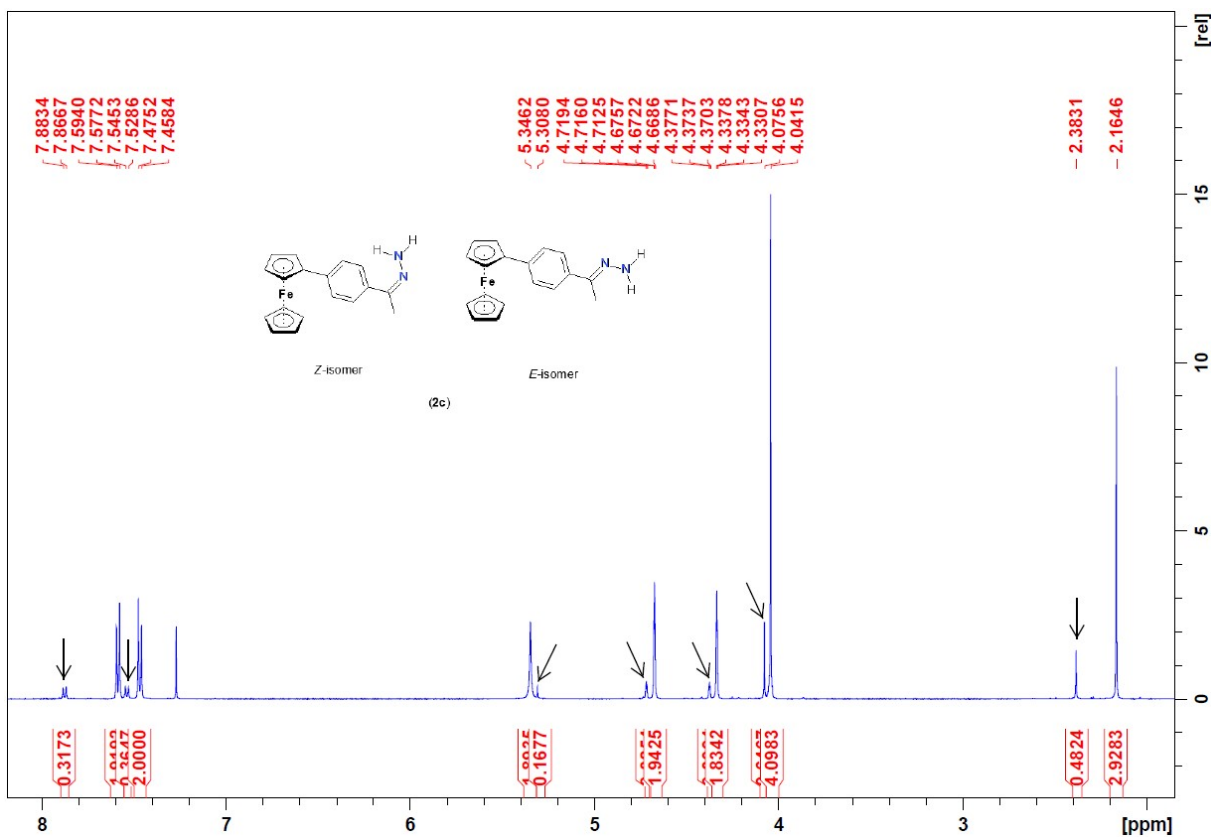


**Figure S2.**  $^1\text{H}$  NMR spectrum of **1b** (500 MHz,  $\text{CDCl}_3$ , 298 K). Arrows denote signals of minor Z-isomer.

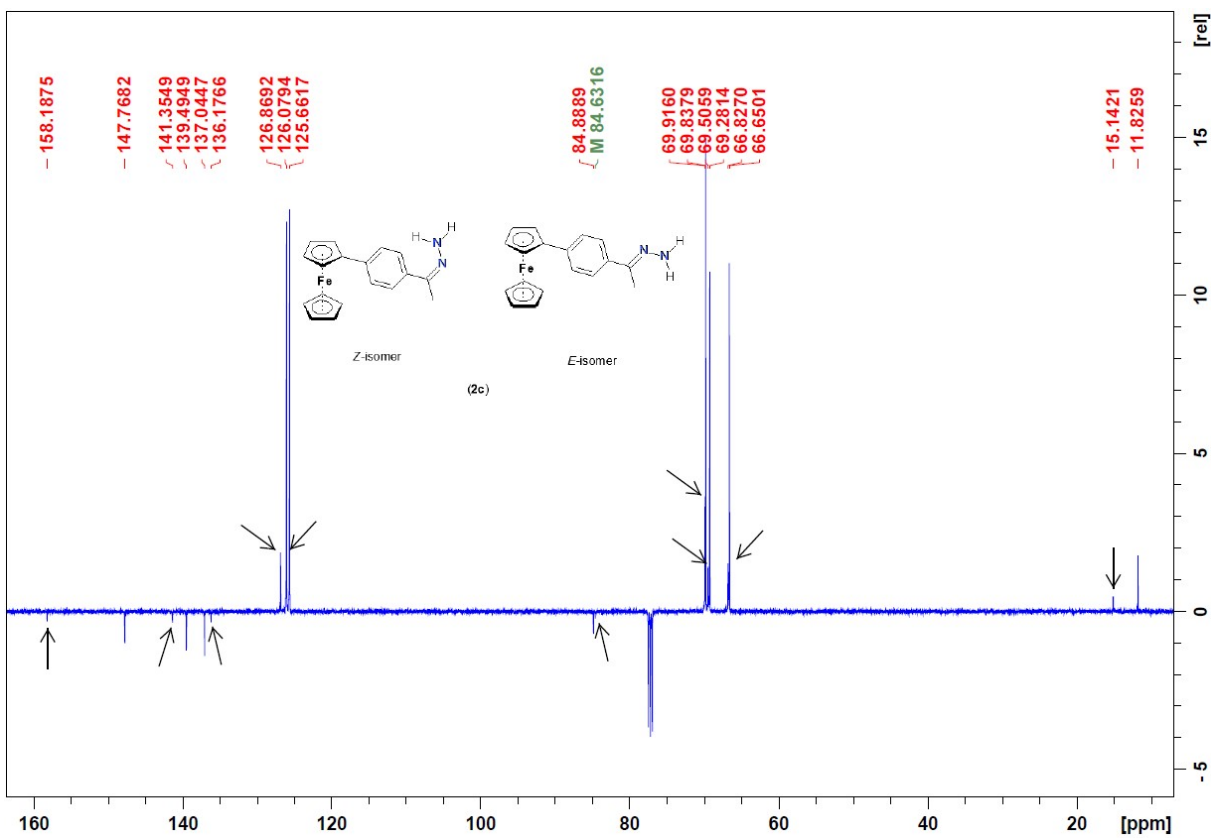


**Figure S3.**  $^{13}\text{C}\{^1\text{H}\}$  APT NMR spectrum of **1b** (125.76 MHz,  $\text{CDCl}_3$ , 298 K). Arrows denote signals of minor Z-isomer.

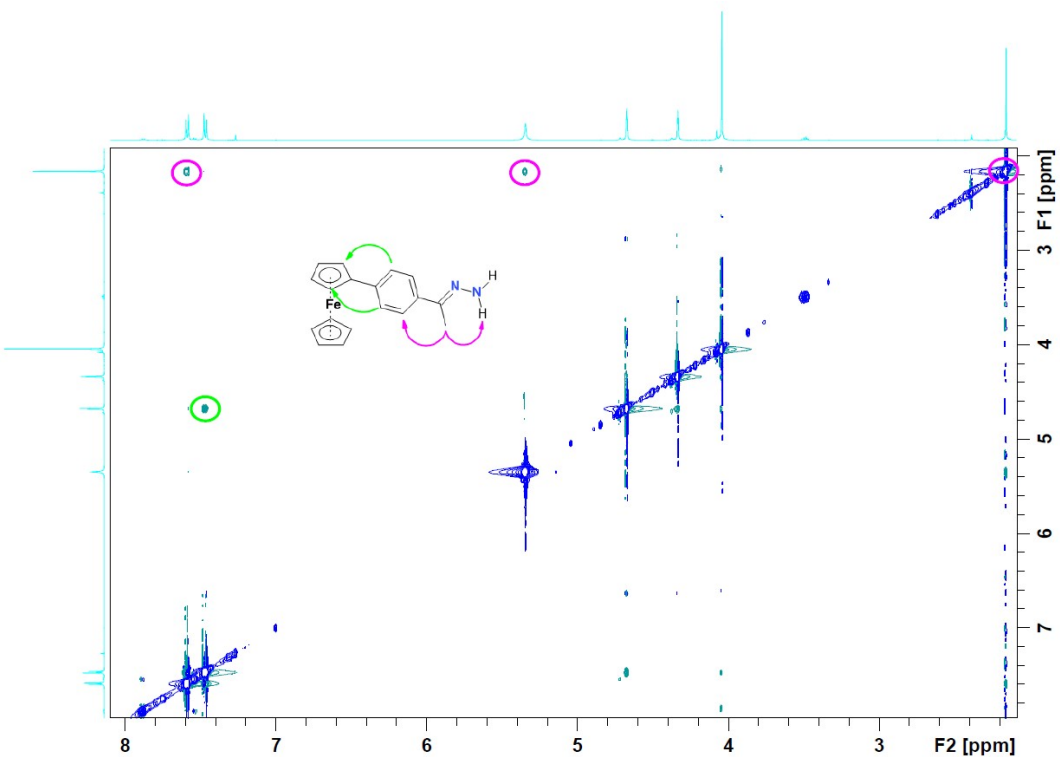


**Figure S4.**  $^1\text{H}-^1\text{H}$  2D-NOESY NMR spectrum of **1b**. Arrows shows  $^1\text{H}-^1\text{H}$  interactions observed for major component, *E*-isomer.

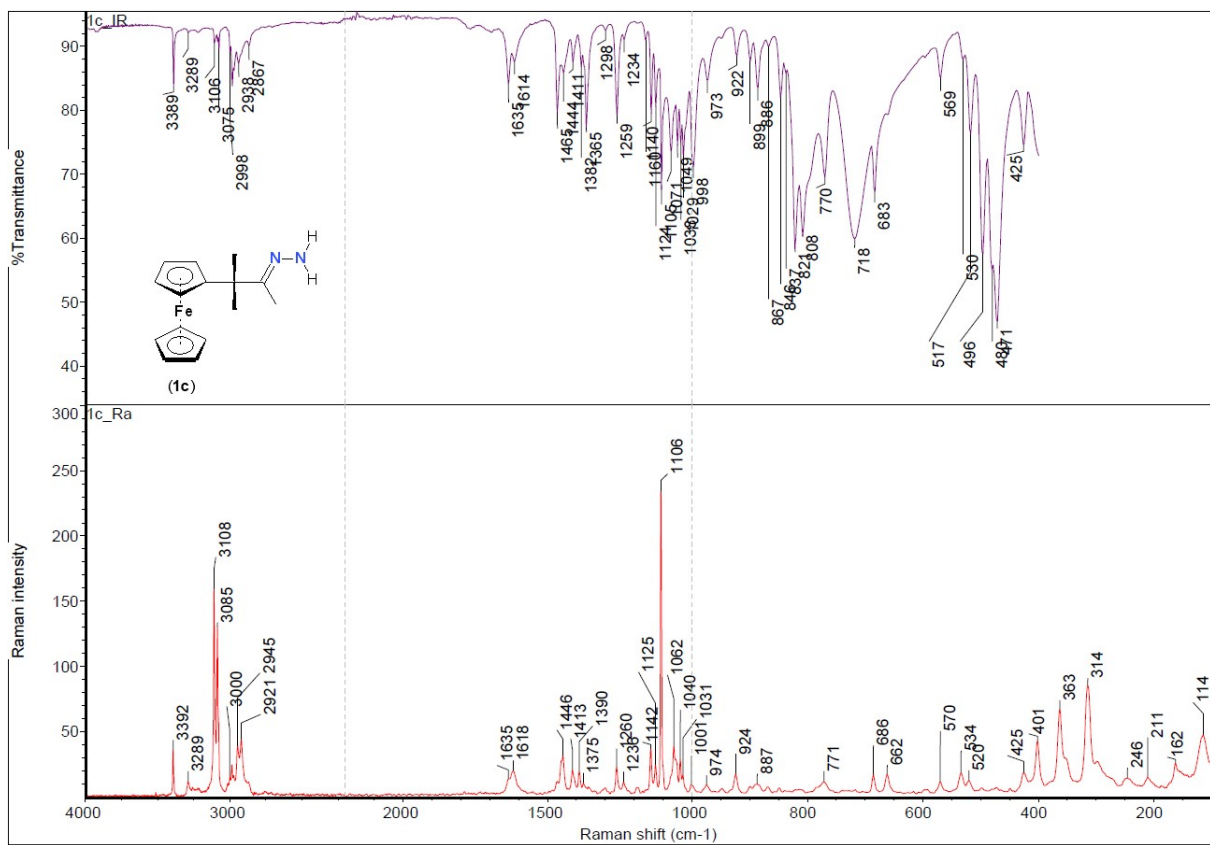


**Figure S5.** Infrared (top) and Raman (bottom) spectra of **1c** measured in the solid state.

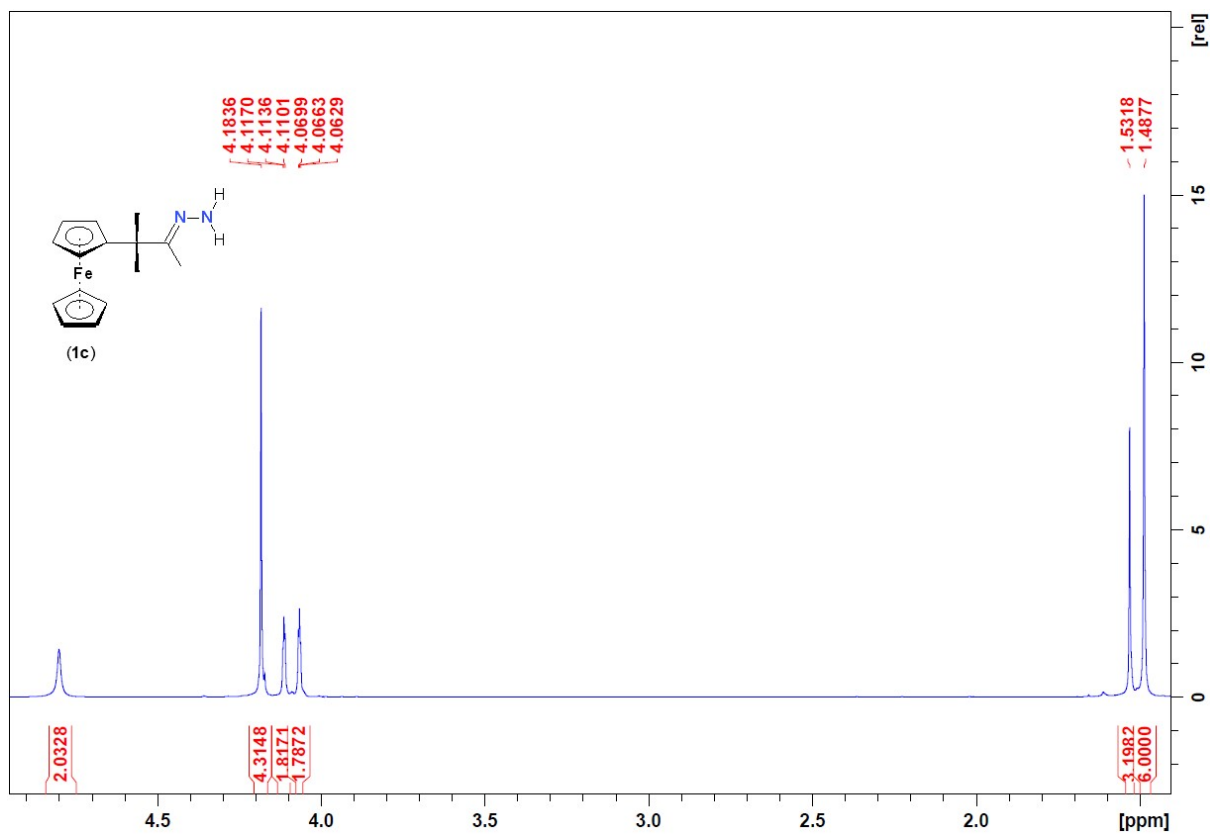


**Figure S6.** <sup>1</sup>H NMR spectrum of **1c** (500 MHz,  $\text{CDCl}_3$ , 298 K).

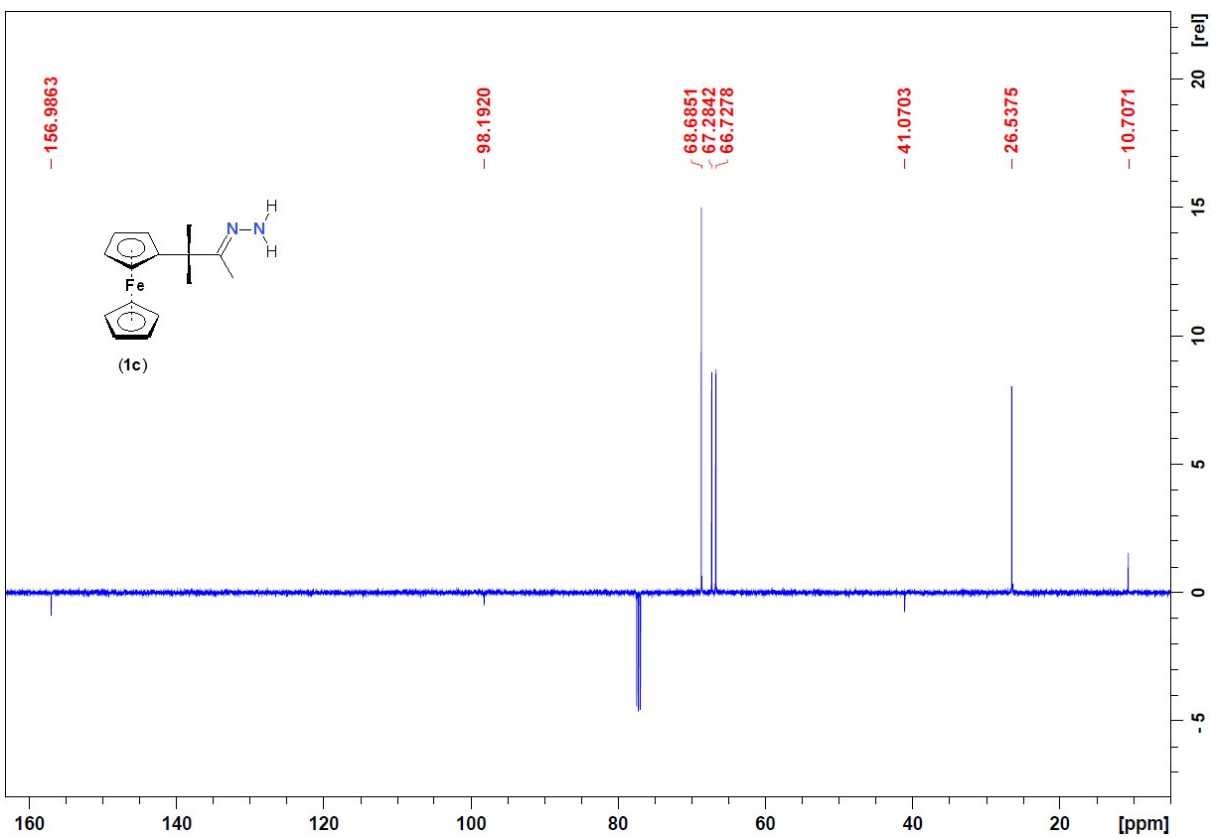


**Figure S7.**  $^{13}\text{C}\{^1\text{H}\}$  APT NMR spectrum of **1c** (125.76 MHz,  $\text{CDCl}_3$ , 298 K).

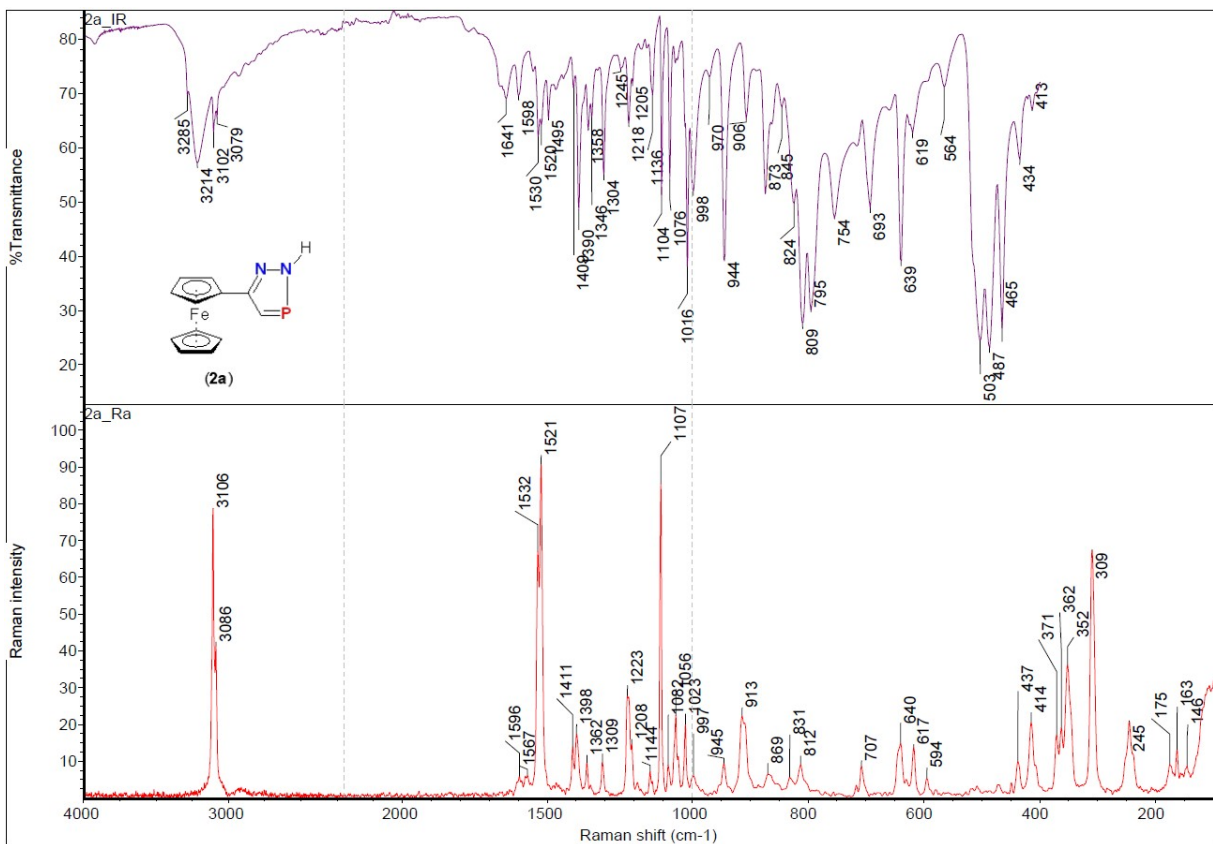


**Figure S8.** Infrared (top) and Raman (bottom) spectra of **2a** measured in the solid state.

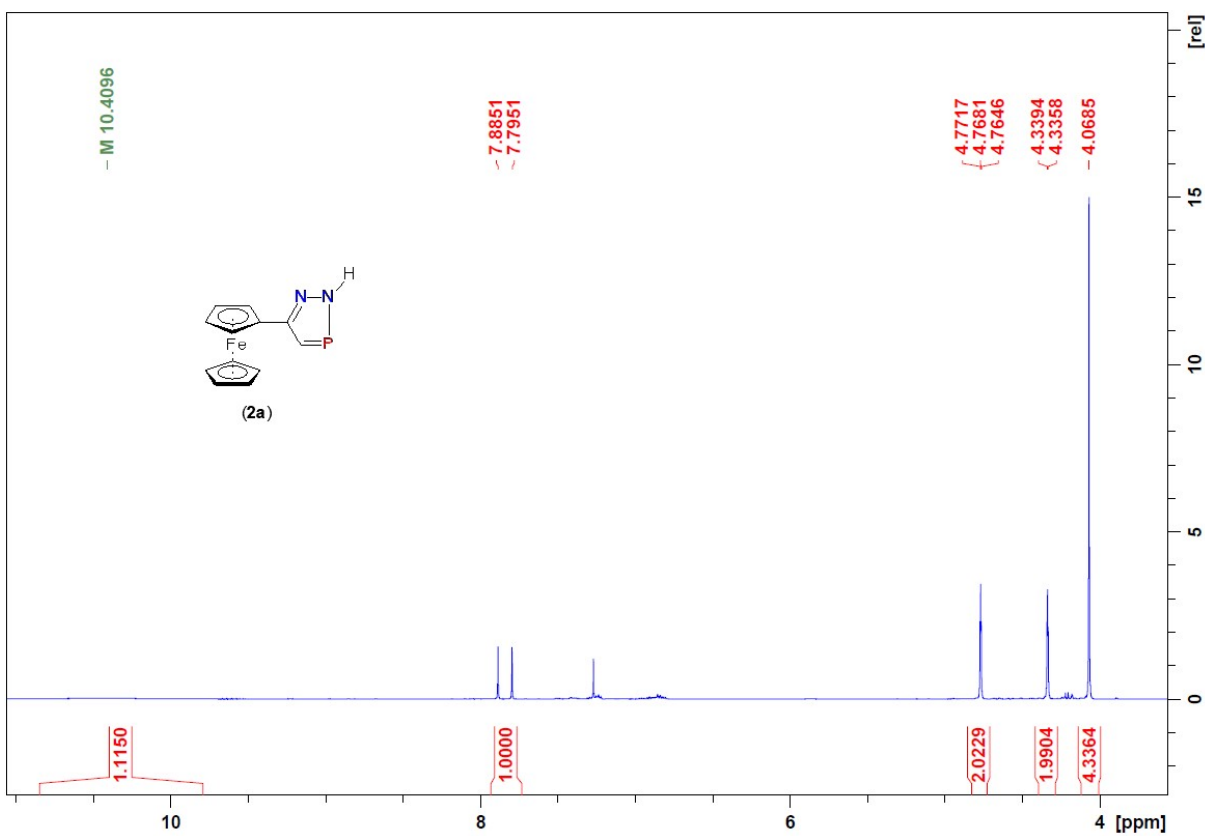


**Figure S9.**  $^1\text{H}$  NMR spectrum of **2a** (500 MHz,  $\text{CDCl}_3$ , 298 K).

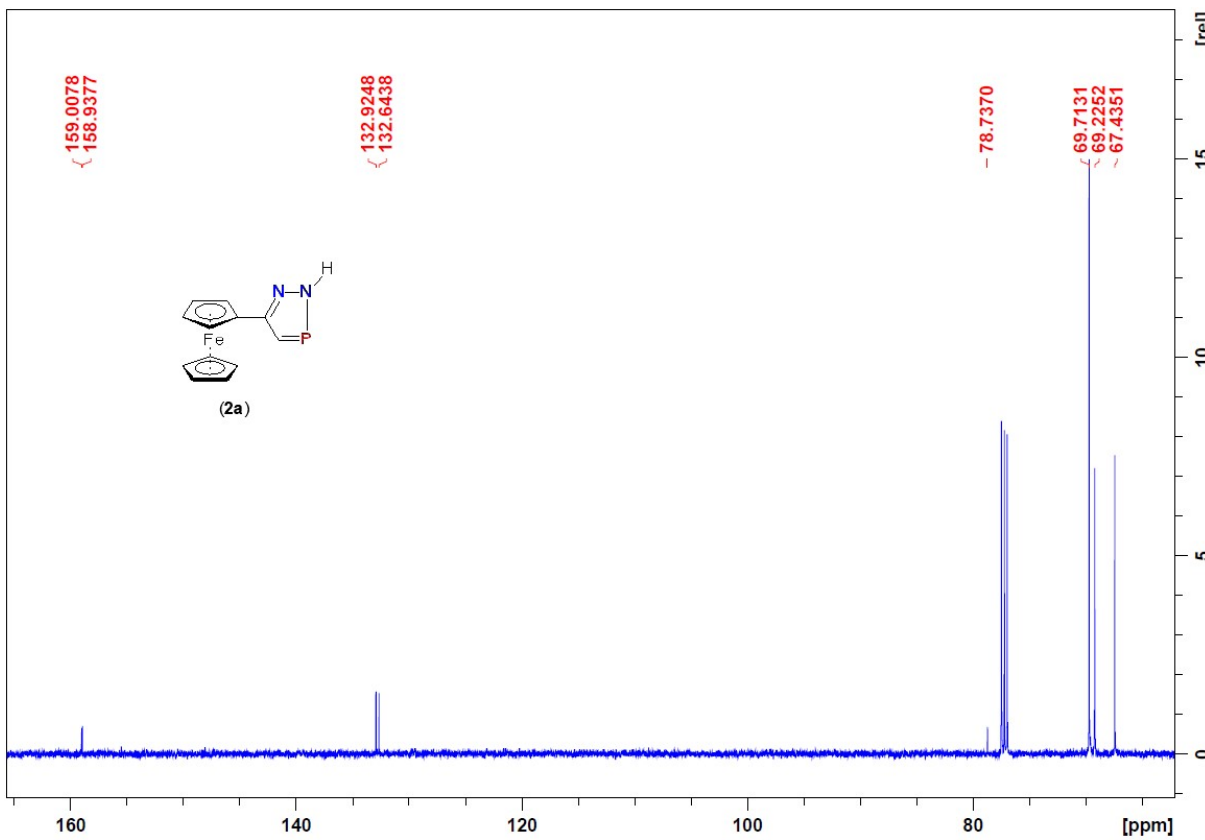


**Figure S10.**  $^{13}\text{C}\{^1\text{H}\}$  NMR spectrum of **2a** (125.76 MHz,  $\text{CDCl}_3$ , 298 K).

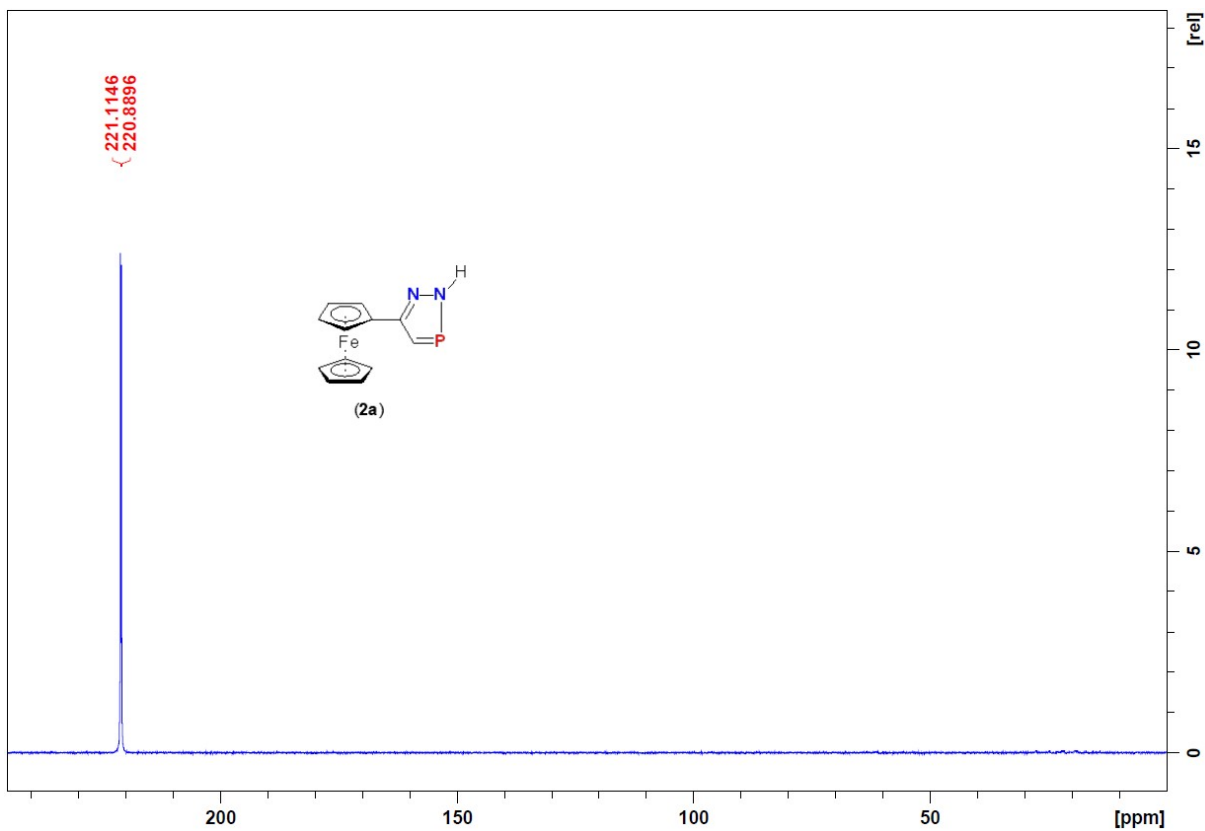


**Figure S11.**  $^{31}\text{P}$  NMR spectrum of **2a** (202.5 MHz,  $\text{CDCl}_3$ , 298 K).

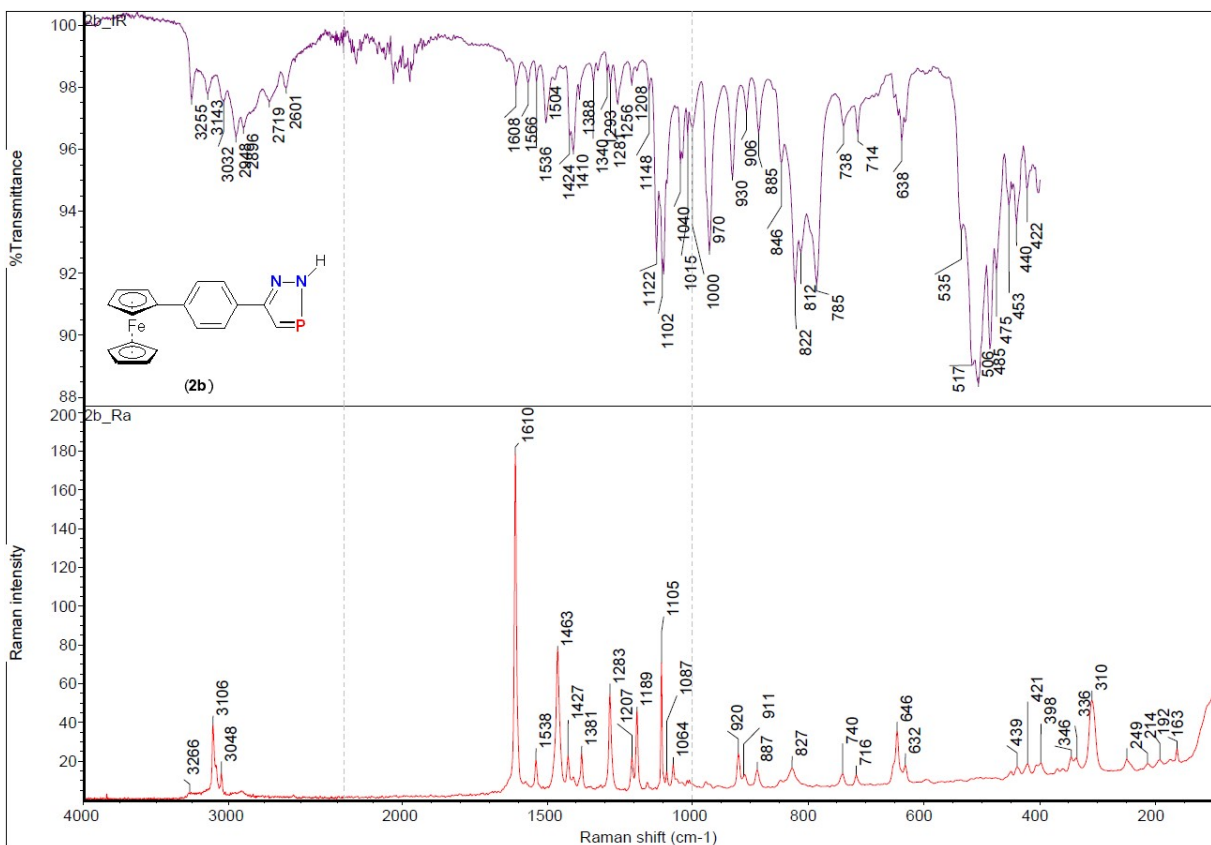


**Figure S12.** Infrared (top) and Raman (bottom) spectra of **2b** measured in the solid state.

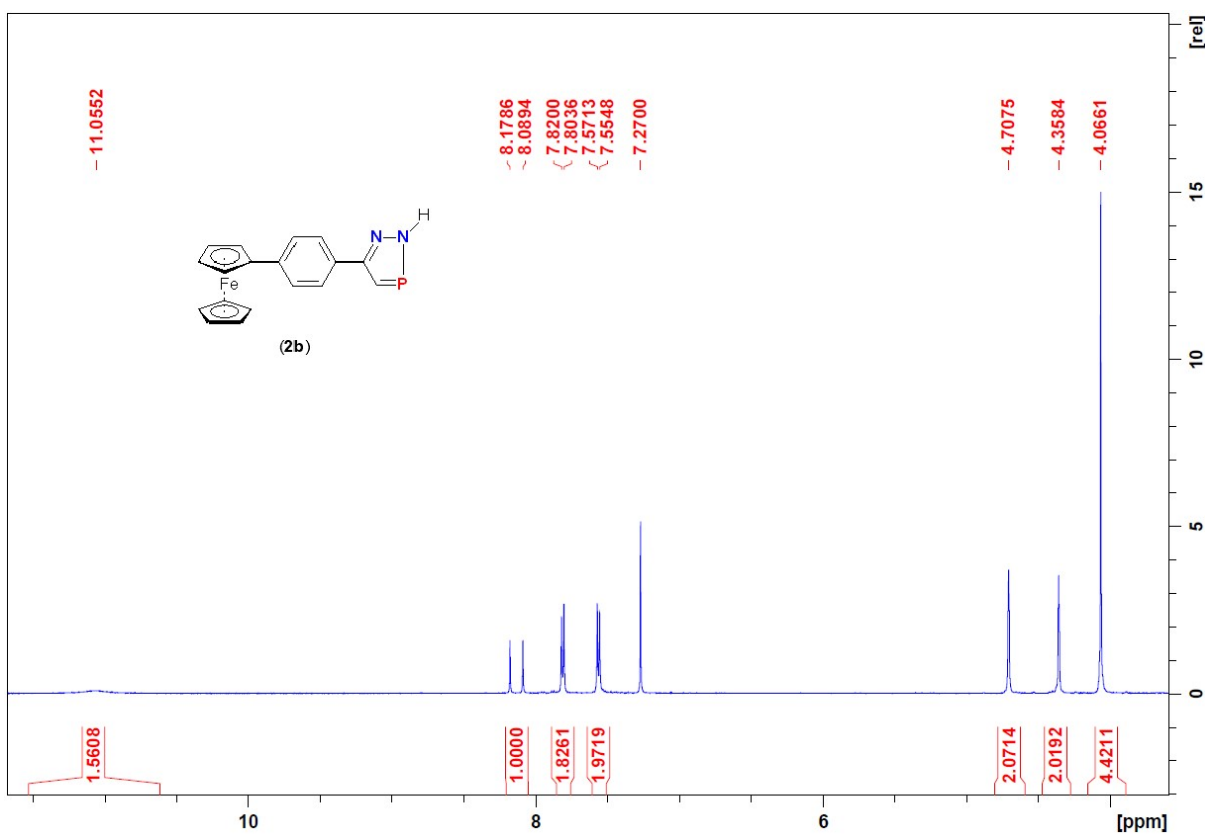


**Figure S13.**  $^1\text{H}$  NMR spectrum of **2b** (500 MHz,  $\text{CDCl}_3$ , 298 K).

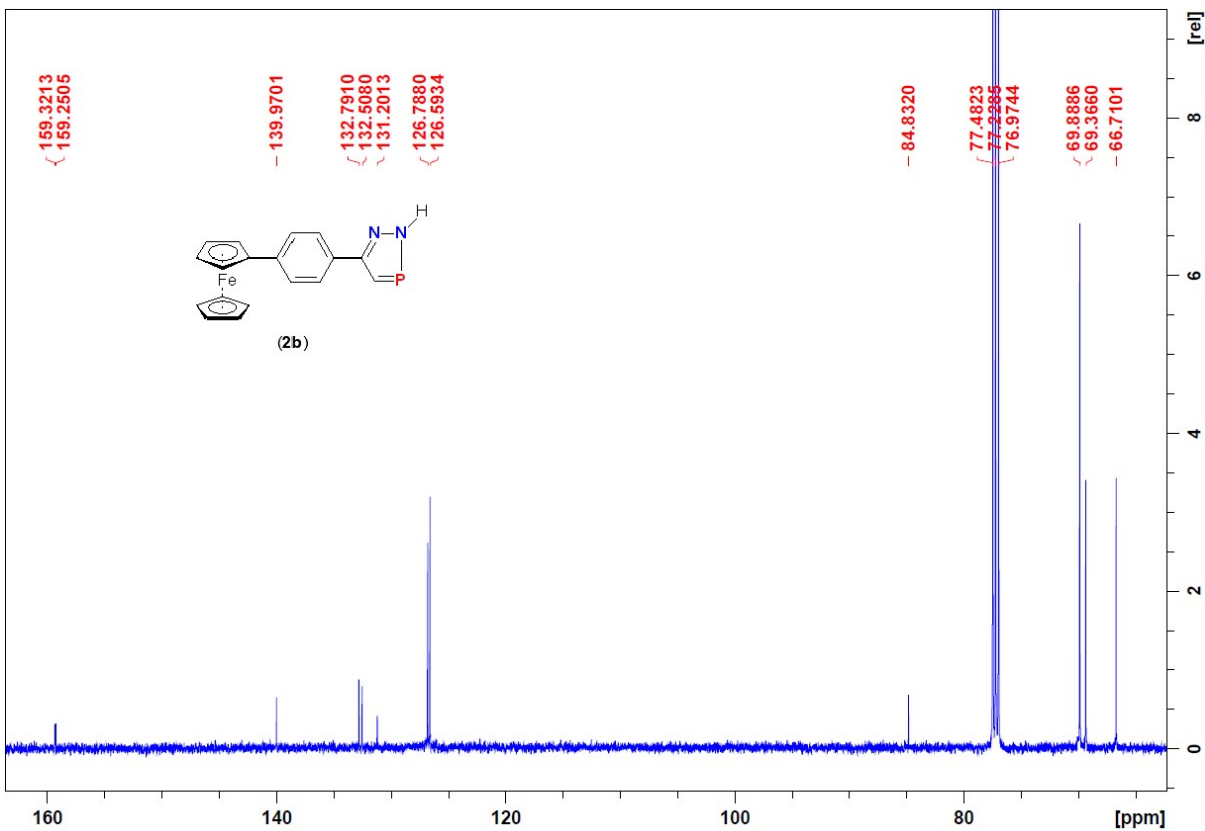


**Figure S14.**  $^{13}\text{C}\{^1\text{H}\}$  NMR spectrum of **2b** (125.76 MHz,  $\text{CDCl}_3$ , 298 K).

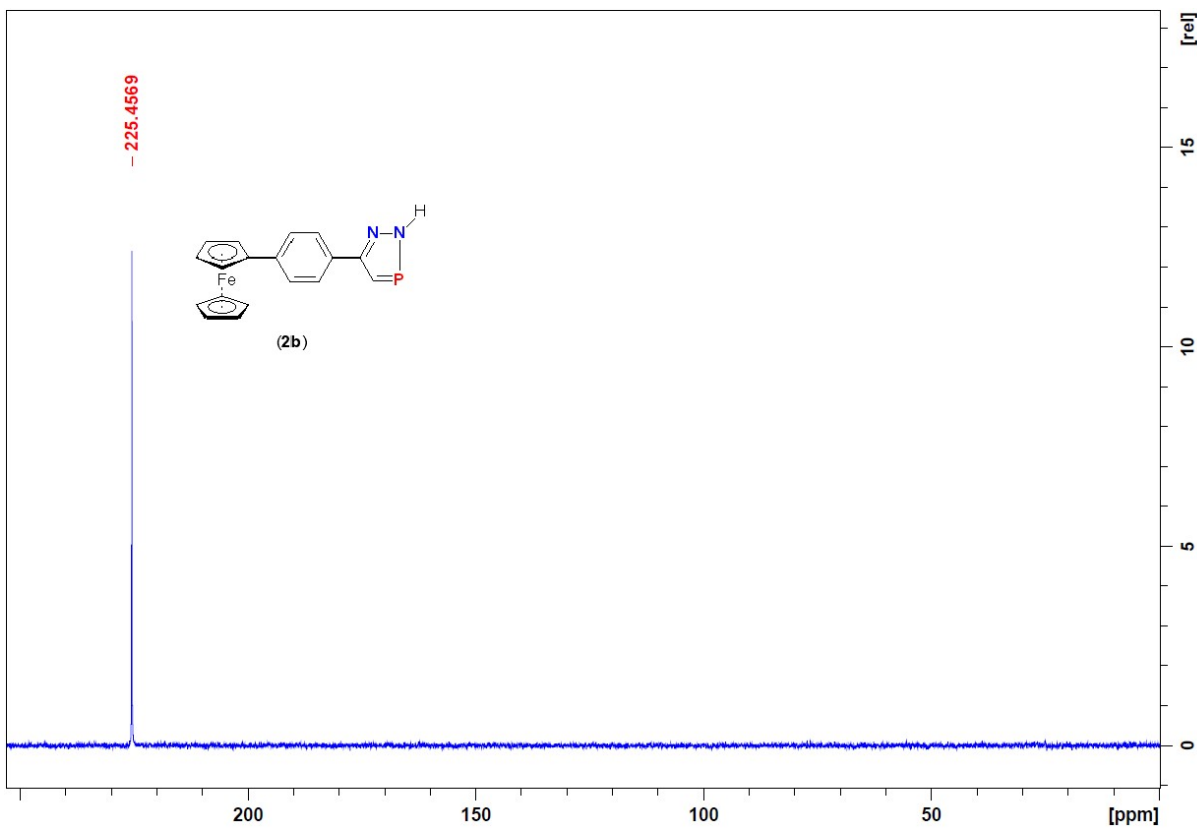


**Figure S15.**  $^{31}\text{P}\{^1\text{H}\}$  NMR spectrum of **2b** (202.5 MHz,  $\text{CDCl}_3$ , 298 K).

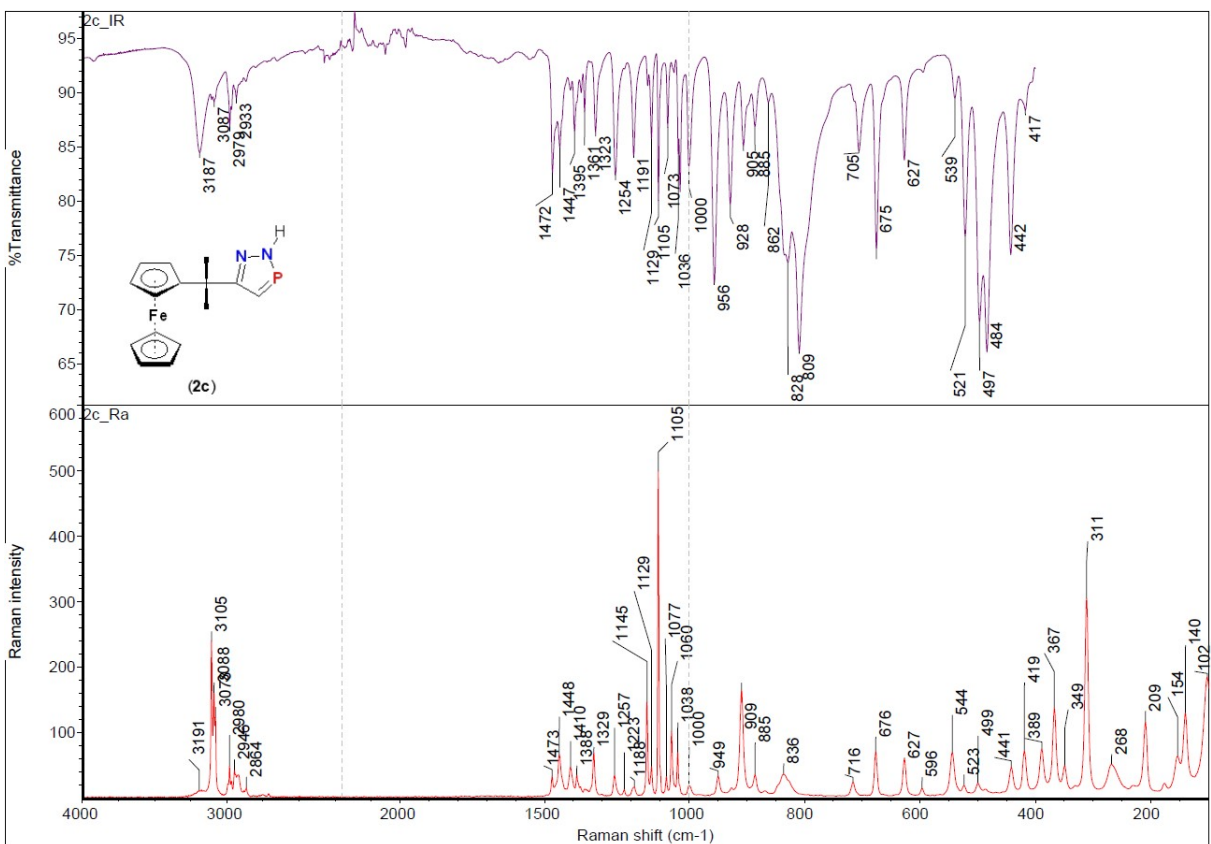


**Figure S16.** Infrared (top) and Raman (bottom) spectra of **2c** measured in the solid state (manually selected single-crystals

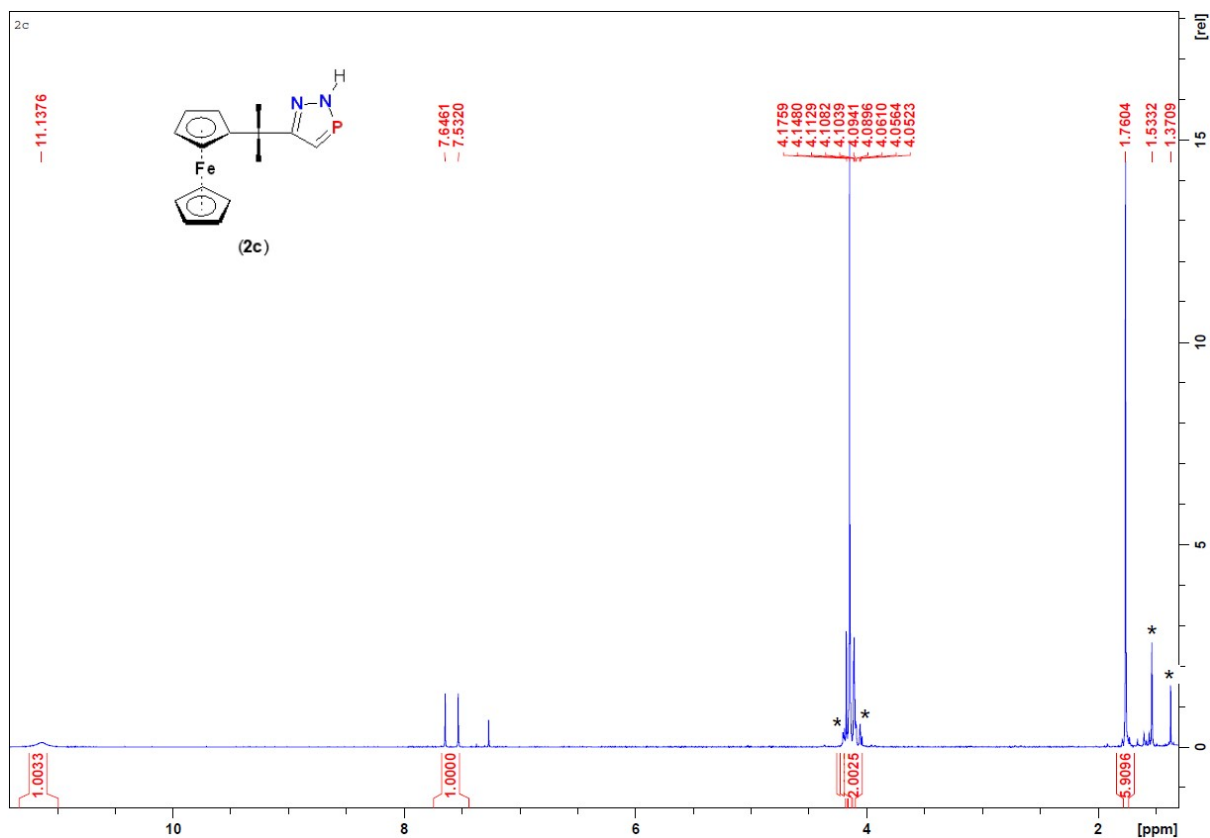


**Figure S17.**  $^1\text{H}$  NMR spectrum of **2c** (500 MHz,  $\text{CDCl}_3$ , 298 K). Asterisks denote signals of azine **3c**.

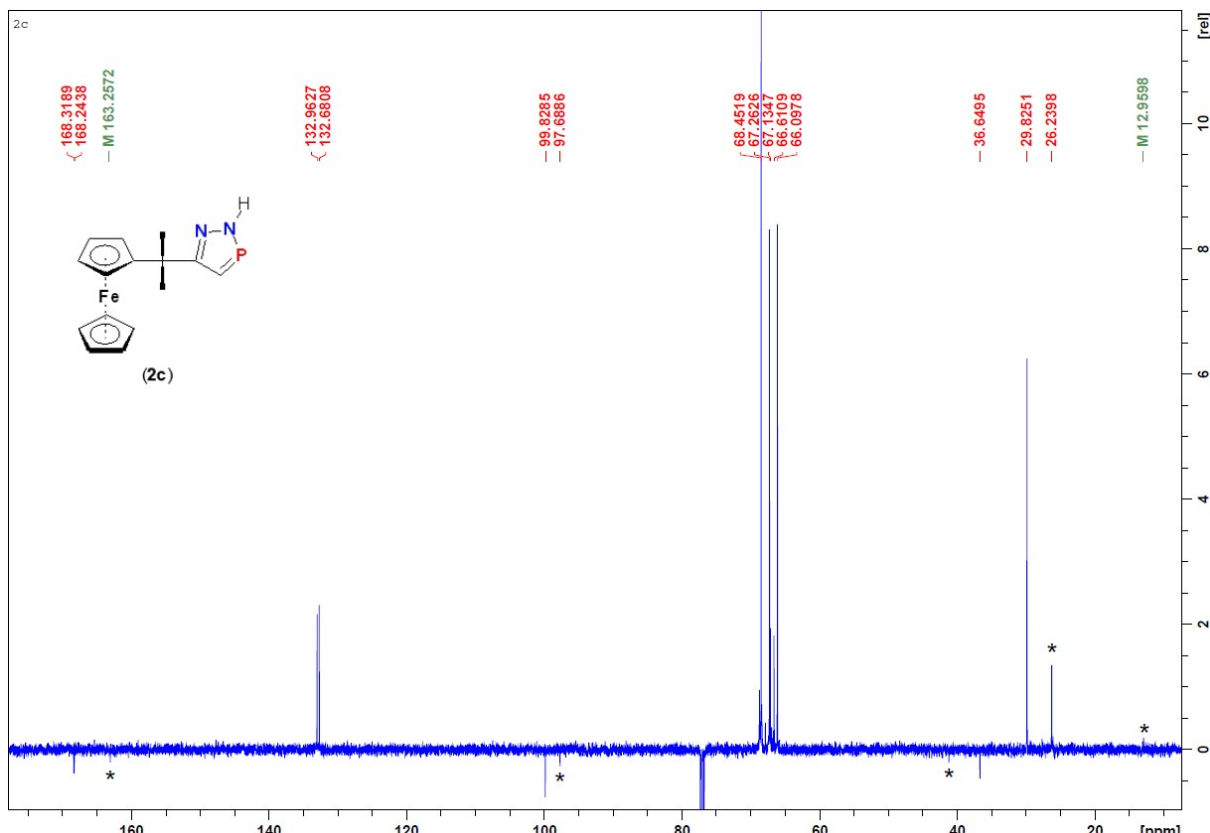


**Figure S18.**  $^{13}\text{C}\{^1\text{H}\}$  APT NMR spectrum of **2c** (125.76 MHz,  $\text{CDCl}_3$ , 298 K). Asterisks denote signals of azine **3c**.

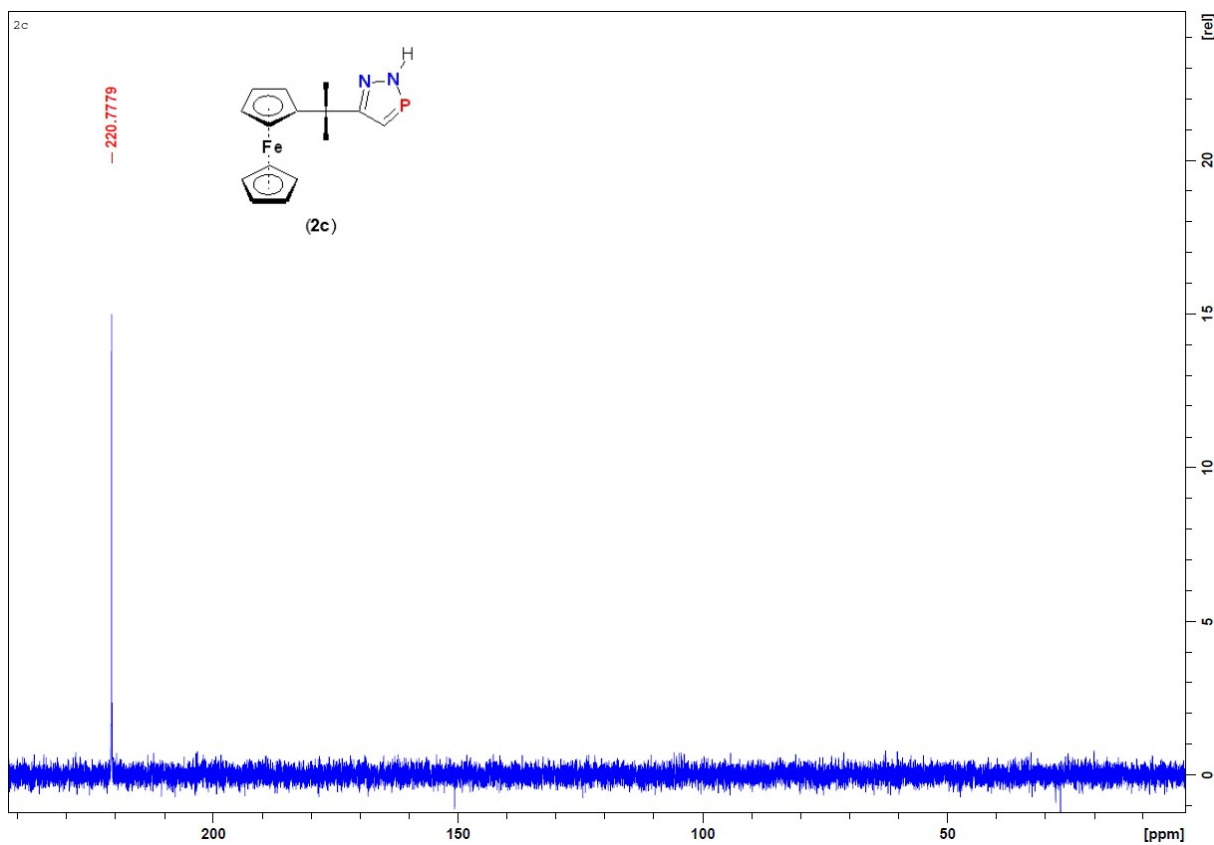


**Figure S19.**  $^{31}\text{P}\{\text{H}\}$  NMR spectrum of **2c** (202.5 MHz,  $\text{CDCl}_3$ , 298 K).

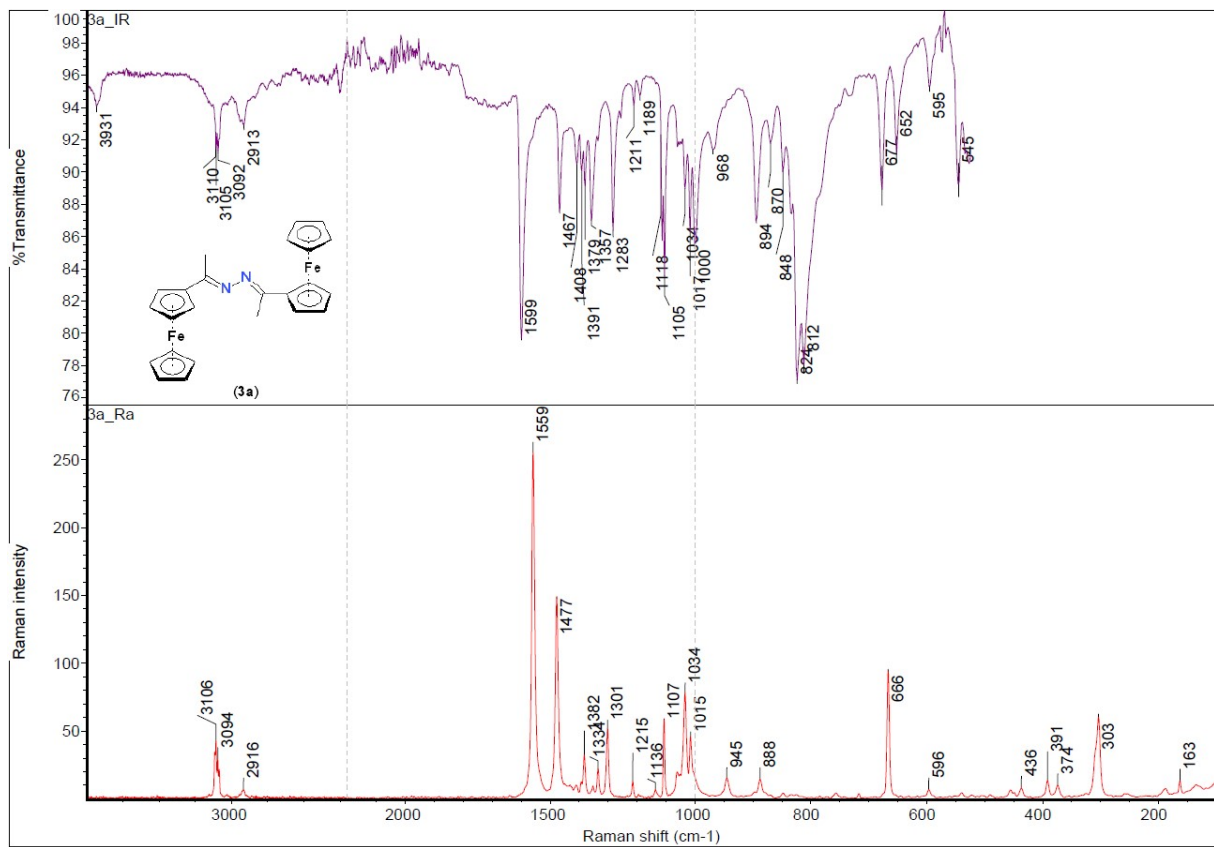


**Figure S20.** Infrared (top) and Raman (bottom) spectra of **3a** measured in the solid state.

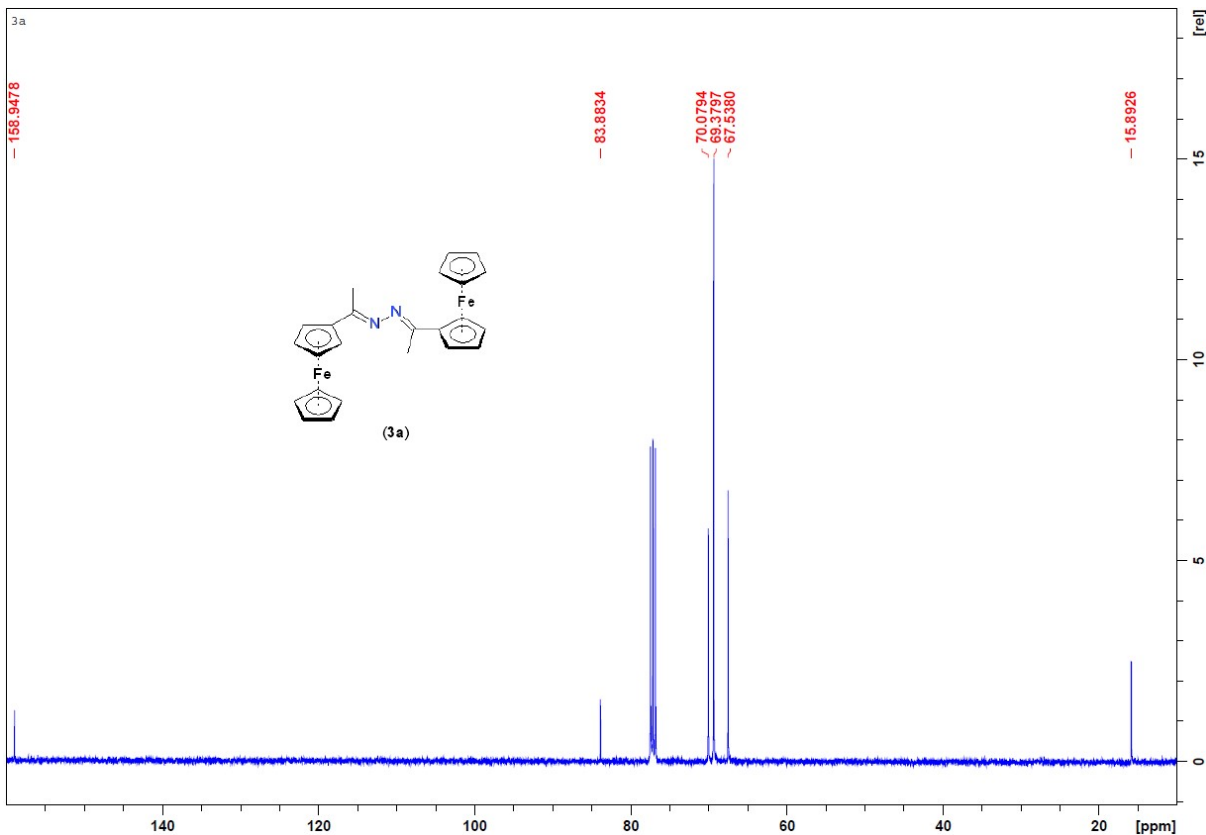
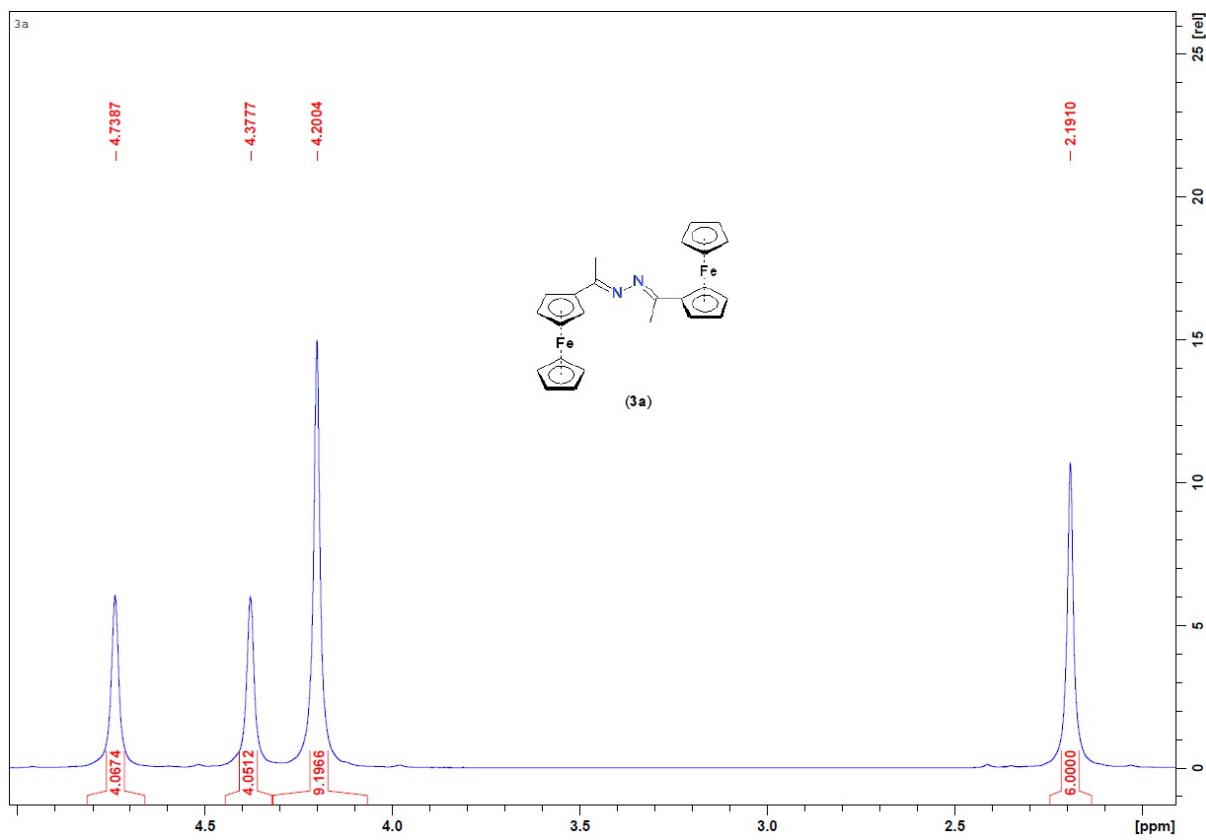


**Figure S22.**  $^{13}\text{C}\{^1\text{H}\}$  NMR spectrum of **3a** (100.61 MHz,  $\text{CDCl}_3$ , 298 K).

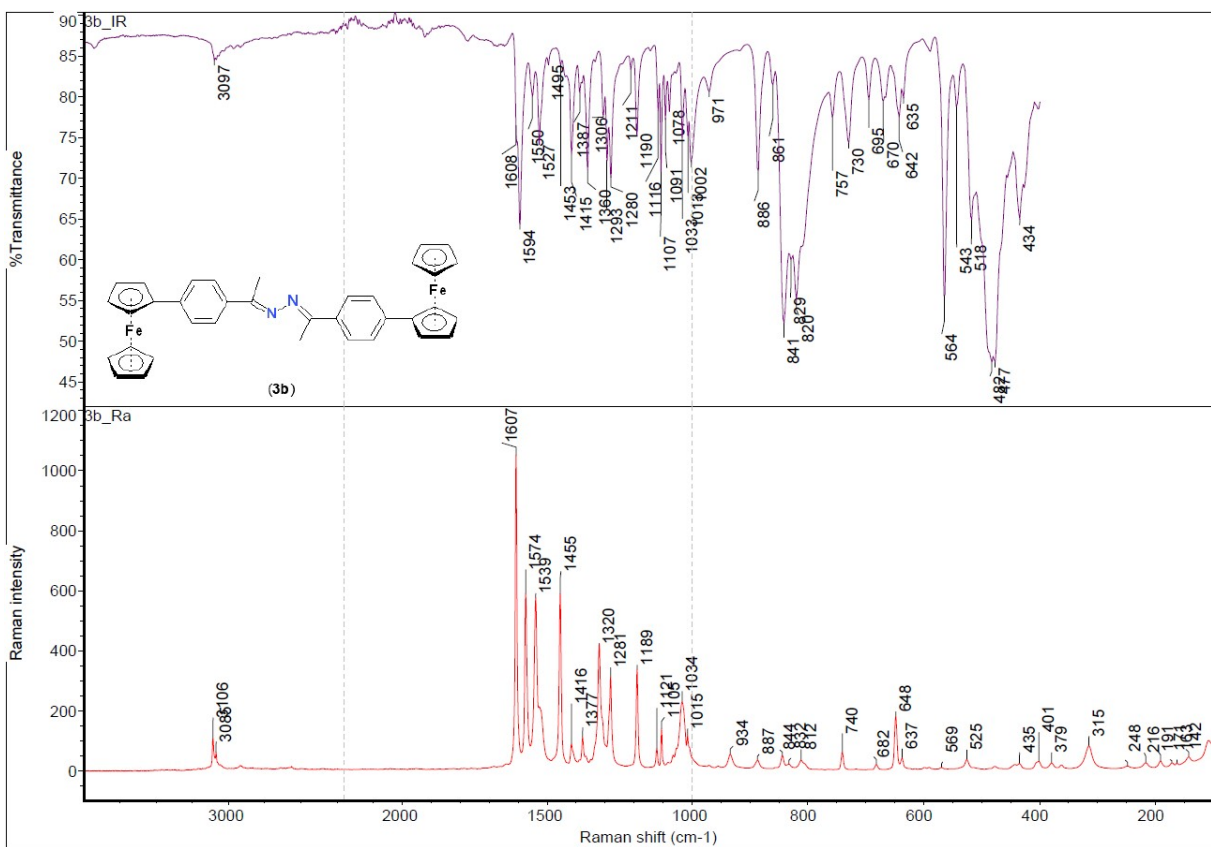


**Figure S23.** Infrared (top) and Raman (bottom) spectra of **3b** measured in the solid state.

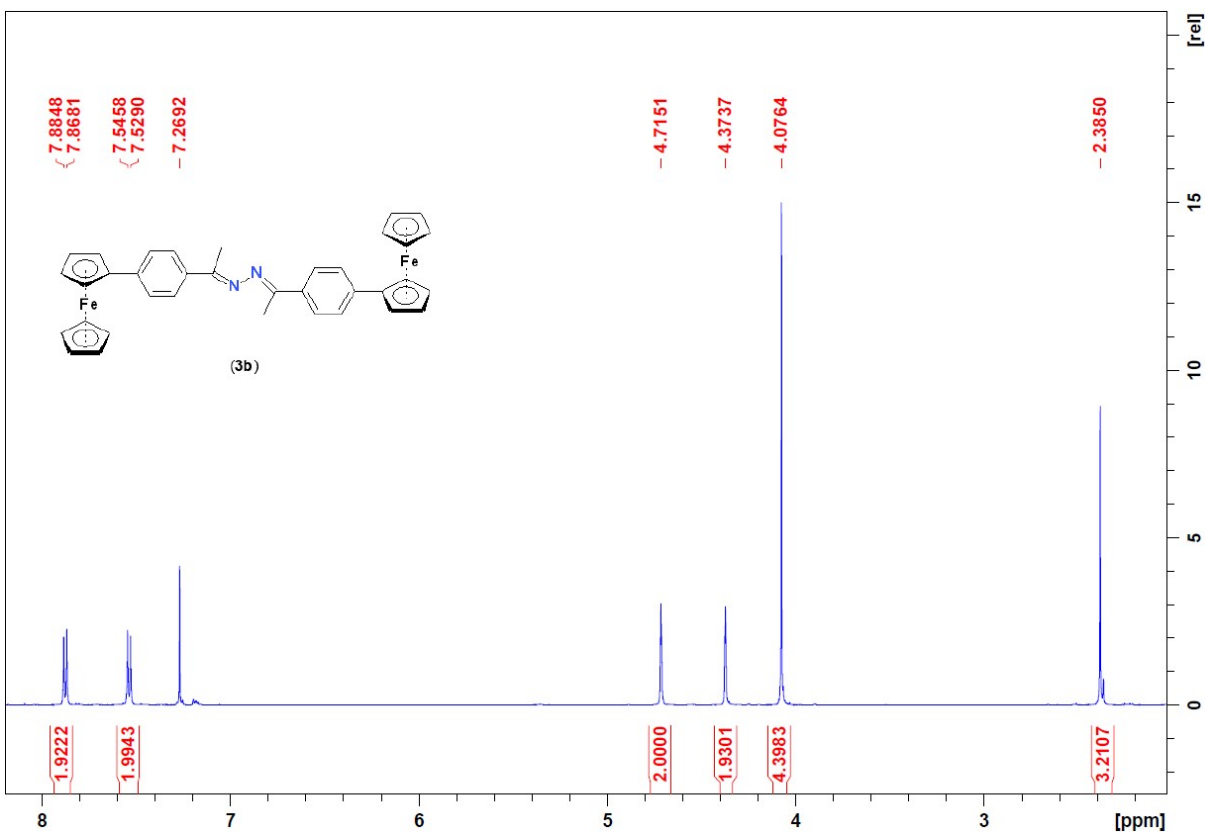


**Figure S24.**  $^1\text{H}$  NMR spectrum of **3b** (500 MHz,  $\text{CDCl}_3$ , 298 K).

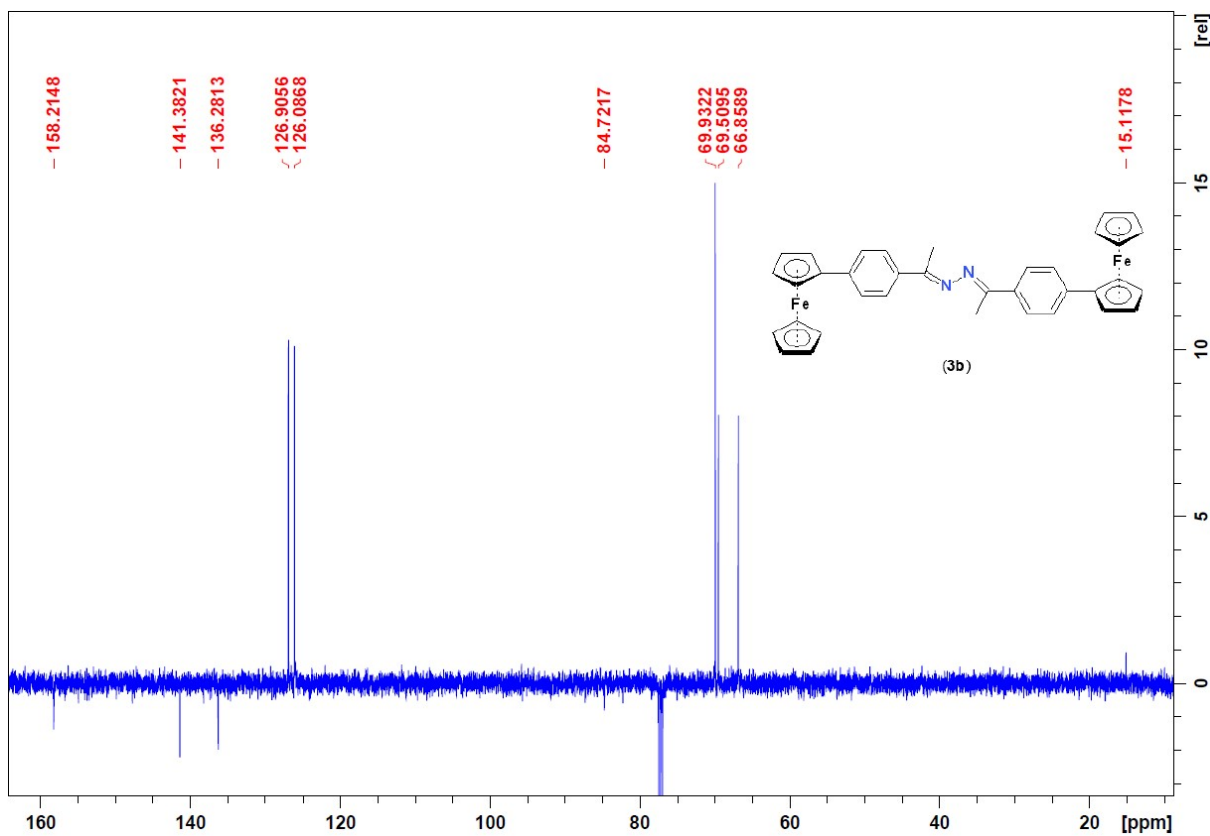


**Figure S25.**  $^{13}\text{C}\{^1\text{H}\}$  APT NMR spectrum of **3b** (125.76 MHz,  $\text{CDCl}_3$ , 298 K).

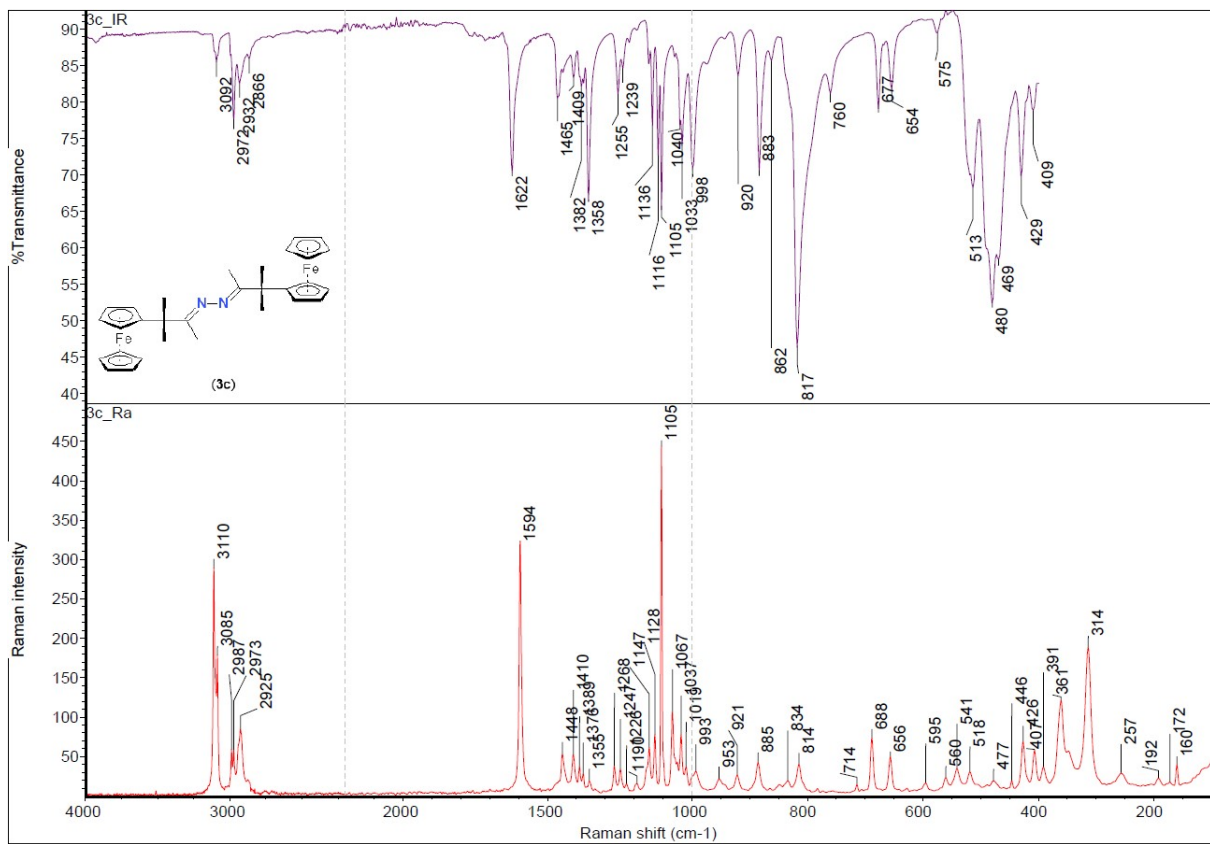


**Figure S26.** Infrared (top) and Raman (bottom) spectra of **3c** measured in the solid state.

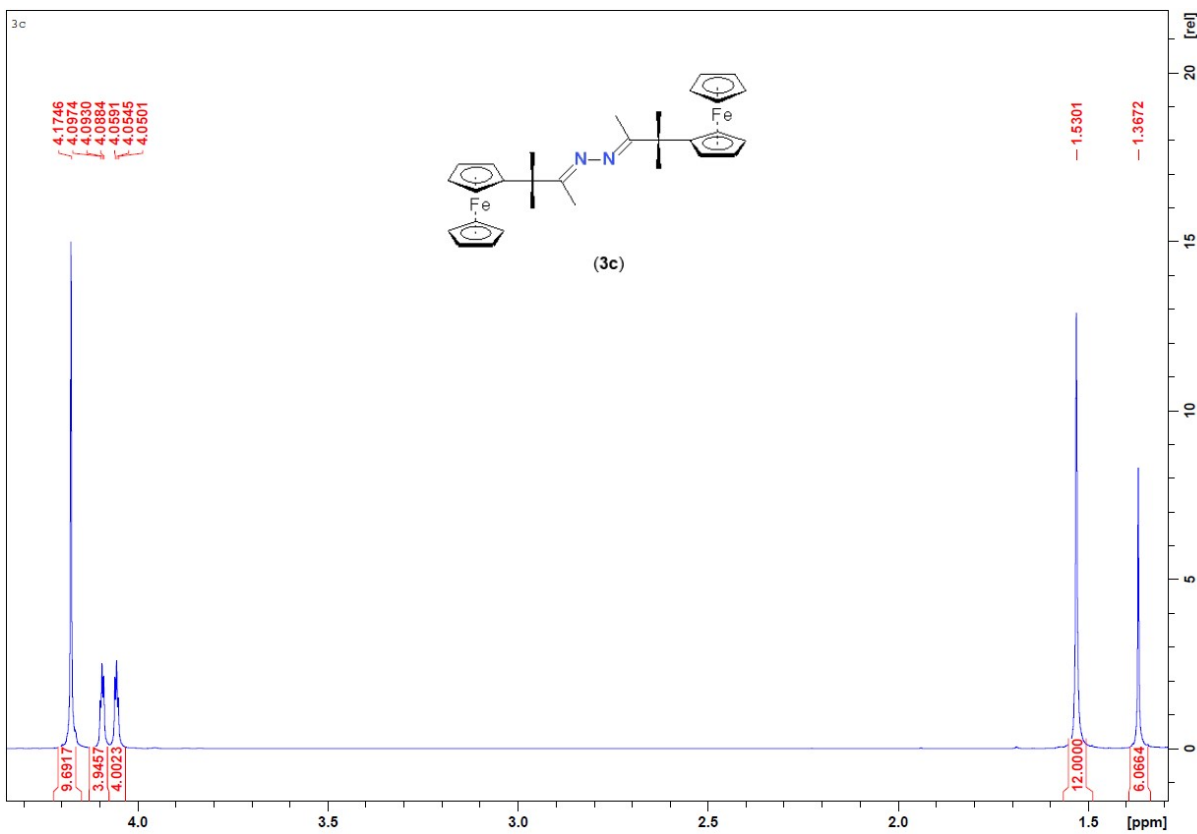


**Figure S27.**  $^1\text{H}$  NMR spectrum of **3c** (400 MHz,  $\text{CDCl}_3$ , 298 K).

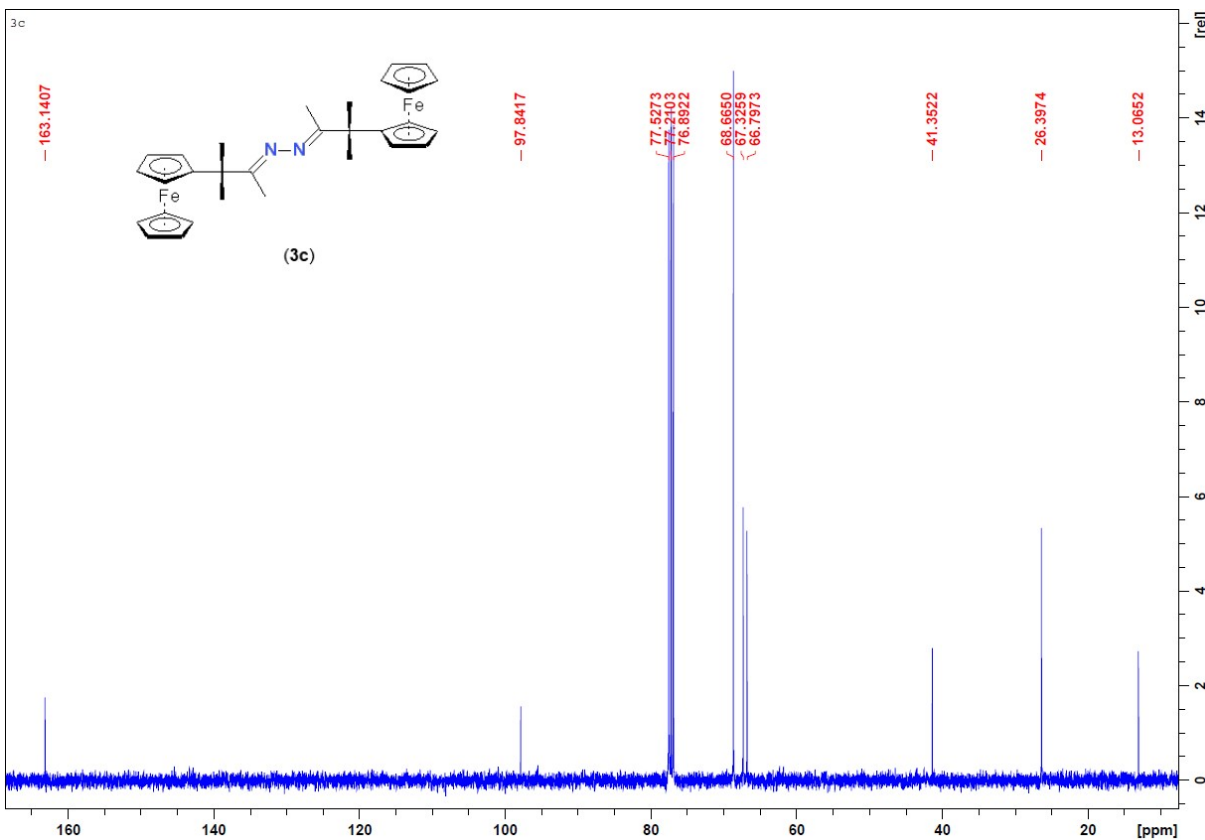


**Figure S28.**  $^{13}\text{C}\{^1\text{H}\}$  NMR spectrum of **3c** (100.61 MHz,  $\text{CDCl}_3$ , 298 K).

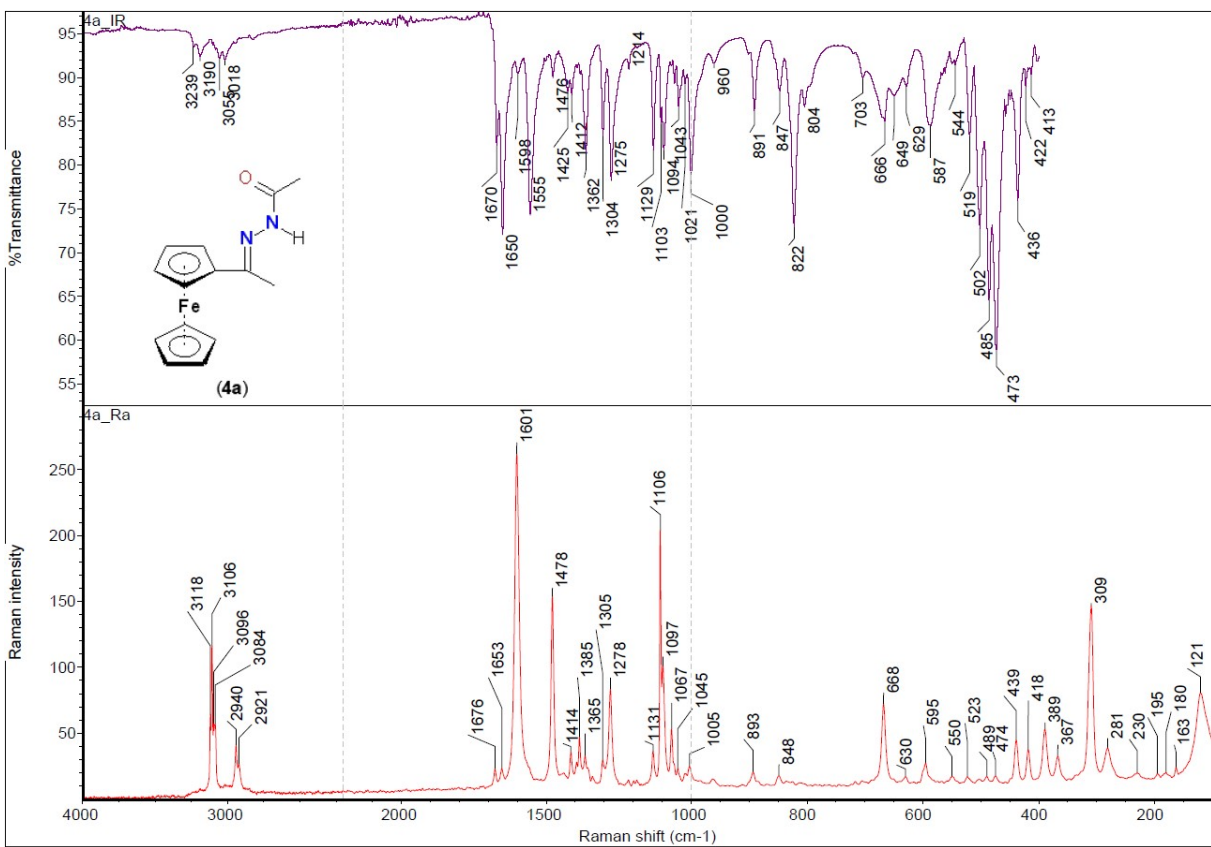


**Figure S29.** Infrared (top) and Raman (bottom) spectra of **4a** measured in the solid state.

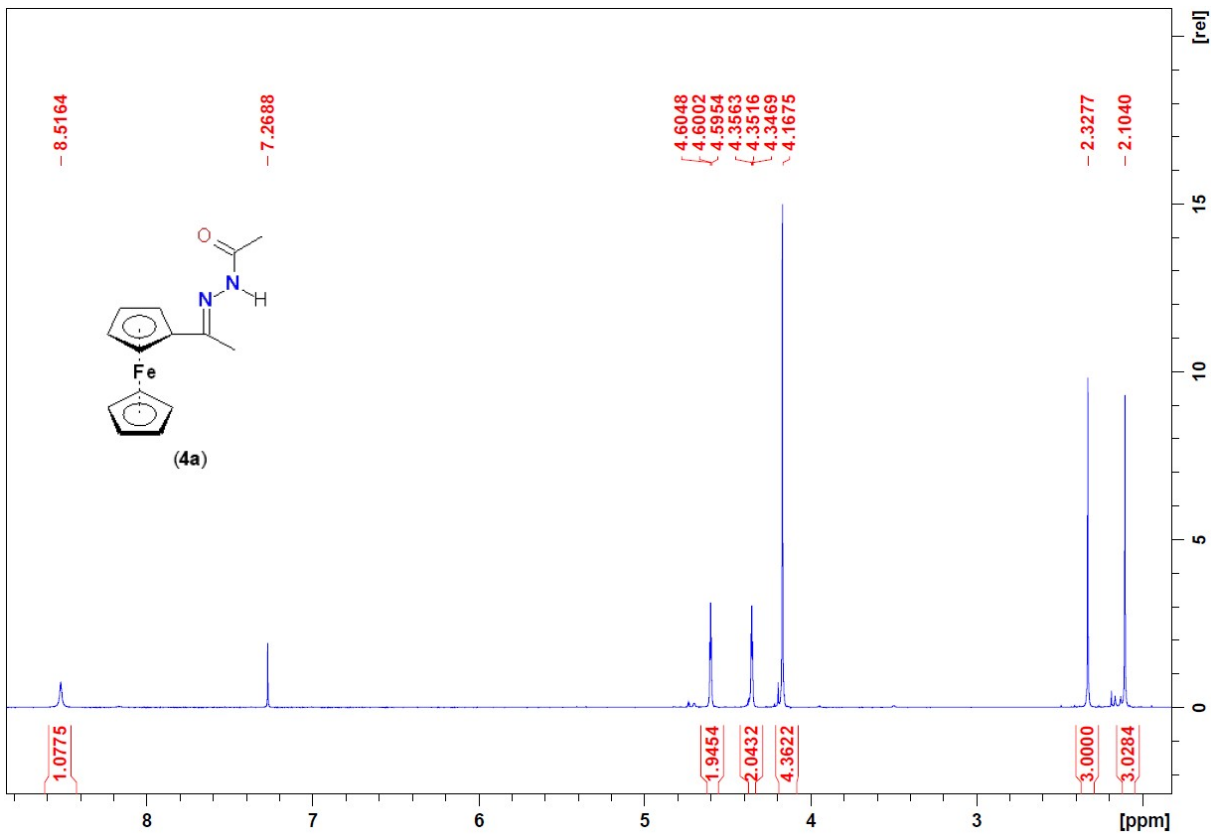


**Figure S30.** <sup>1</sup>H NMR spectrum of **4a** (400 MHz, CDCl<sub>3</sub>, 298 K).

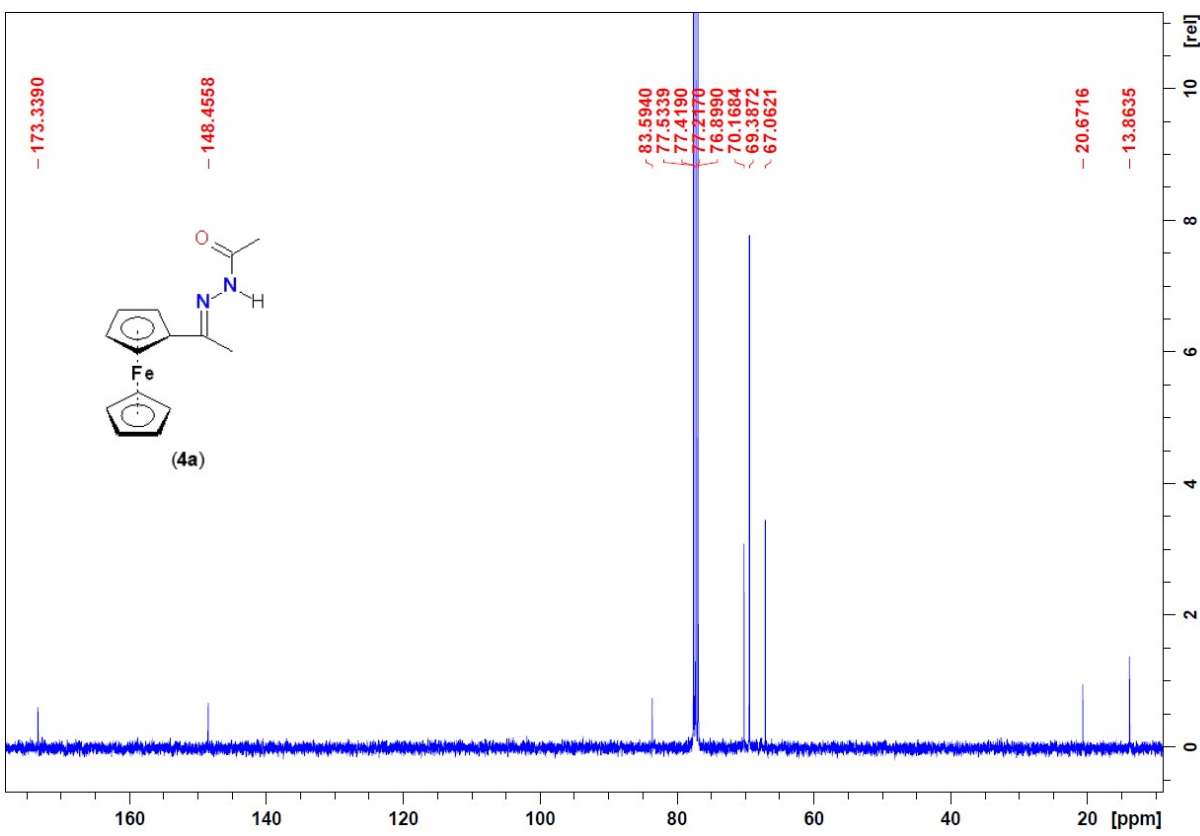


**Figure S31.**  $^{13}\text{C}\{^1\text{H}\}$  NMR spectrum of **4a** (100.61 MHz,  $\text{CDCl}_3$ , 298 K).

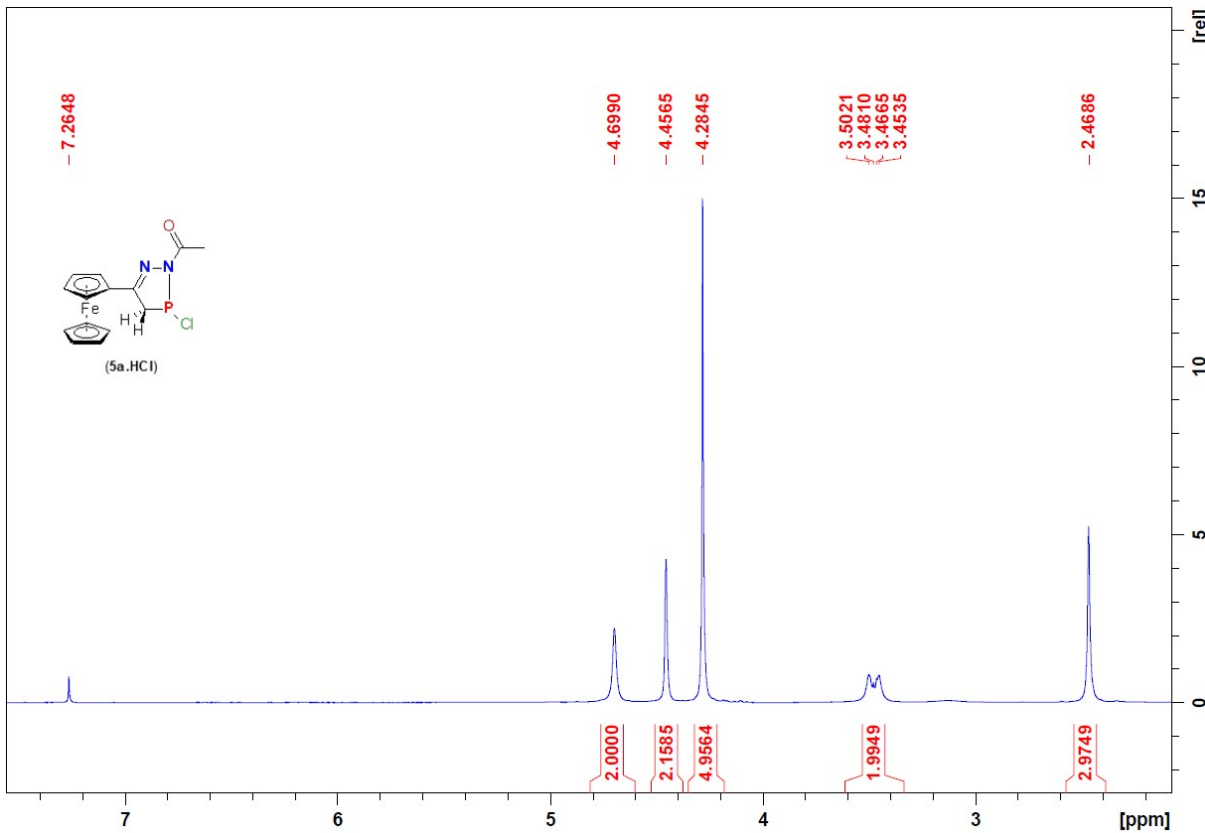


**Figure S32.**  $^1\text{H}$  NMR spectrum of **5a.HCl** (500 MHz,  $\text{CDCl}_3$ , 250 K).

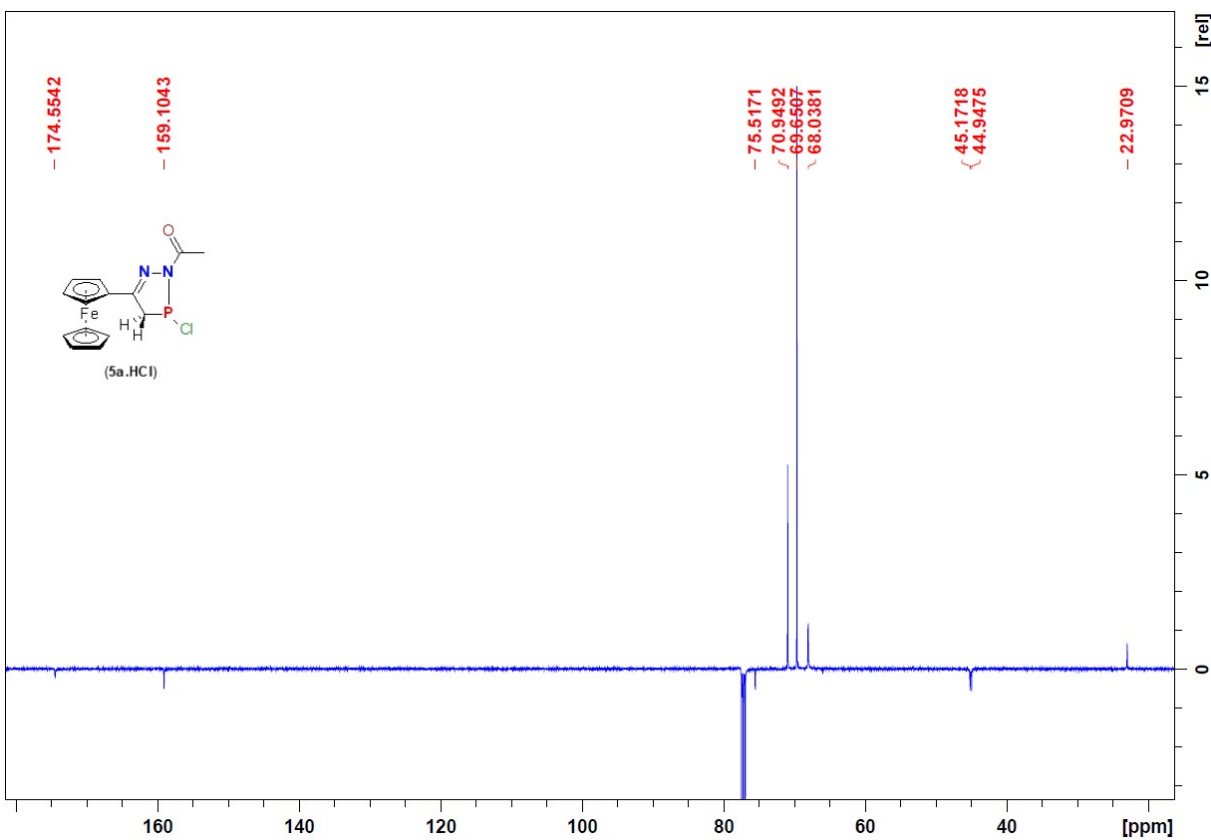


**Figure S33.**  $^{13}\text{C}\{\text{H}\}$  NMR spectrum of **5a.HCl** (125.76 MHz, CDCl<sub>3</sub>, 250 K).

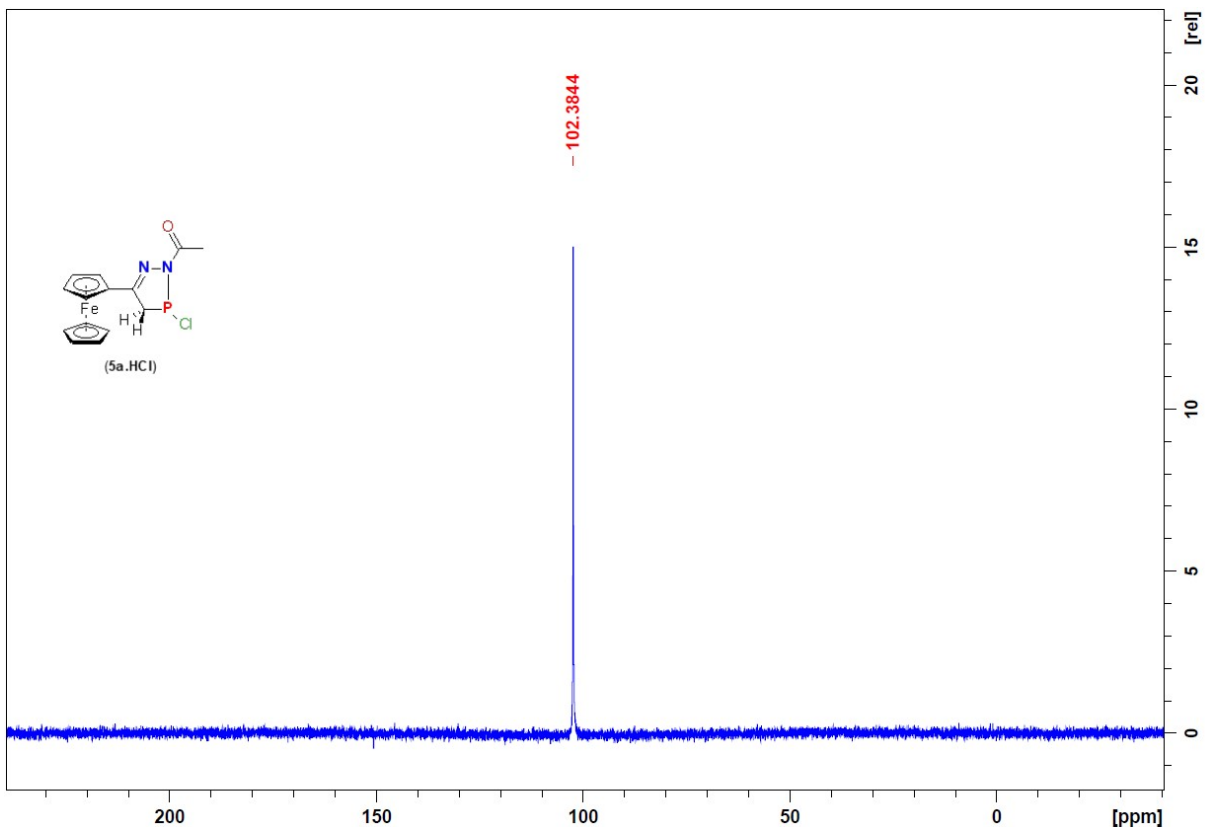


**Figure S34.**  $^{31}\text{P}\{\text{H}\}$  NMR spectrum of **5a.HCl** (161.98 MHz, CDCl<sub>3</sub>, 250 K).

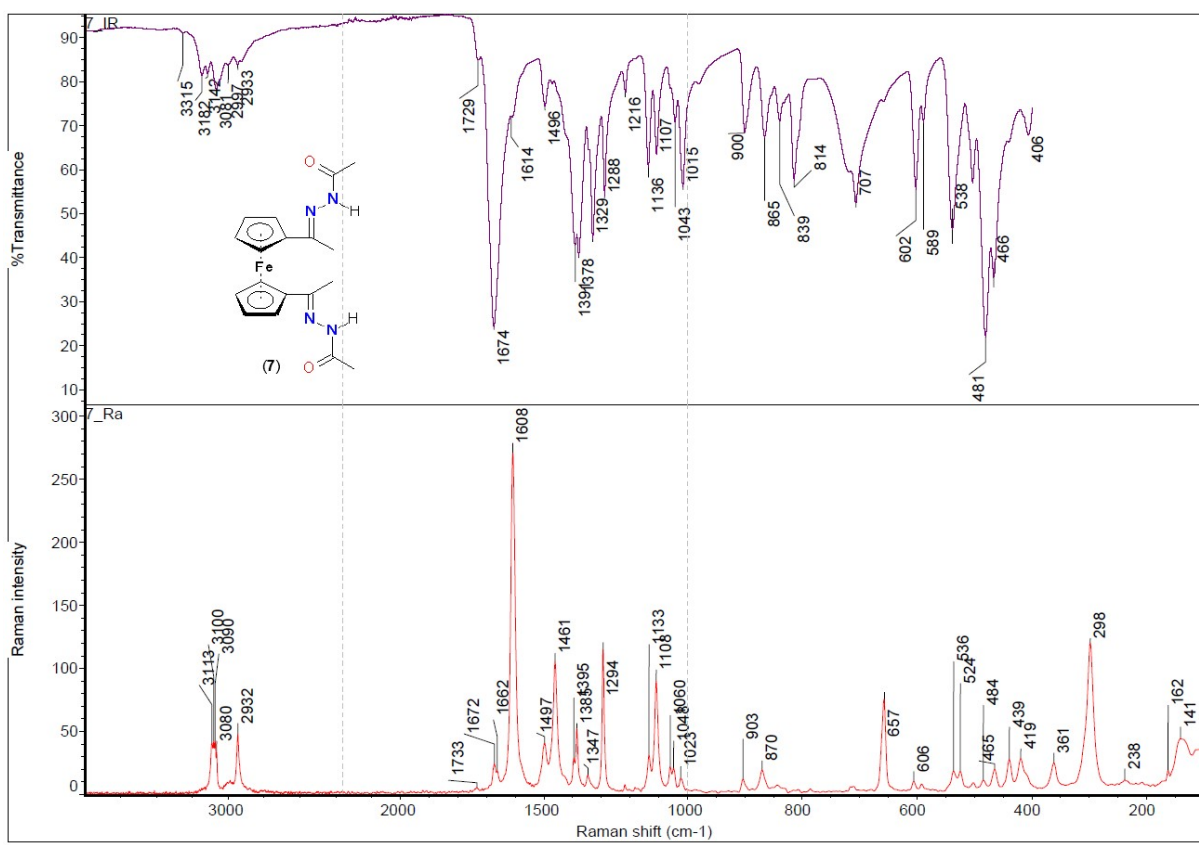


**Figure S35.** Infrared (top) and Raman (bottom) spectra of **7** measured in the solid state.

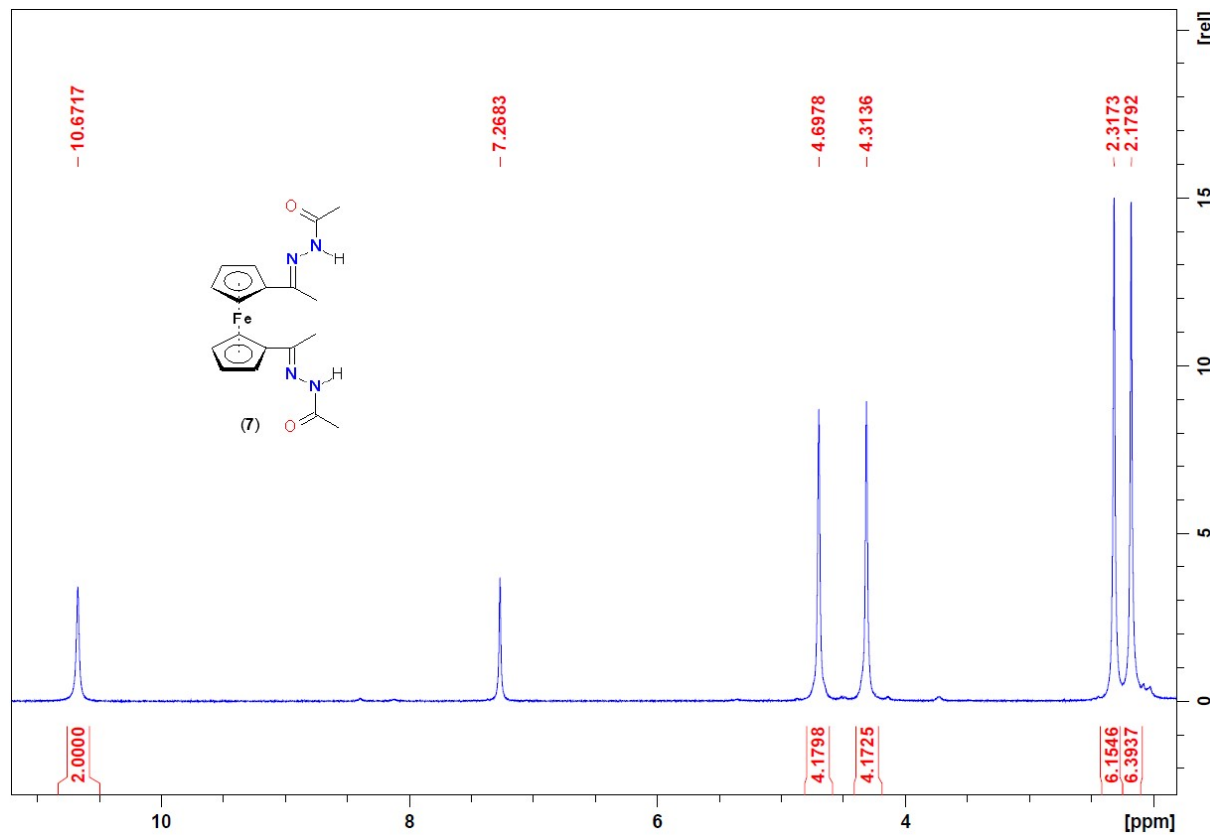


**Figure S36.** <sup>1</sup>H NMR spectrum of **7** (500 MHz, CDCl<sub>3</sub>, 298 K).

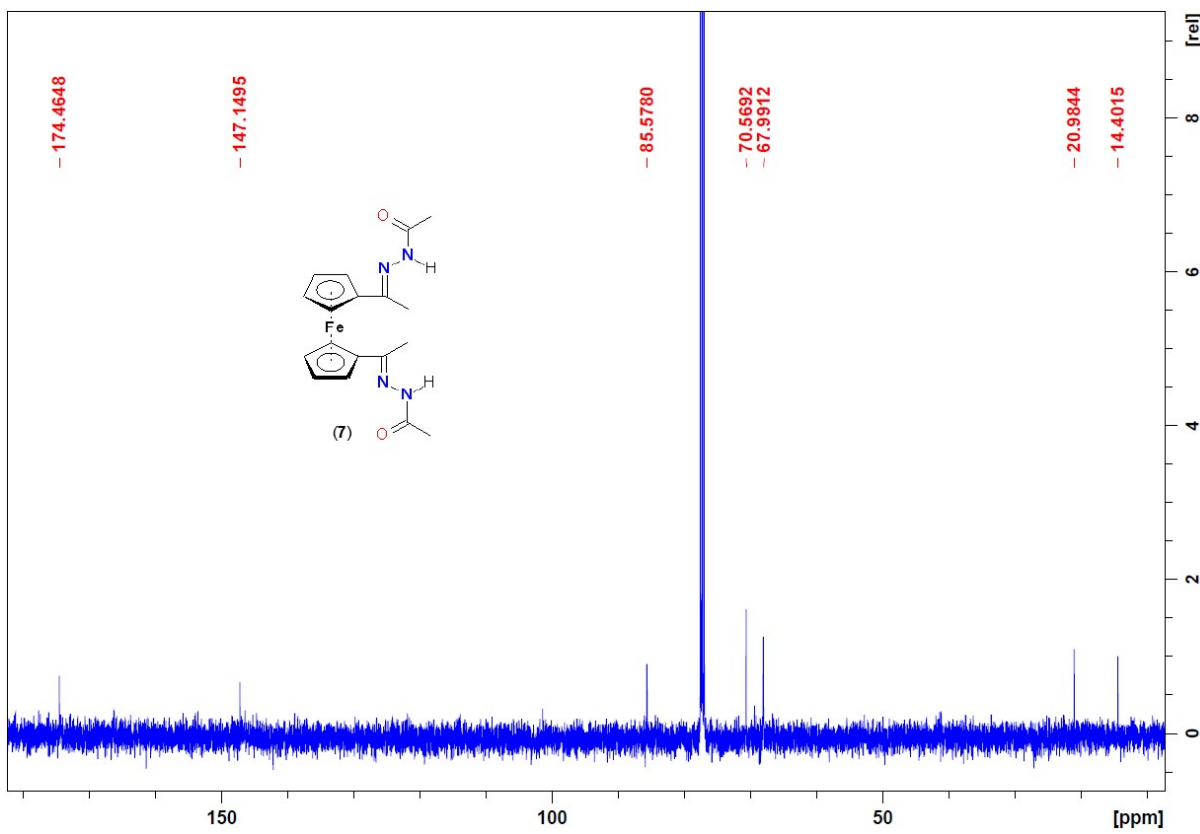


**Figure S37.**  $^{13}\text{C}\{^1\text{H}\}$  NMR spectrum of **7** (125.76 MHz,  $\text{CDCl}_3$ , 298 K).

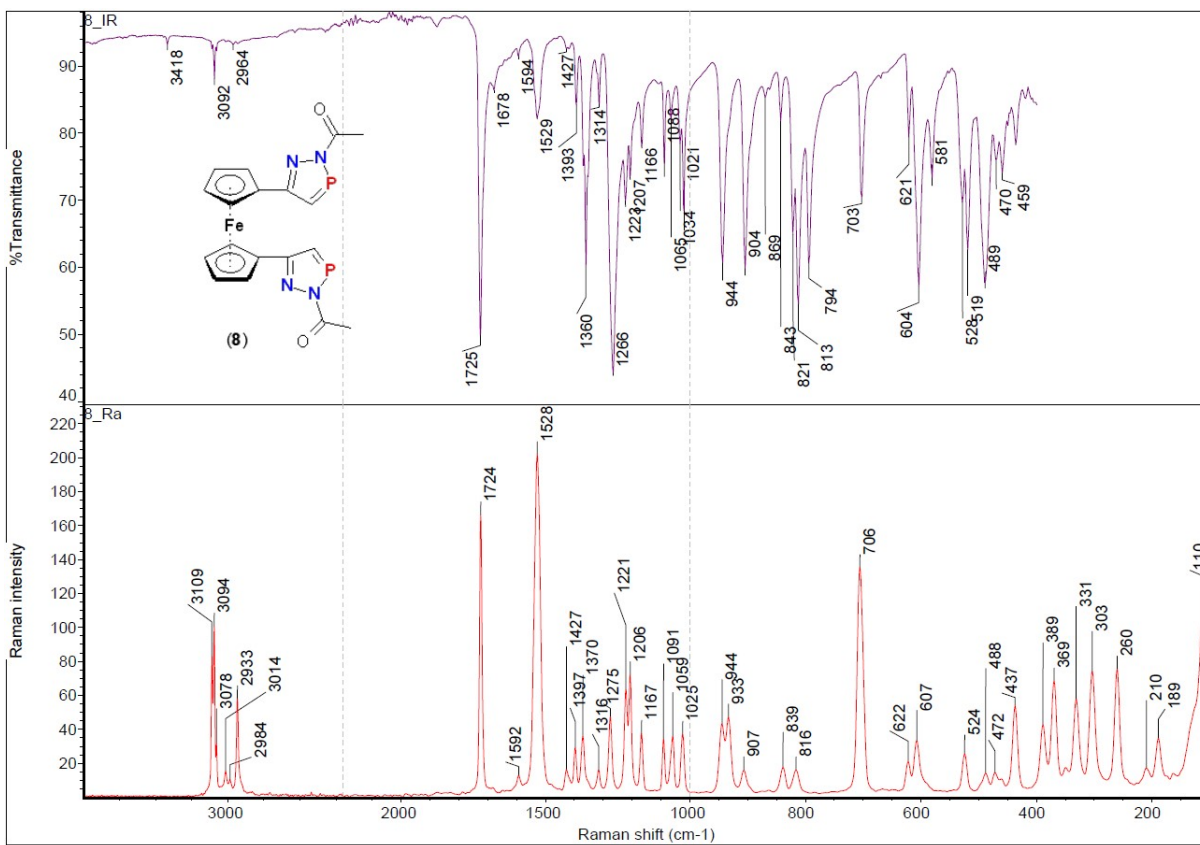


**Figure S38.** Infrared (top) and Raman (bottom) spectra of **8** measured in the solid state.

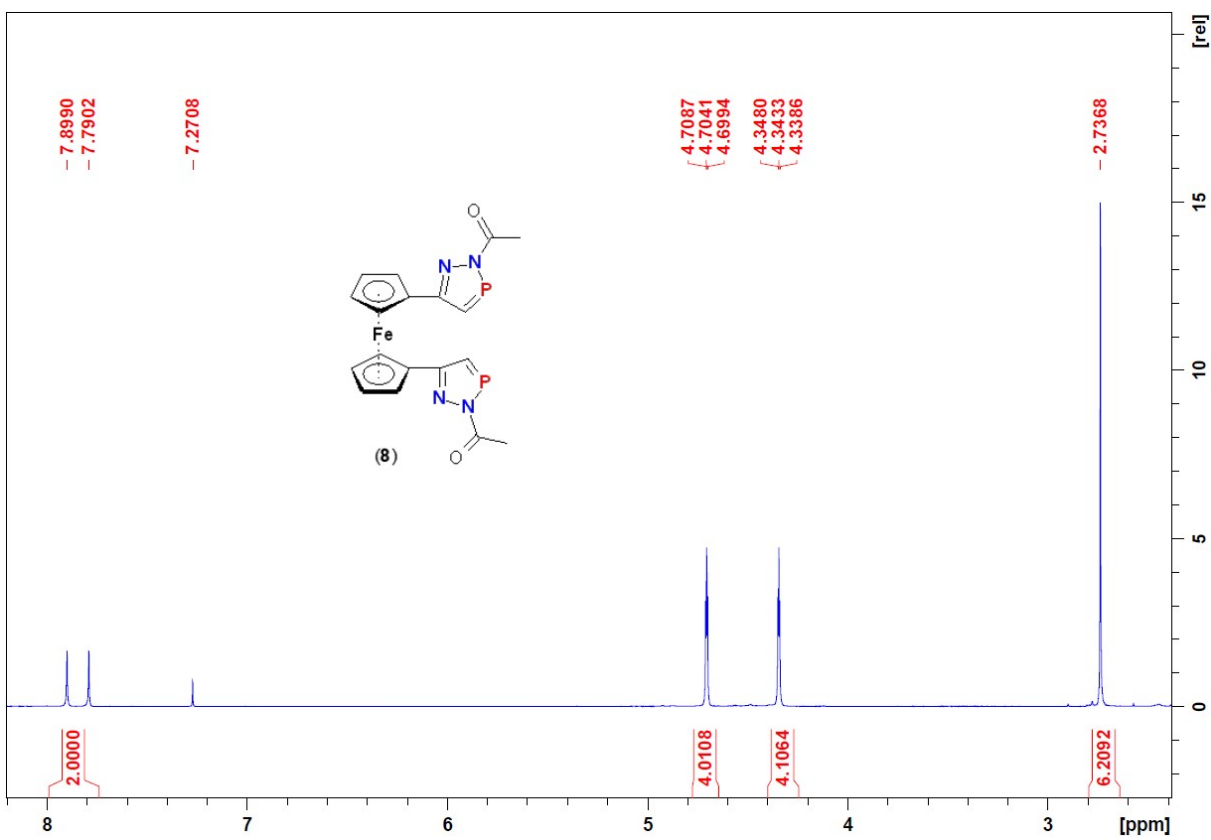


**Figure S39.**  $^1\text{H}$  NMR spectrum of **8** (400 MHz,  $\text{CDCl}_3$ , 298 K).

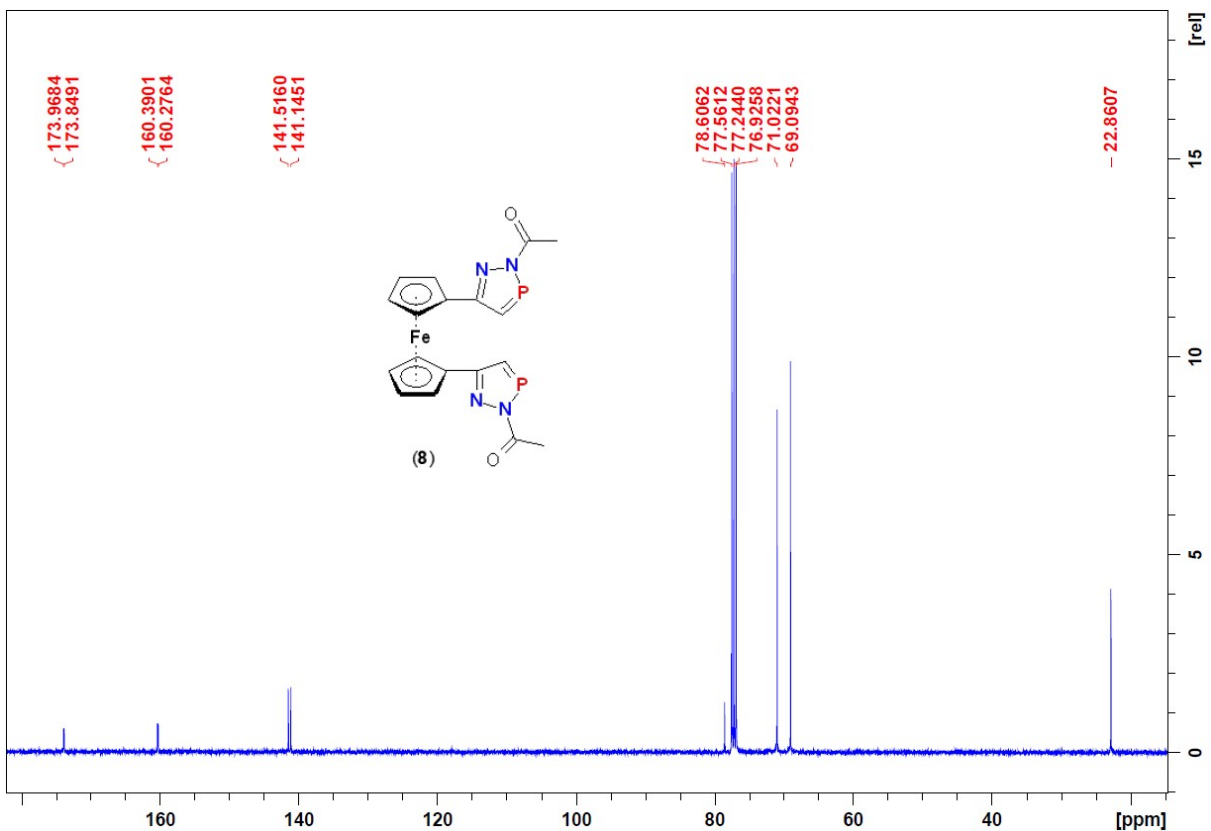


**Figure S40.**  $^{13}\text{C}\{^1\text{H}\}$  NMR spectrum of **8** (100.61 MHz,  $\text{CDCl}_3$ , 298 K).

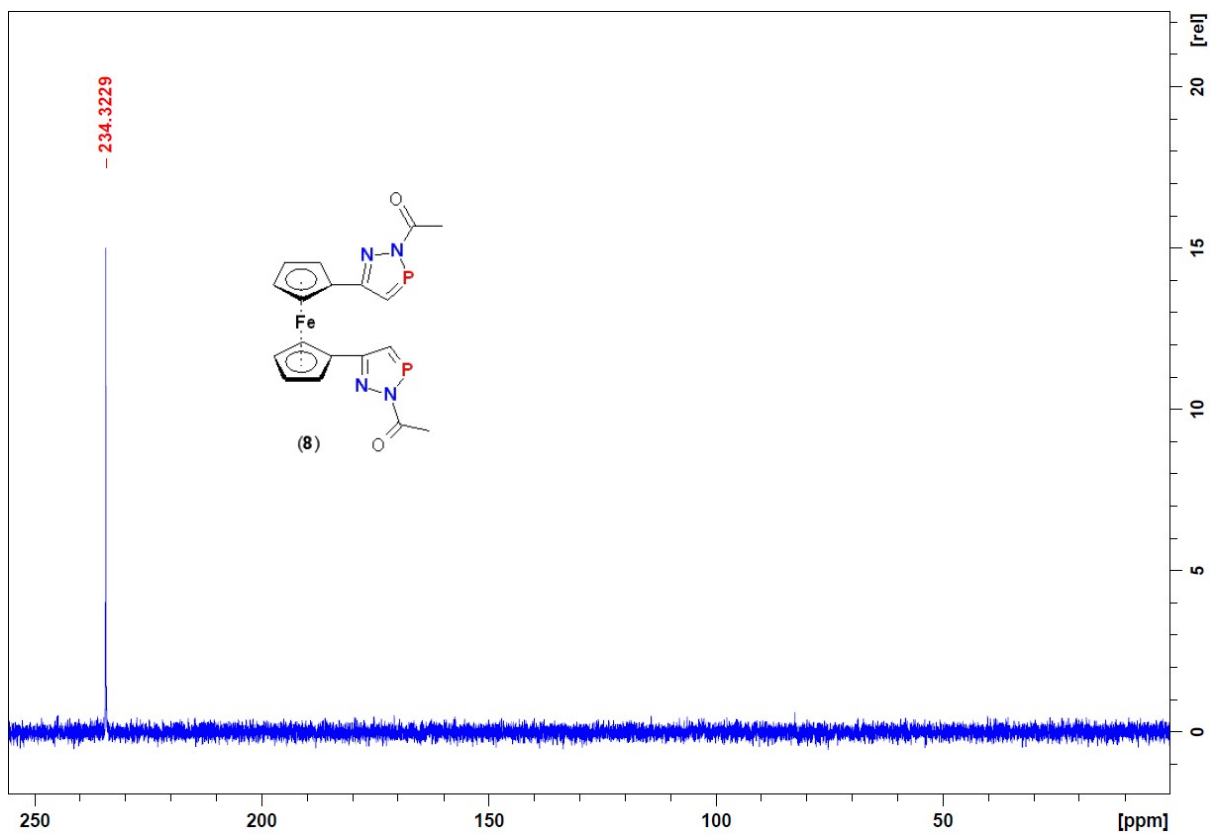


**Figure S41.**  $^1\text{H}$  NMR spectrum of **8** (161.98 MHz,  $\text{CDCl}_3$ , 298 K).

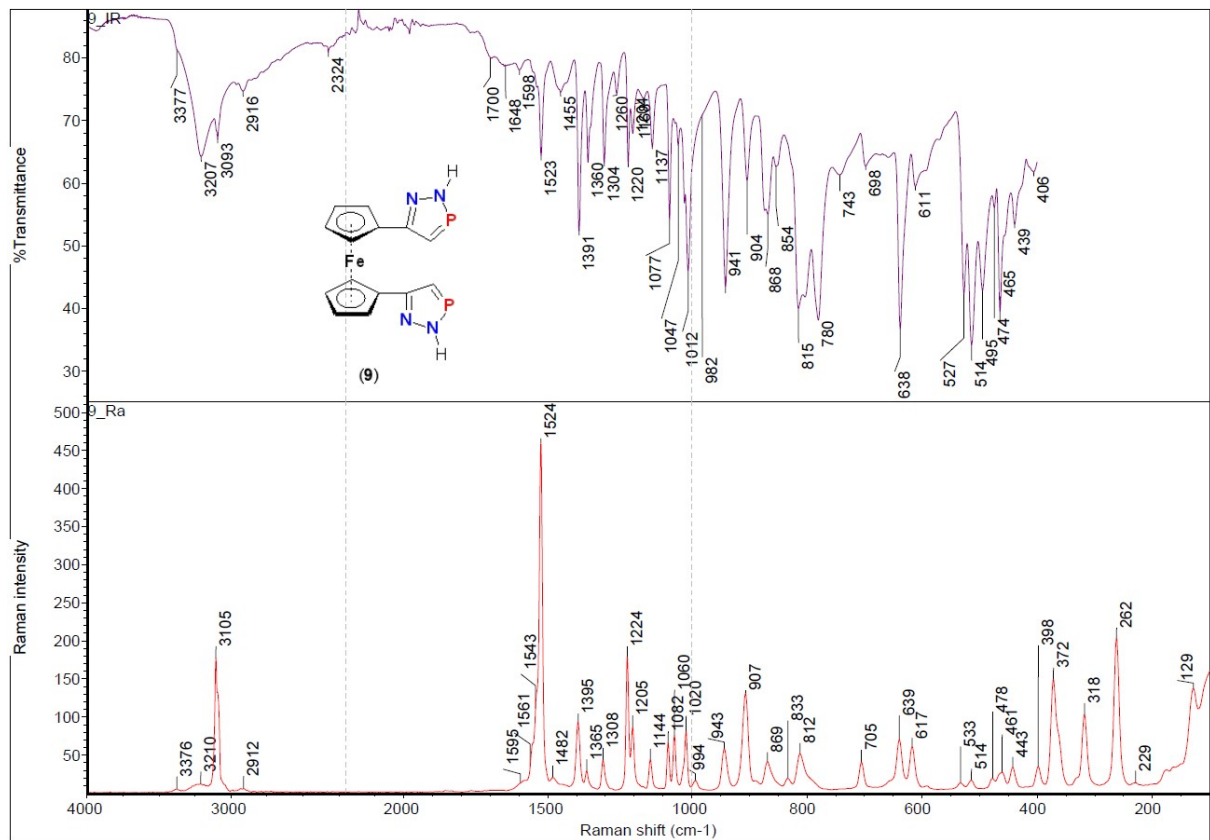


**Figure S42.** Infrared (top) and Raman (bottom) spectra of **9** measured in the solid state.

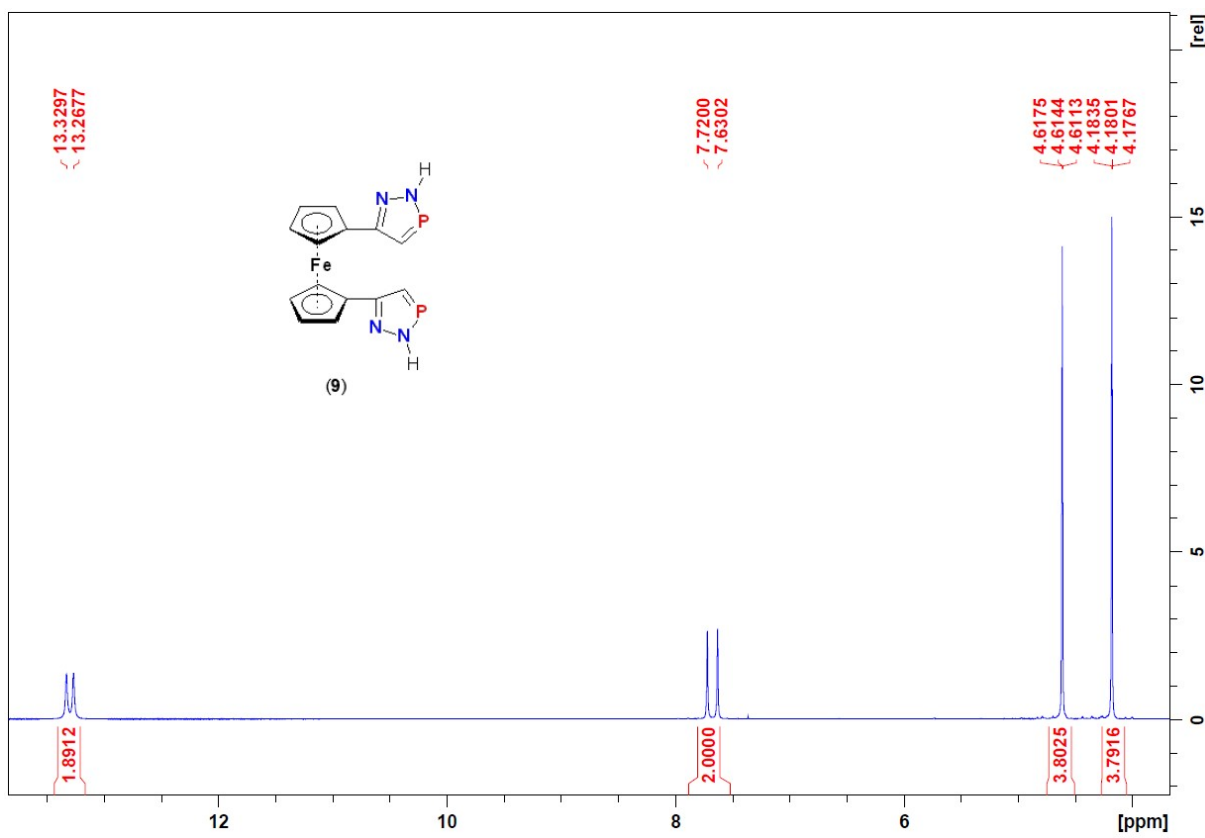


**Figure S43.**  $^1\text{H}$  NMR spectrum of **9** (500 MHz, dmso-d6, 298 K).

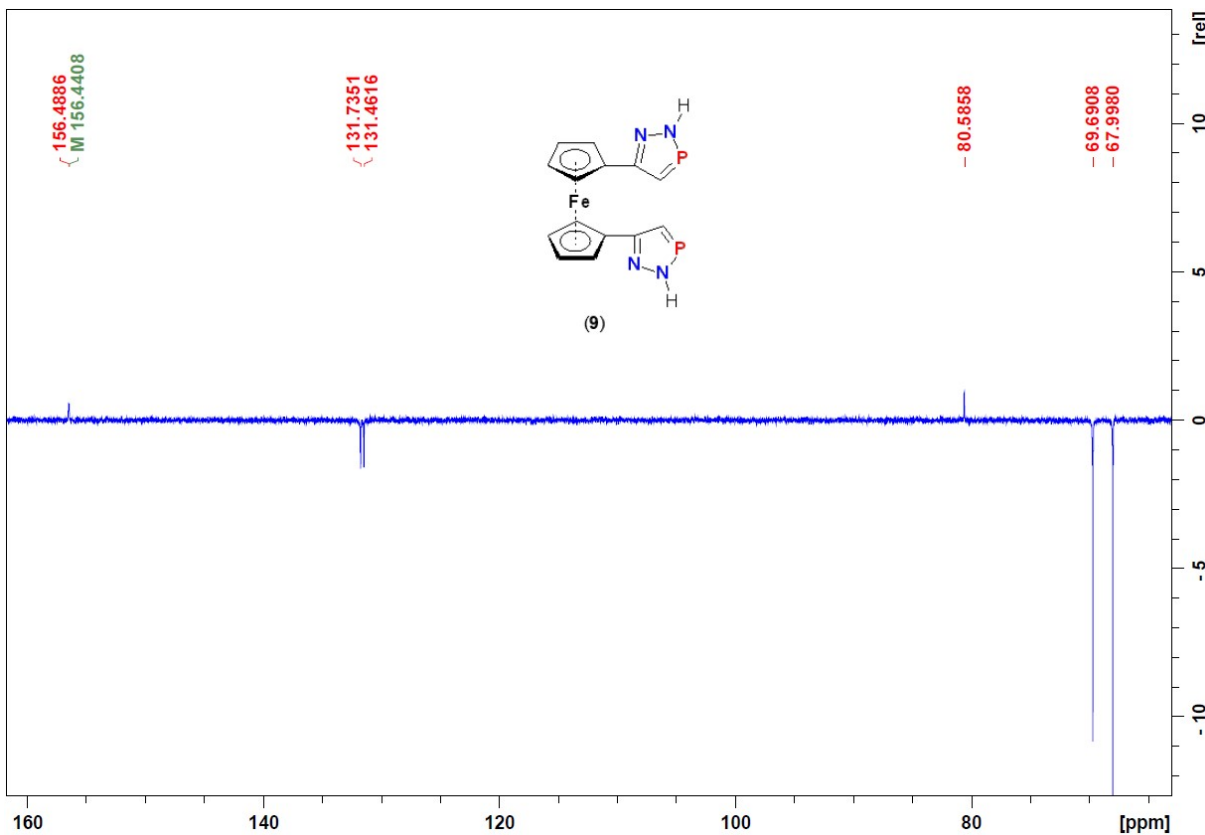


**Figure S44.**  $^{13}\text{C}\{^1\text{H}\}$  NMR APT spectrum of **9** (125.76 MHz, dmso-d6, 298 K).

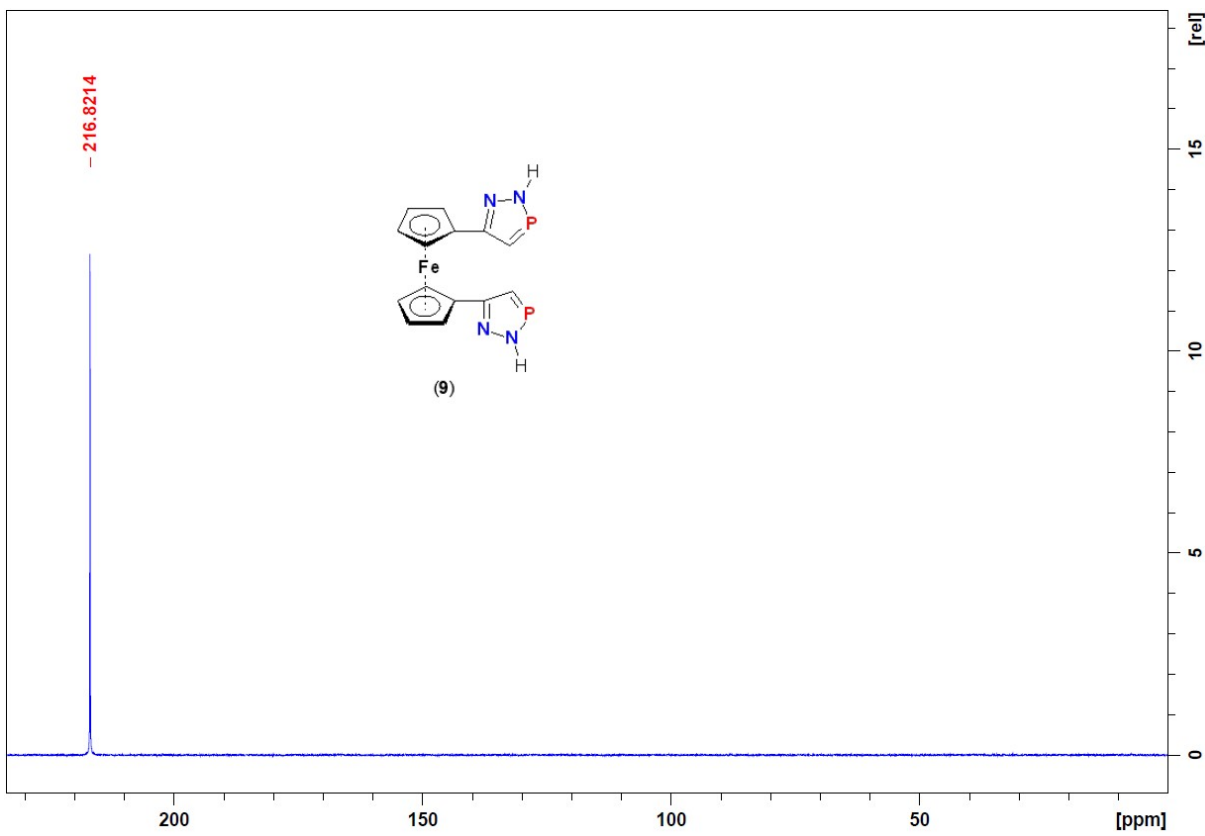


**Figure S45.**  $^{31}\text{P}\{^1\text{H}\}$  NMR spectrum of **9** (202.5 MHz, dmso-d6, 298 K).

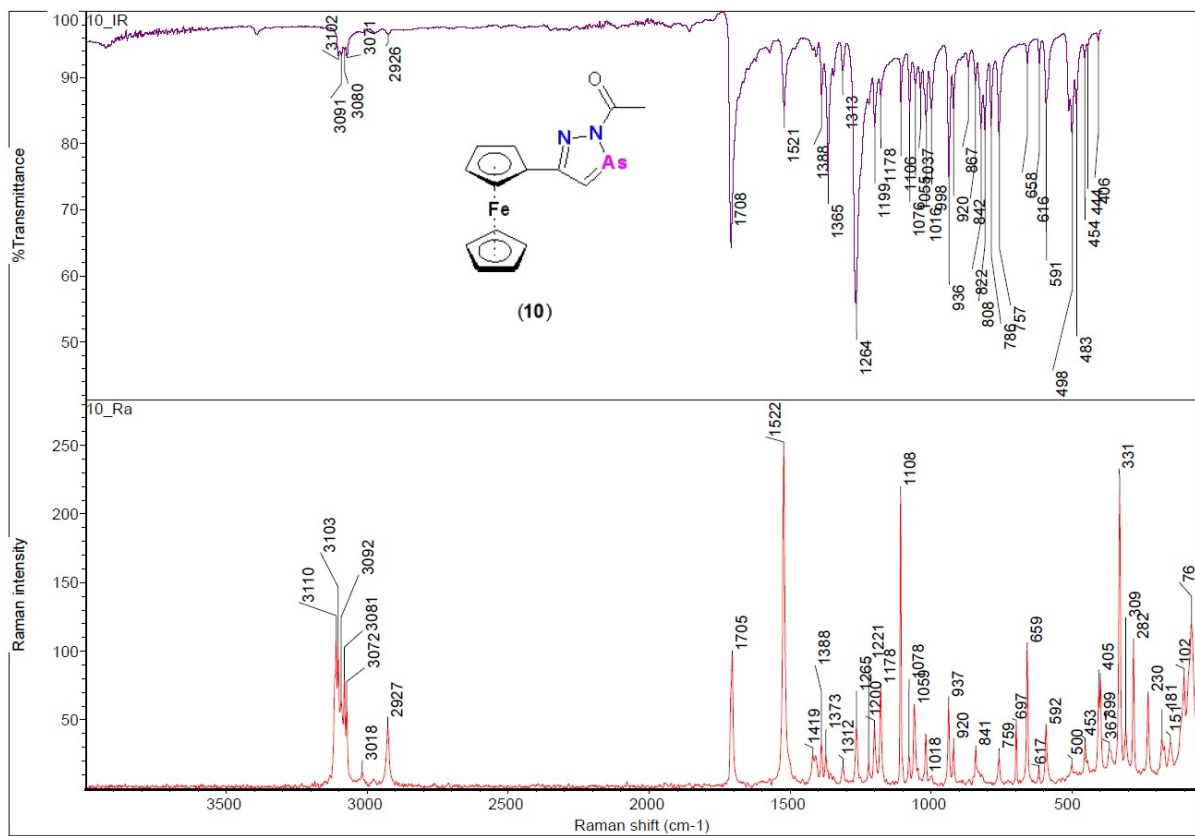


**Figure S46.** Infrared (top) and Raman (bottom) spectra of **10** measured in the solid state.

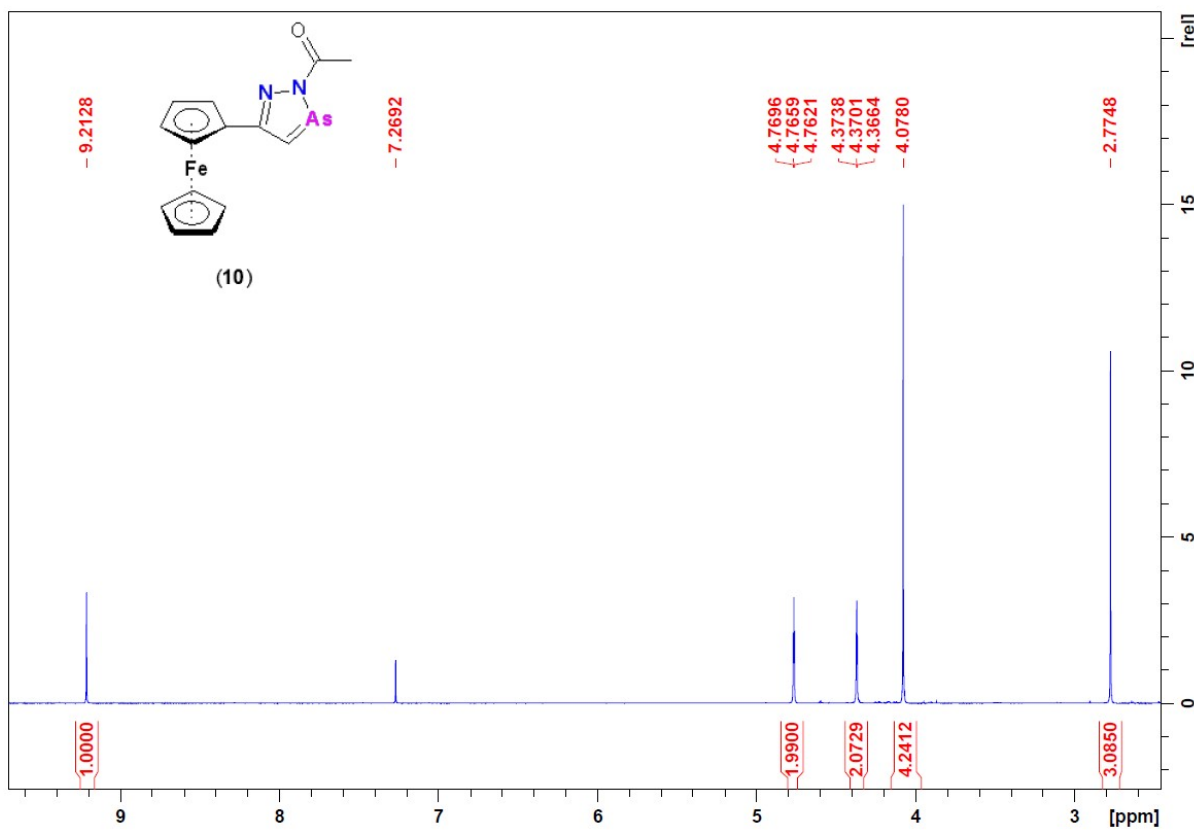


**Figure S47.**  $^1\text{H}$  NMR spectrum of **10** (500 MHz,  $\text{CDCl}_3$ , 298 K).

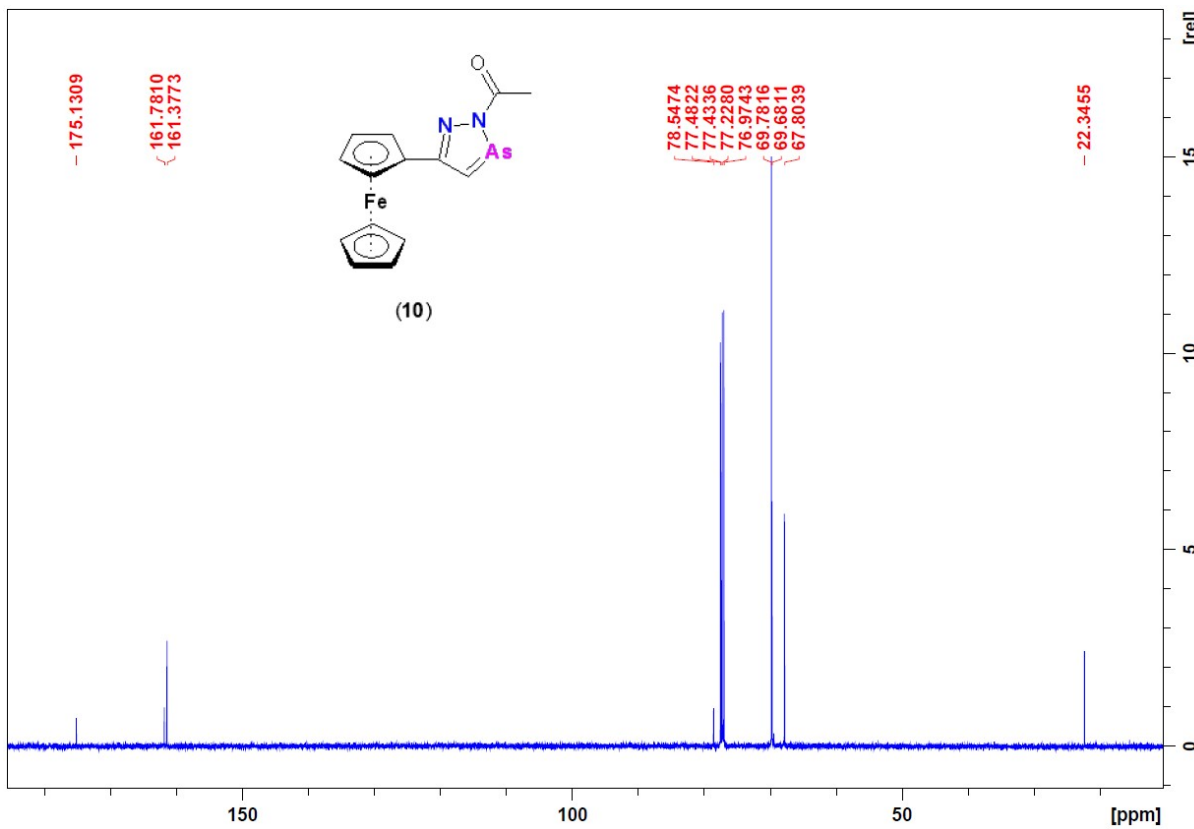


**Figure S48.**  $^{13}\text{C}\{^1\text{H}\}$  NMR spectrum of **10** (125.76 MHz,  $\text{CDCl}_3$ , 298 K).

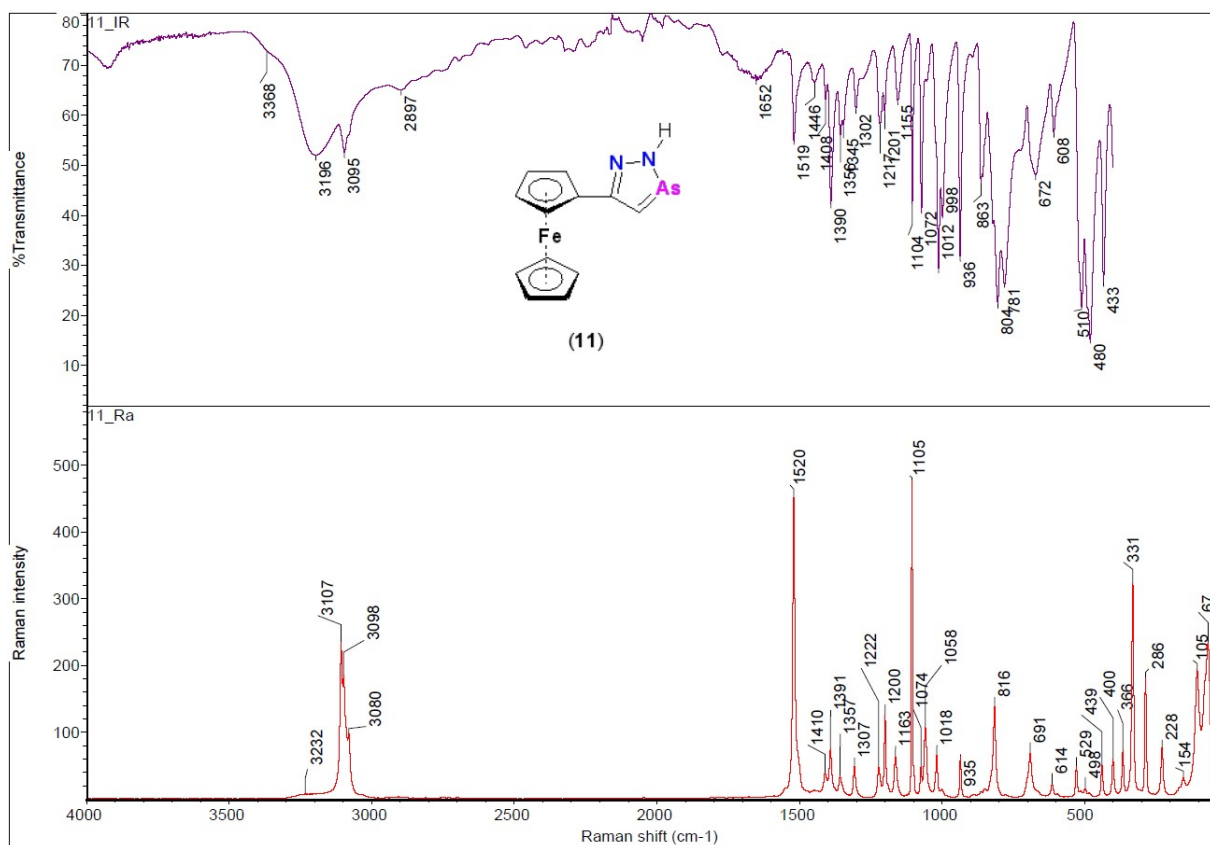


**Figure S49.** Infrared (top) and Raman (bottom) spectra of **11** measured in the solid state.

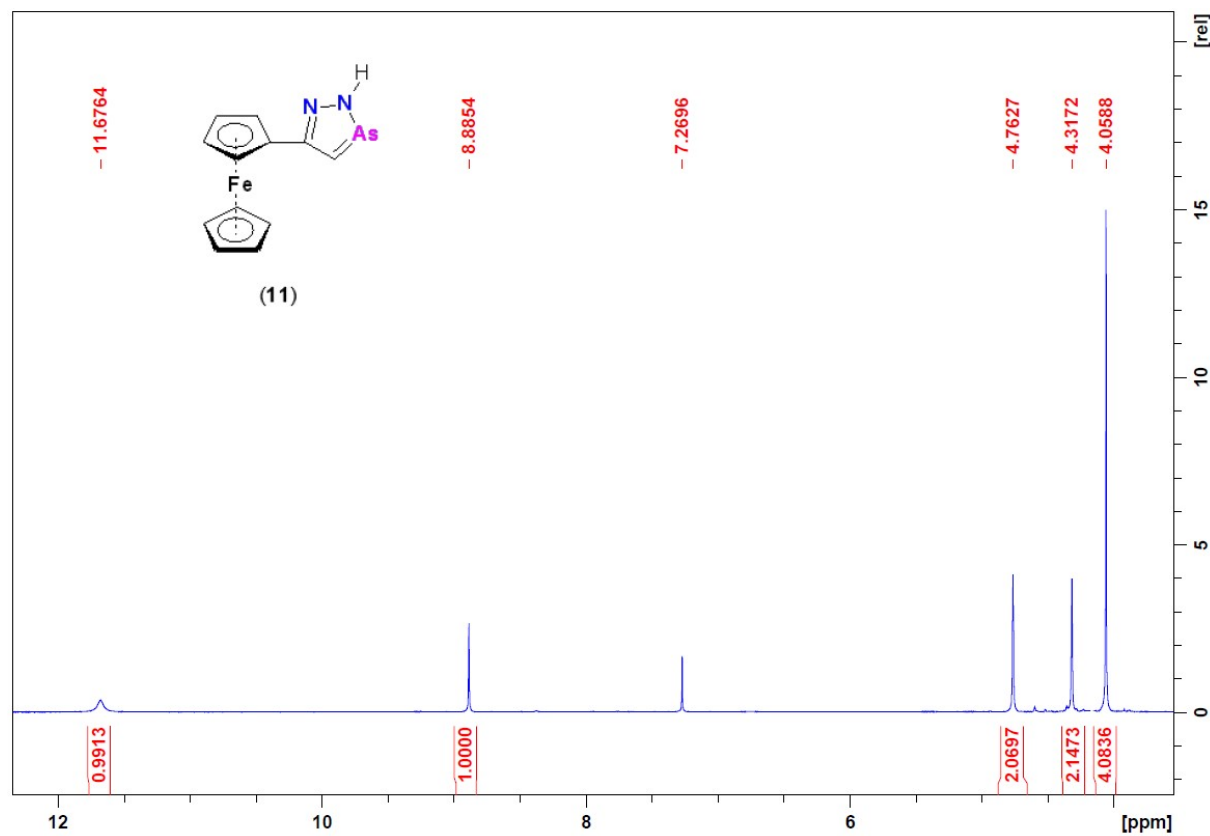


**Figure S50.** <sup>1</sup>H NMR spectrum of **11** (500 MHz, CDCl<sub>3</sub>, 298 K).

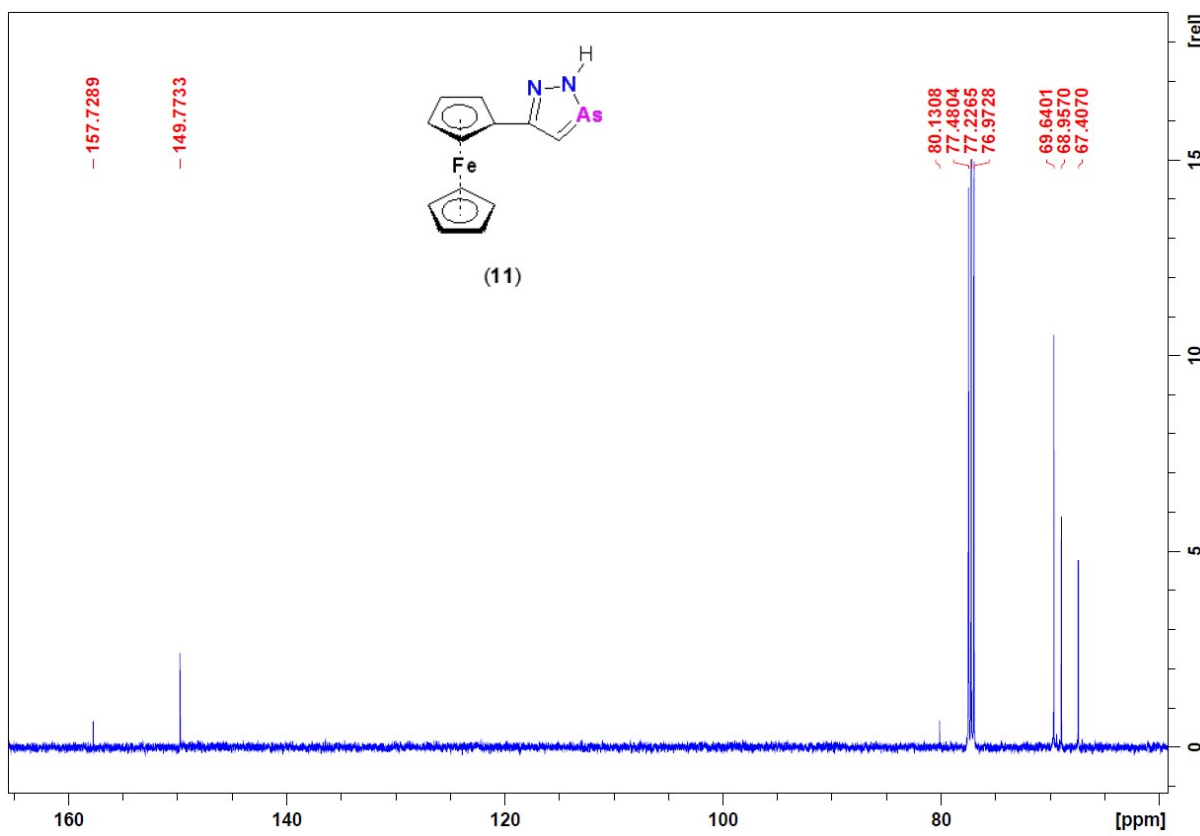


**Figure S51.**  $^{13}\text{C}\{^1\text{H}\}$  NMR spectrum of **11** (125.76 MHz,  $\text{CDCl}_3$ , 298 K).

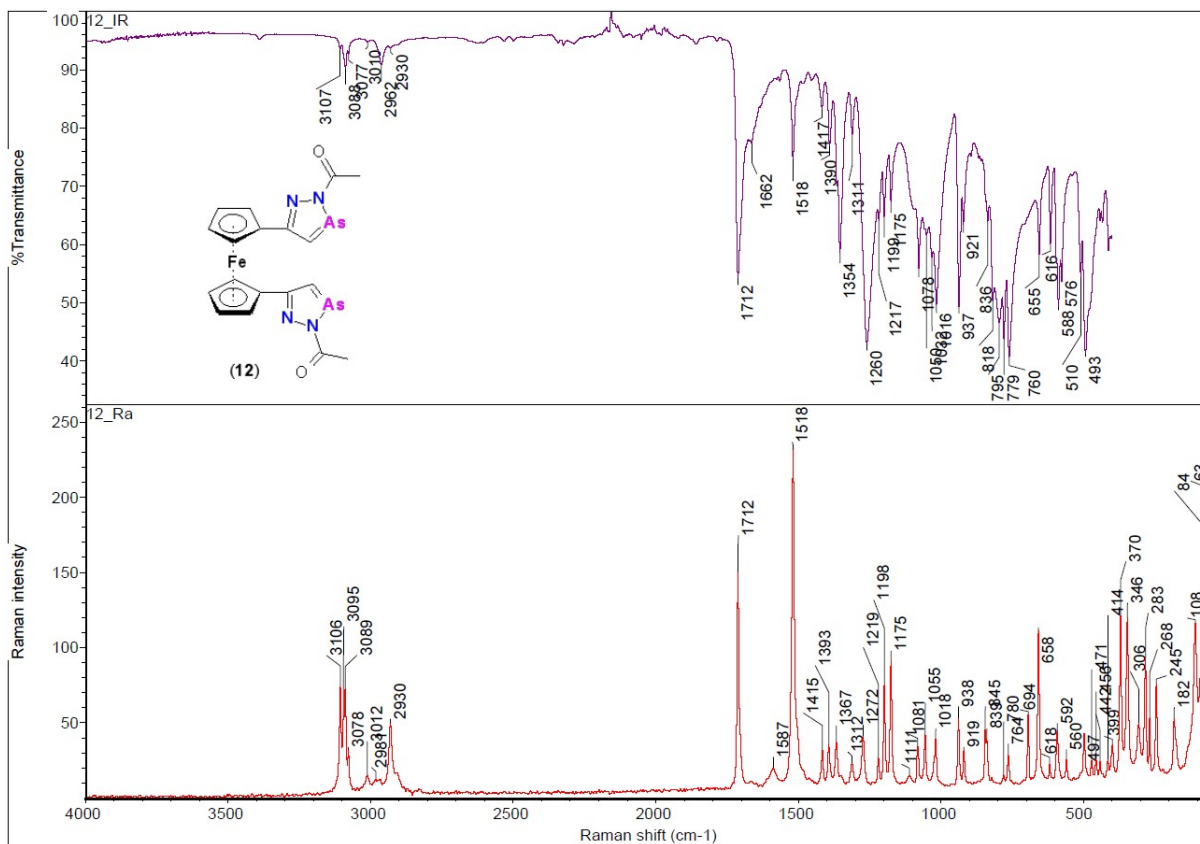


**Figure S52.** Infrared (top) and Raman (bottom) spectra of **12** measured in the solid state.

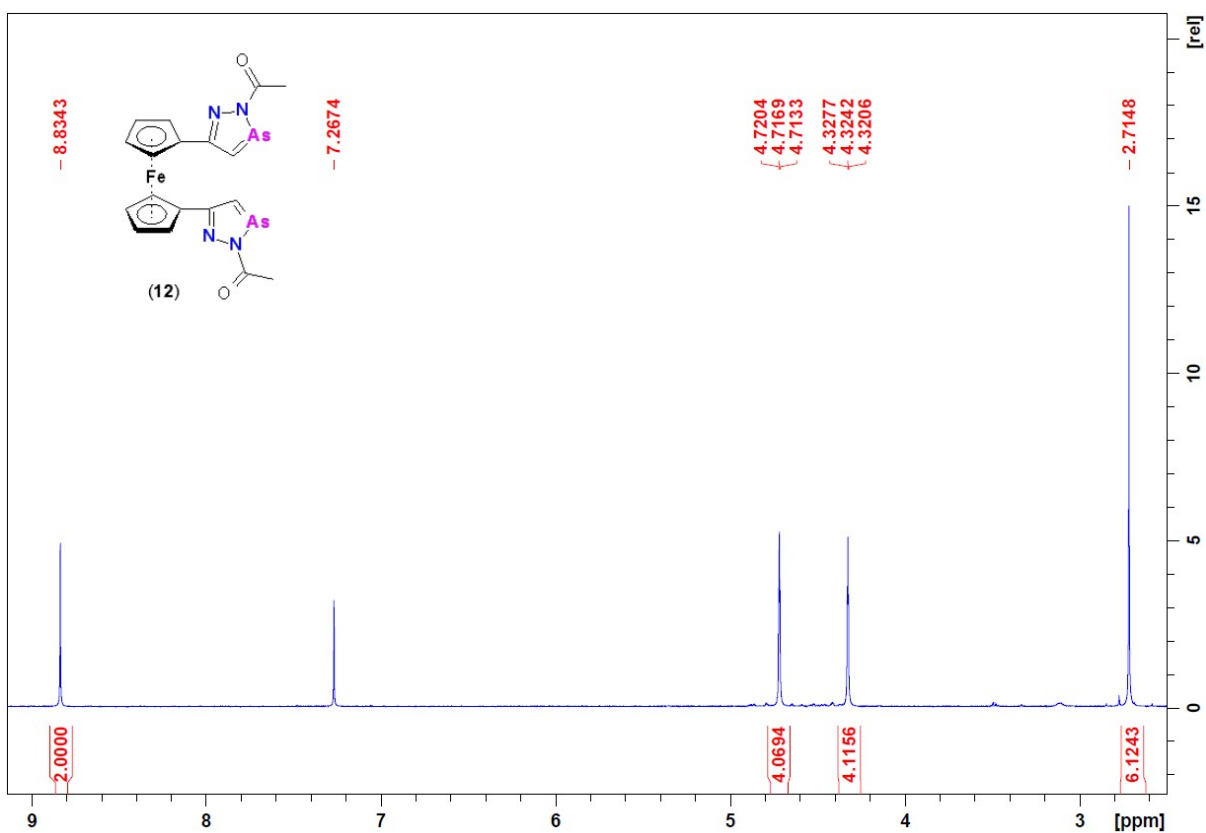


**Figure S53.**  $^1\text{H}$  NMR spectrum of **12** (500 MHz,  $\text{CDCl}_3$ , 298 K).

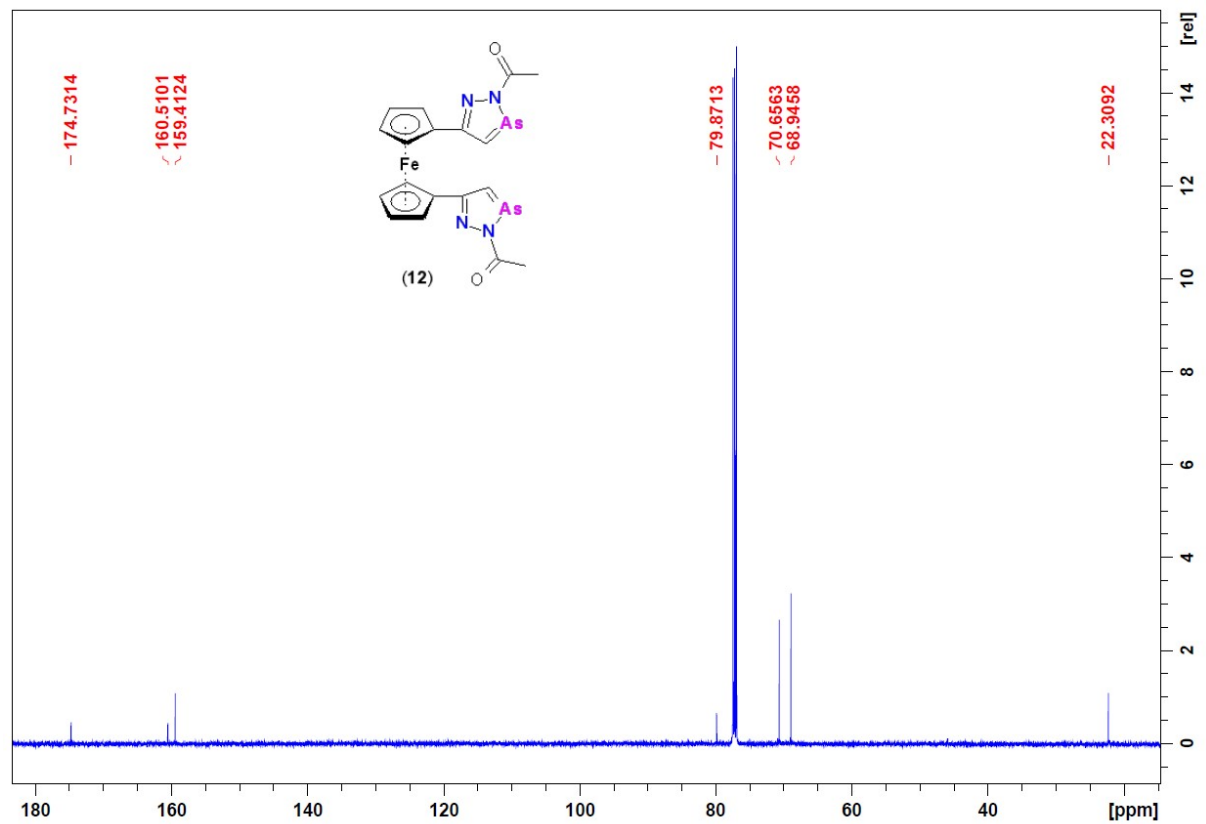


**Figure S54.**  $^{13}\text{C}\{^1\text{H}\}$  NMR spectrum of **12** (125.76 MHz,  $\text{CDCl}_3$ , 298 K).

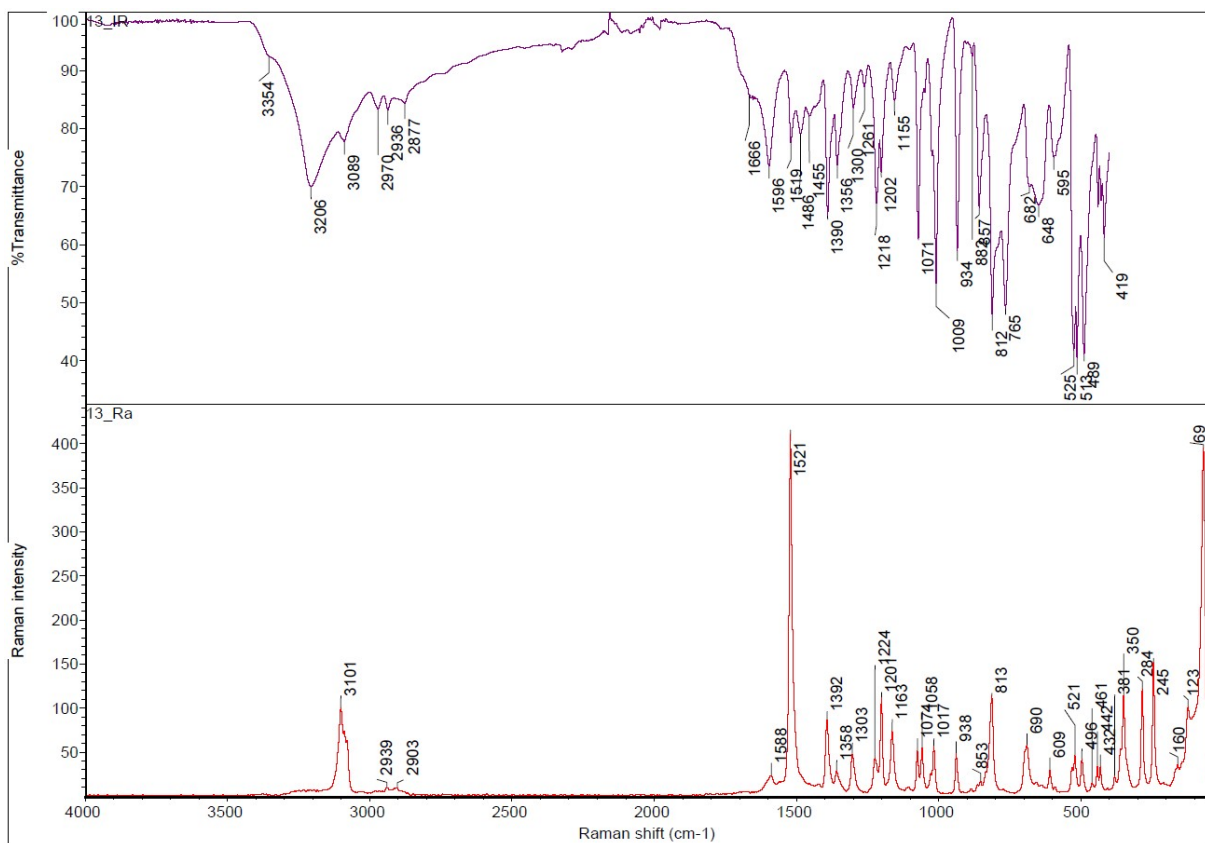


**Figure S55.** Infrared (top) and Raman (bottom) spectra of **13** measured in the solid state.

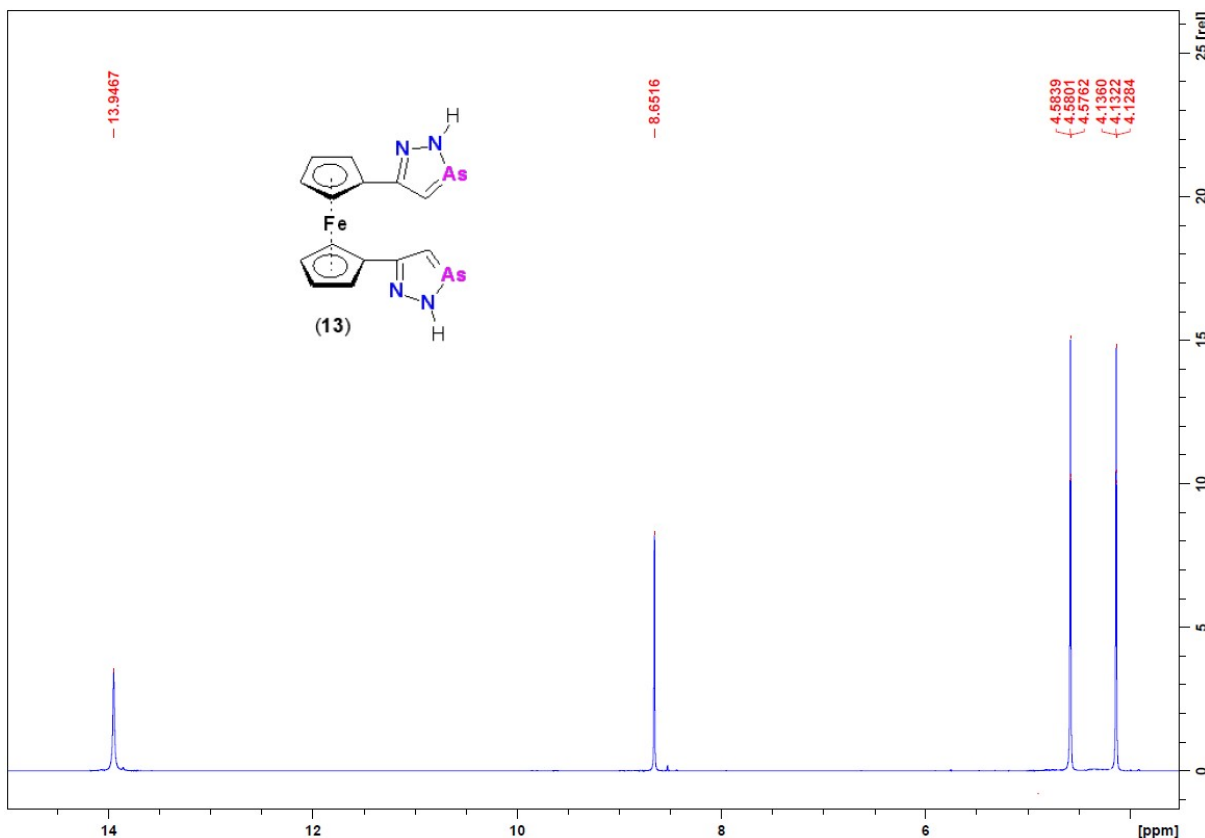


**Figure S56.** <sup>1</sup>H NMR spectrum of **13** (500 MHz, dmso-d<sub>6</sub>, 298 K).

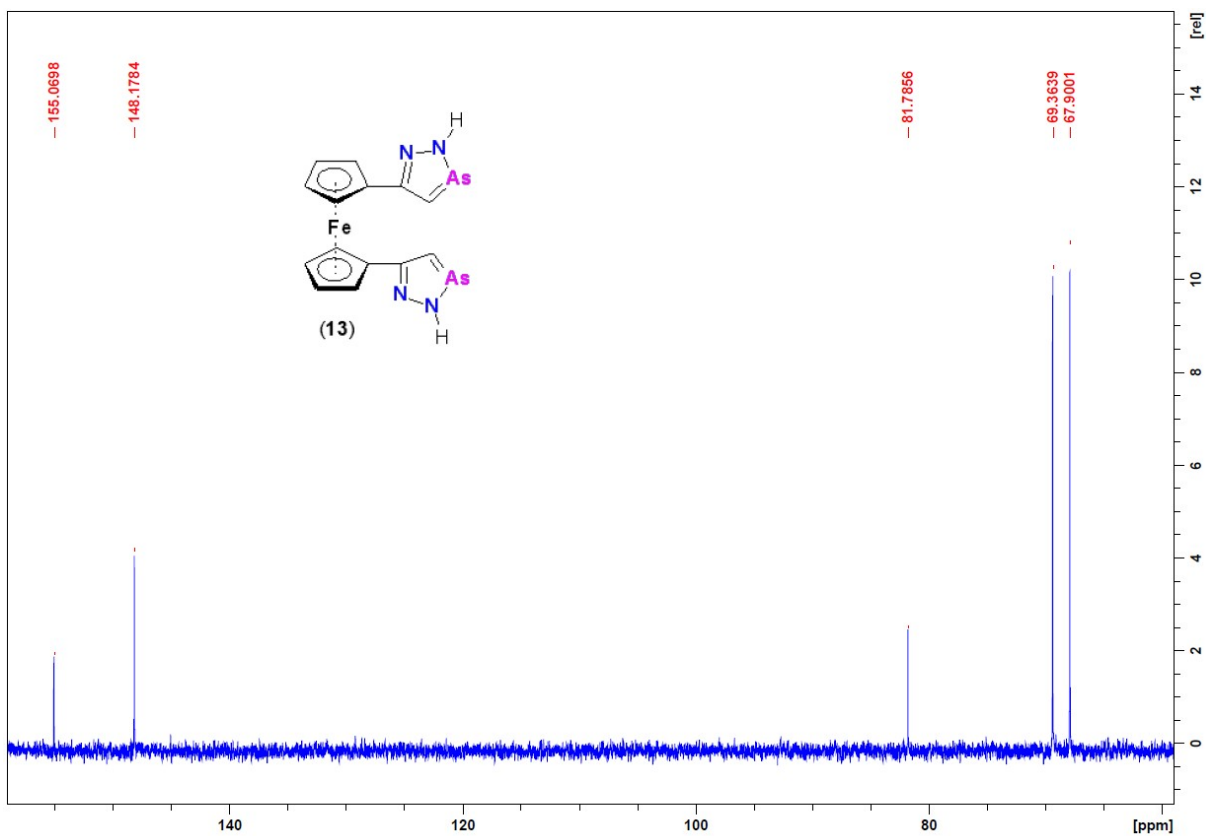


**Figure S57.**  $^{13}\text{C}\{^1\text{H}\}$  NMR spectrum of **13** (125.76 MHz, dmso-d6, 298 K).

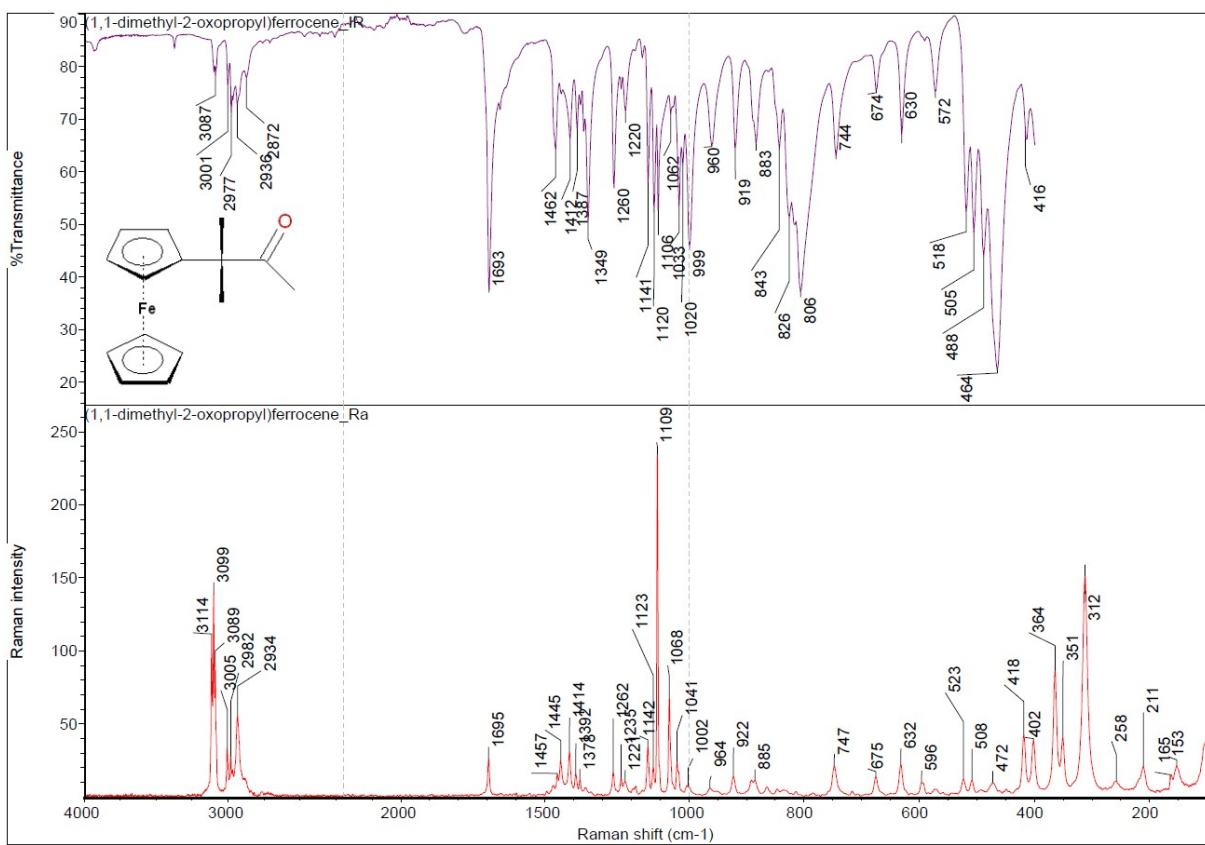


**Figure S58.** Infrared (top) and Raman (bottom) spectra of (1,1-dimethyl-2-oxopropyl)ferrocene.

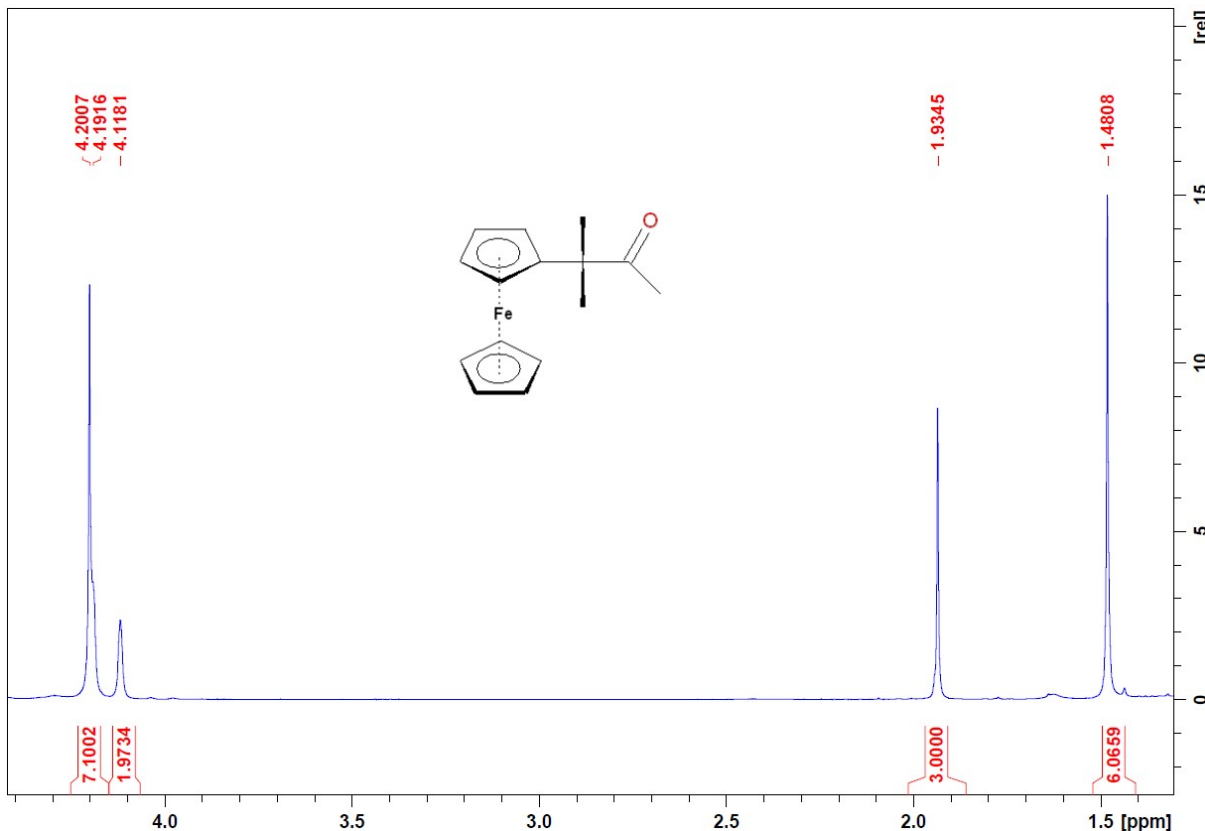


**Figure S59.** <sup>1</sup>H NMR spectrum of (1,1-dimethyl-2-oxopropyl)ferrocene (500 MHz, CDCl<sub>3</sub>, 298 K).

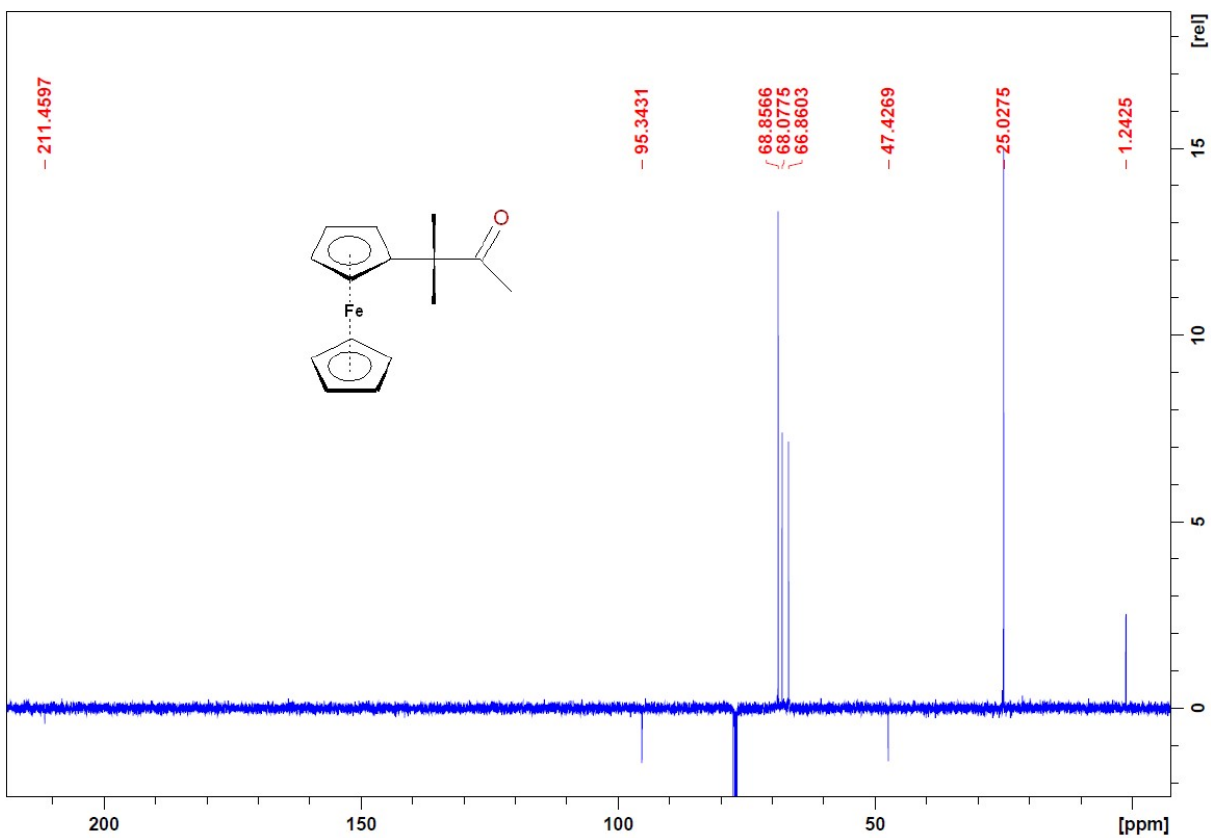


**Figure S60.**  $^{13}\text{C}\{^1\text{H}\}$  APT NMR spectrum of (1,1-dimethyl-2-oxopropyl)ferrocene (125.76 MHz,  $\text{CDCl}_3$ , 298 K).

## Crystallographic and refinement data for studied compounds

**Table S1.** Crystal data, data collection and processing parameters for **1a**, **2a**, **2b**, **2c**, **3c**, **4a-1** and **4a-2**.

Compound	<b>1a</b>	<b>2a</b>	<b>2b</b>	<b>2c</b>	<b>3c</b>	<b>4a-1</b>	<b>4a-2</b>
Empirical formula	C <sub>12</sub> H <sub>14</sub> FeN <sub>2</sub>	C <sub>12</sub> H <sub>11</sub> FeN <sub>2</sub> P	C <sub>18</sub> H <sub>15</sub> FeN <sub>2</sub> P	C <sub>15</sub> H <sub>17</sub> FeN <sub>2</sub> P	C <sub>30</sub> H <sub>36</sub> Fe <sub>2</sub> N <sub>2</sub>	C <sub>14</sub> H <sub>16</sub> FeN <sub>2</sub> O	C <sub>14</sub> H <sub>16</sub> FeN <sub>2</sub> O
<i>a</i> (Å)	28.021 (2)	41.9024 (10)	19.1416 (10)	7.3267 (5)	7.5627 (10)	16.3414 (11)	9.7872 (5)
<i>b</i> (Å)	7.3169 (5)	10.1534 (3)	9.7740 (6)	10.2286 (7)	10.1352 (14)	7.8369 (5)	12.8584 (5)
<i>c</i> (Å)	10.7673 (8)	21.7438 (5)	8.2857 (5)	18.5961 (11)	16.263 (2)	19.833 (1)	20.2069 (9)
<i>α</i> (°)	90	90	90	90	90	90	90
<i>β</i> (°)	101.809 (2)	104.147 (1)	94.672 (2)	90.660 (2)	98.888 (5)	90	90
<i>γ</i> (°)	90	90	90	90	90	90	90
<i>Z</i>	8	32	4	4	2	8	8
M <sub>r</sub>	242.10	270.05	346.14	312.12	536.31	284.14	284.14
Space group	<i>C</i> 2	<i>C</i> 2/ <i>c</i>	<i>P</i> 2 <sub>1</sub> / <i>c</i>	<i>P</i> 2 <sub>1</sub> / <i>n</i>	<i>P</i> 2 <sub>1</sub> / <i>c</i>	<i>P</i> <i>b</i> <i>c</i> <i>a</i>	<i>P</i> 2 <sub>1</sub> 2 <sub>1</sub> 2 <sub>1</sub>
<i>V</i> (Å <sup>3</sup> )	2160.9 (3)	8970.4 (4)	1545.0 (2)	1393.5 (2)	1231.6 (3)	2539.9 (3)	2543.0 (2)
<i>D<sub>x</sub></i> /g.cm <sup>-3</sup>	1.488	1.600	1.488	1.488	1.446	1.486	1.484
<i>μ</i> (mm <sup>-1</sup> )	1.36	1.46	1.08	1.18	1.20	1.18	1.17
Reflections measured	32050	94553	35672	31521	29953	20629	24400
- independent ( <i>R</i> <sub>int</sub> ) <sup>a)</sup>	4817 (0.042)	9768 (0.064)	3555 (0.083)	3219 (0.108)	2937 (0.128)	2766 (0.142)	5560 (0.081)
- observed [ <i>I</i> >2σ( <i>I</i> )]	4458	7977	2922	2451	2560	1879	4644
Parameters refined	286	581	203	178	158	165	332
Max/min Δ <i>ρ</i> /e.Å <sup>-3</sup>	2.37 / -1.57	0.33 / -0.42	0.90 / -0.38	0.31 / -0.44	2.00 / -0.57	0.39 / -0.42	0.32 / -0.34
GOF <sup>b)</sup>	1.18	1.02	1.16	1.02	1.10	0.99	0.98
<i>R</i> <sup>c)</sup> / <i>wR</i> <sup>c)</sup>	0.053 / 0.137	0.033 / 0.065	0.045 / 0.106	0.037 / 0.073	0.084 / 0.245	0.047 / 0.097	0.039 / 0.067

<sup>a)</sup>  $R_{\text{int}} = \sum |F_o^2 - F_{o,\text{mean}}^2| / \sum F_o^2$ .

<sup>b)</sup> GOF = [Σ(w(F<sub>o</sub><sup>2</sup> - F<sub>c</sub><sup>2</sup>)<sup>2</sup>)/(N<sub>diffs</sub> - N<sub>params</sub>)]<sup>1/2</sup> for all data.

<sup>c)</sup>  $R(F) = \sum |F_o| - |F_c| / \sum |F_o|$  for observed data;  $wR(F^2) = [\sum(w(F_o^2 - F_c^2)^2) / (\sum w(F_o^2)^2)]^{1/2}$  for all data.

**Table S1** (continue). Crystal data and structure refinement of **4a** (two polymorphs), **5a**, **8**, **9** and **10**.

Compound	<b>5a</b>	<b>8</b>	<b>9</b>	<b>10</b>
Empirical formula	C <sub>14</sub> H <sub>13</sub> FeN <sub>2</sub> OP	C <sub>18</sub> H <sub>16</sub> FeN <sub>4</sub> O <sub>2</sub> P <sub>2</sub>	C <sub>14</sub> H <sub>12</sub> FeN <sub>4</sub> P <sub>2</sub>	C <sub>14</sub> H <sub>13</sub> AsFeN <sub>2</sub> O
<i>a</i> (Å)	11.6640 (8)	8.8683 (7)	9.7557 (4)	11.5955 (13)
<i>b</i> (Å)	7.3497 (5)	9.7413 (7)	12.9751 (5)	7.3503 (8)
<i>c</i> (Å)	15.3627 (10)	21.2822 (12)	13.2097 (6)	15.4894 (15)
<i>α</i> (°)	90	90	65.892 (2)	90
<i>β</i> (°)	91.718 (2)	90	70.324 (2)	92.284 (4)
<i>γ</i> (°)	90	90	72.391 (2)	90
<i>Z</i>	4	4	4	4
M <sub>r</sub>	312.08	438.14	354.07	356.03
Space group	<i>P</i> 2 <sub>1</sub> / <i>n</i>	<i>P</i> ccn	<i>P</i> 1̄	<i>P</i> 2 <sub>1</sub> / <i>n</i>
<i>V</i> (Å <sup>3</sup> )	1316.4 (2)	1838.5 (2)	1410.4 (1)	1319.1 (2)
<i>D<sub>x</sub></i> /g.cm <sup>-3</sup>	1.575	1.583	1.667	1.793
<i>μ</i> (mm <sup>-1</sup> )	1.26	1.02	1.29	3.624
Reflections measured	27273	14825	43018	25512
- independent ( <i>R</i> <sub>int</sub> ) <sup>a)</sup>	3028 (0.041)	2118 (0.076)	6159 (0.055)	3058 (0.075)
- observed [ <i>I</i> >2 <i>σ</i> ( <i>I</i> )]	2763	1621	5149	2535
Parameters refined	210	124	395	173
Max/min Δ <i>ρ</i> /e.Å <sup>-3</sup>	0.46 / -0.41	0.40 / -0.35	0.34 / -0.33	0.69 / -0.62
GOF <sup>b)</sup>	1.19	1.08	1.04	1.10
<i>R</i> <sup>c)</sup> / <i>wR</i> <sup>c)</sup>	0.027 / 0.077	0.037 / 0.081	0.029 / 0.064	0.046 / 0.089

<sup>a)</sup>  $R_{\text{int}} = \sum |F_o^2 - F_{o,\text{mean}}^2| / \sum F_o^2$ .

<sup>b)</sup> GOF = [Σ(*w*(*F<sub>o</sub>*<sup>2</sup> - *F<sub>c</sub>*<sup>2</sup>)<sup>2</sup>)/(*N<sub>diffs</sub>* - *N<sub>params</sub>*)]<sup>1/2</sup> for all data.

<sup>c)</sup>  $R(F) = \sum | |F_o| - |F_c| | / \sum |F_o|$  for observed data;  $wR(F^2) = [ \sum (w(F_o^2 - F_c^2)^2) / (\sum w(F_o^2)^2) ]^{1/2}$  for all data.

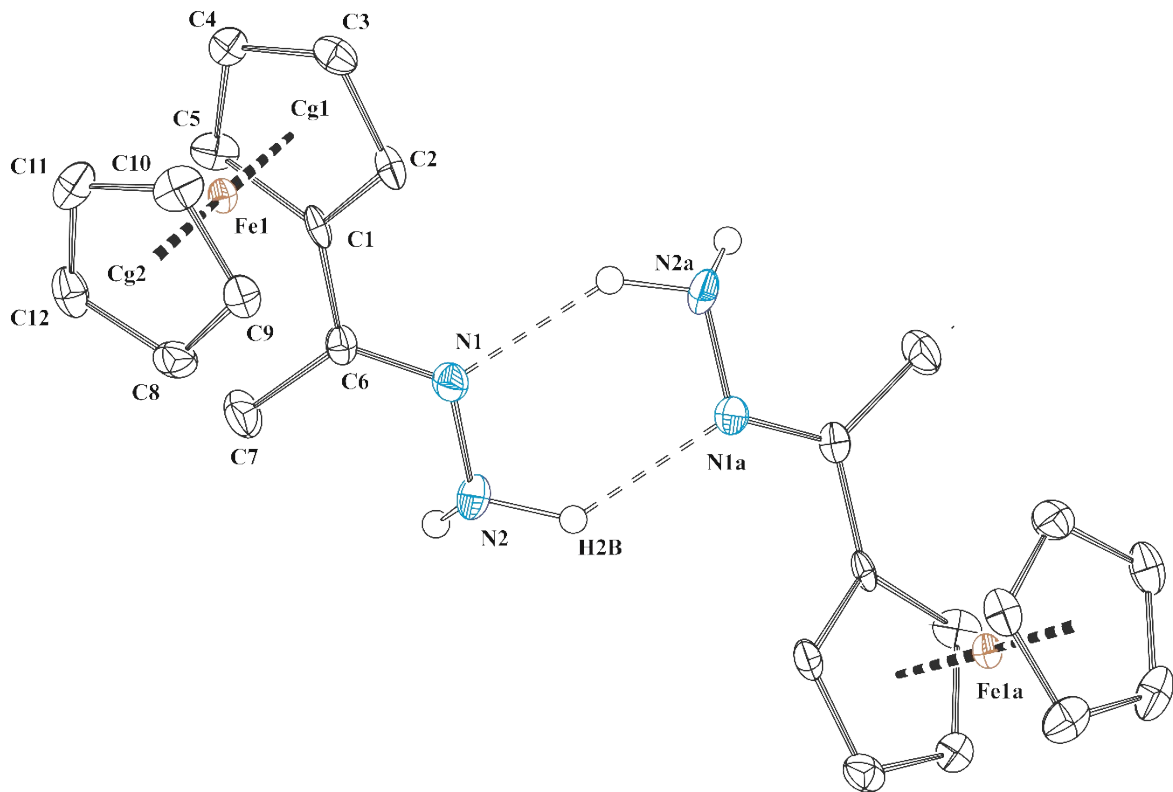


**Figure S61.** The ORTEP plot of **1a** at 30% probability showing its molecular structure and hydrogen-bonding scheme. Hydrogen atoms bonded to carbons are omitted for clarity. Selected bonds ( $\text{\AA}$ ) and angles ( $^\circ$ ): Fe1–Cg1 1.644(4), Fe1–Cg2 1.653(4), C1–C6 1.474(12), C6–N1 1.291(10), N1–N2 1.422(10), C1–C6–N1 114.9(7), C6–N1–N2 115.6(7). Hydrogen-bond geometry ( $\text{\AA}$ ,  $^\circ$ ): N2…N1a 3.028(10), N2–H2B…N1a 134. Symmetry code: (a)  $1 - x, y, -z$ .

In the crystal structure of **1a** two crystallographically independent molecules are present each being connected *via* two hydrogen-bonds toward adjacent molecule. The structure of one of them is depicted in Figure S61, together with neighboring molecule showing hydrogen-bonding interactions; crystallographic data are listed in Table S1. Cyclopentadienyl rings in **1a** are almost eclipsed with dihedral angle C1–Cg1…Cg2–C8 of  $3.6(6)^\circ$ , hydrazone function plane defined by atoms C6, C7, N1 and N2 makes an angle of  $17.6(6)^\circ$  with cyclopentadienyl ring plane C1 – C5. Interatomic distances and angles of **1a** are comparable to known monosubstituted ferrocene compounds.<sup>S1</sup>

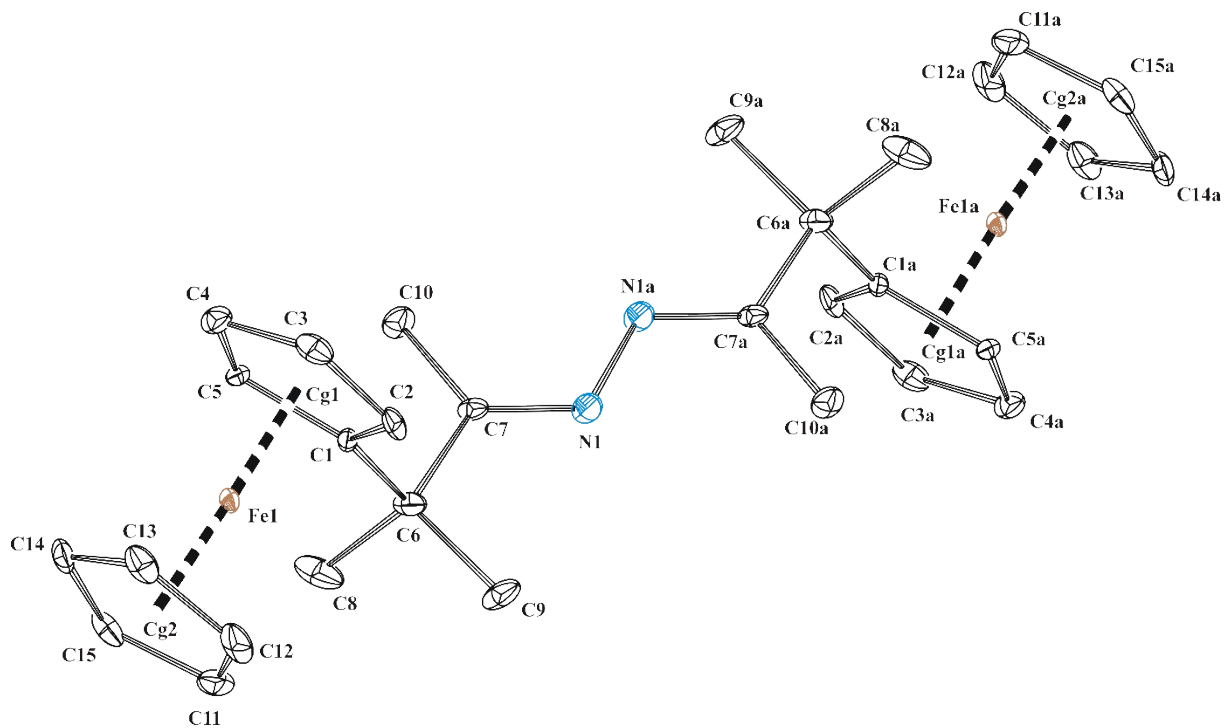


**Figure S62.** Molecular structure of azine **3c** with ORTEP spheres drawn at 30% probability level; hydrogen atoms are omitted for clarity. Selected bonds ( $\text{\AA}$ ) and angles ( $^\circ$ ): Fe1–Cg1 1.645(3), Fe1–Cg2 1.652(4), C1–C6 1.522(9), C6–C7 1.526(9), C7–N1 1.277(9), N1–N1a 1.423(9), C1–C6–C7 107.3(5), C6–C7–N1 117.6(6), C7–N1–N1a 114.0(6). Symmetry code: (a) 1 - x, - y, 1 - z.

Solid state structure of **3c** presents Figure S62, crystallographic data are given in Table S1. Molecule of azine **3c** possesses an inversion center bisecting single bond N1–N1a. Azine backbone is almost planar with ferrocenyl fragments located on the opposite sides of the plane defined by atoms C6, C7, C10, N1, N1a, C10a, C7a and C6a. The torsion angle C7–N1–N1a–C7a of 180.0(6) $^\circ$  reflects an (*E,E*)-configuration at iminic function together with *trans* conformation about N1–N1a bond as was reported previously for other organometallic azines.<sup>S2, S3</sup>

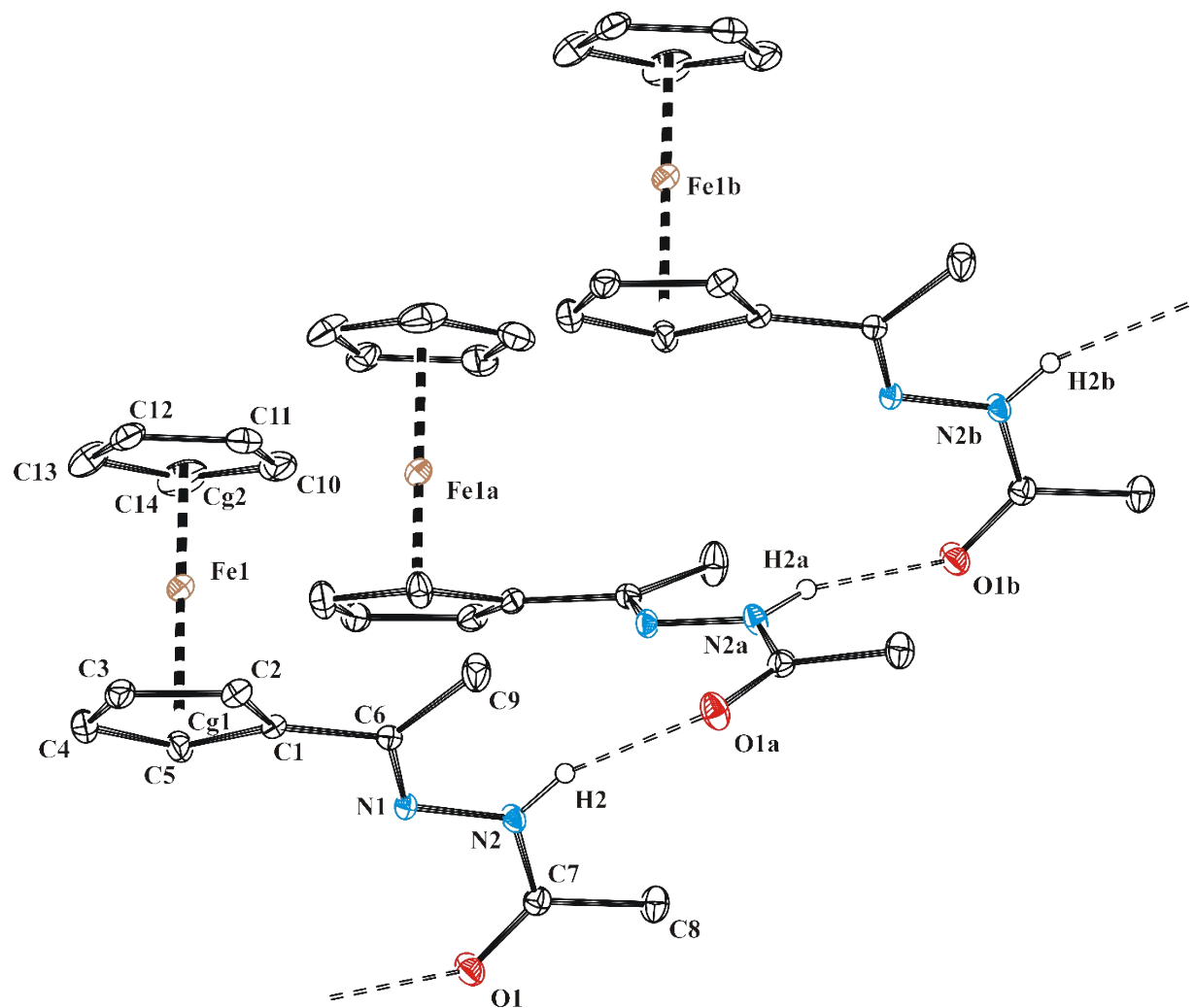


**Figure S63.** Molecular structure and hydrogen-bonding scheme of **4a-1** shown at 30% probability. Hydrogen atoms not involved in hydrogen bonding are omitted for clarity. Selected bonds ( $\text{\AA}$ ) and angles ( $^\circ$ ): Fe1–Cg1 1.6448(14), Fe1–Cg2 1.6482(16), C1–C6 1.475(4), C6–N1 1.289(4), N1–N2 1.389(3), N2–C7 1.349(4), C7–O1 1.226(4), C1–C6–N1 114.9(3), C6–N1–N2 116.4(2), N1–N2–C7 118.4(2), N2–C7–O1 123.5(3). Hydrogen-bond geometry ( $\text{\AA}$ ,  $^\circ$ ): N2 $\cdots$ O1a 2.941(3), N2–H2 $\cdots$ O2 162. Symmetry codes: (a)  $\frac{1}{2} - x, -\frac{1}{2} + y, z$ ; (b)  $x, -1 + y, z$ .

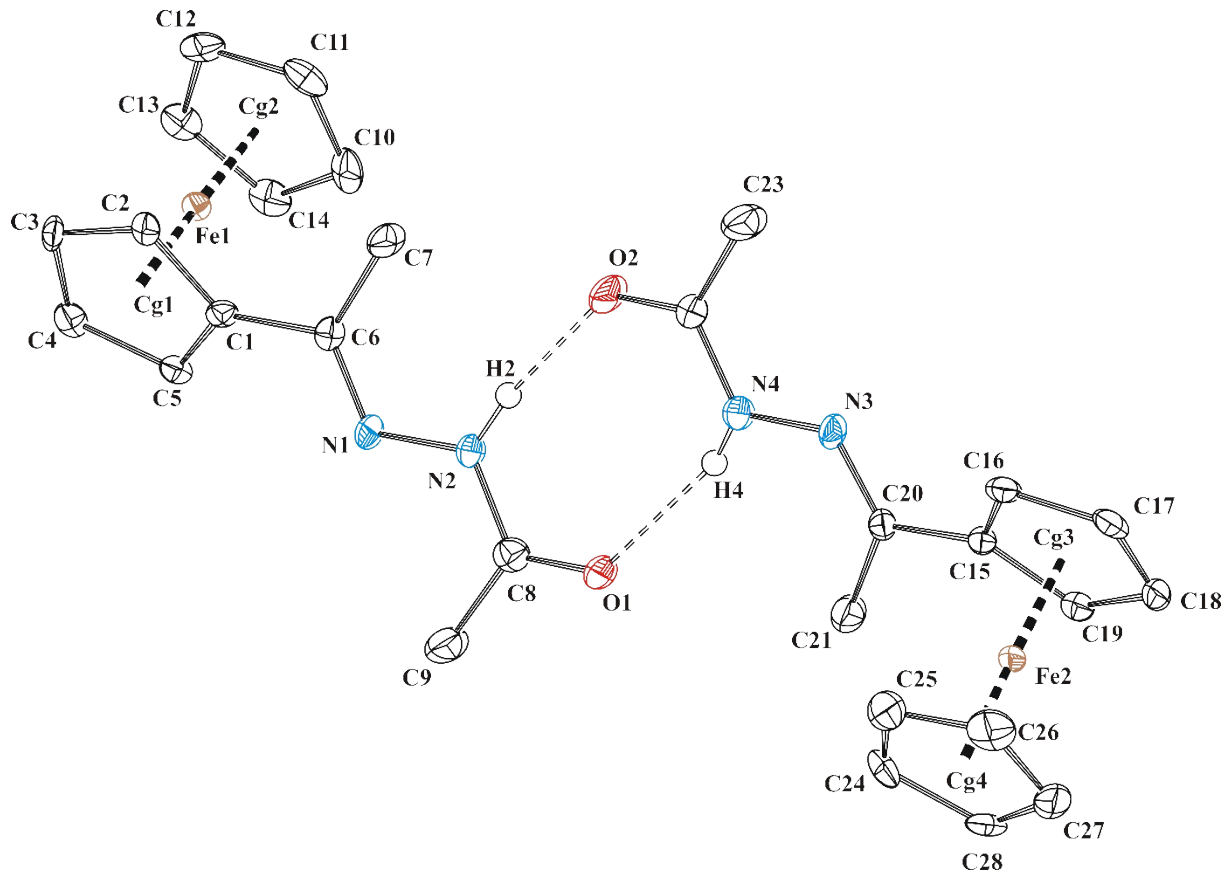


**Figure S64.** Molecular structure and hydrogen-bonding scheme of **4a-2** shown at 30% probability. Hydrogen atoms not involved in hydrogen bonding are omitted for clarity. Selected bonds ( $\text{\AA}$ ) and angles ( $^\circ$ ): Fe1–Cg1 1.6442(18), Fe1–Cg2 1.6478(19), C1–C6 1.460(5), C6–N1 1.287(5), N1–N2 1.390(4), N2–C8 1.350(5), C8–O1 1.239(5), Fe2–Cg3 1.6463(19), Fe2–Cg4 1.646(2), C15–C20 1.477(5), C20–N3 1.286(5), N3–N4 1.394(4), N4–C22 1.352(5), C22–O2 1.235(5), C1–C6–N1 116.5(4), C6–N1–N2 116.3(4), N1–N2–C8 119.9(4), N2–C8–O1 120.0(4), C15–C20–N3 115.1(3), C20–N3–N4 116.8(4), N3–N4–C22 119.1(4), N4–C22–O2 119.7(4). Hydrogen-bond geometry ( $\text{\AA}$ ,  $^\circ$ ): N2…O2 2.978(5), N2–H2…O2 164, N4…O1 3.016(5), N4–H4…O1 162.

Acetylferrocene acetylhydrazone **4a** crystallizes in two different space groups *Pbca* (**4a-1**) and *P2<sub>1</sub>2<sub>1</sub>2<sub>1</sub>* (**4a-2**) when single-crystals were grown from methanol and hexane, respectively. The interatomic distances and angles observed in both polymorphs are identical within the experimental error, see Figures S63 and S64; crystallographic data gives Table S1. Acetylhydrazone function is almost planar and makes an angle of 31.4° with substituted cyclopentadienyl ring in **4a-1** (28.6 and 32.4° in **4a-2**). Each molecule in **4a-1** is connected toward two adjacent molecules *via* hydrogen bonds giving infinite chains along *b* cell axis. By contrast, asymmetric unit of **4a-2** consists of two crystallographically independent molecules mutually connected *via* two hydrogen-bonds.

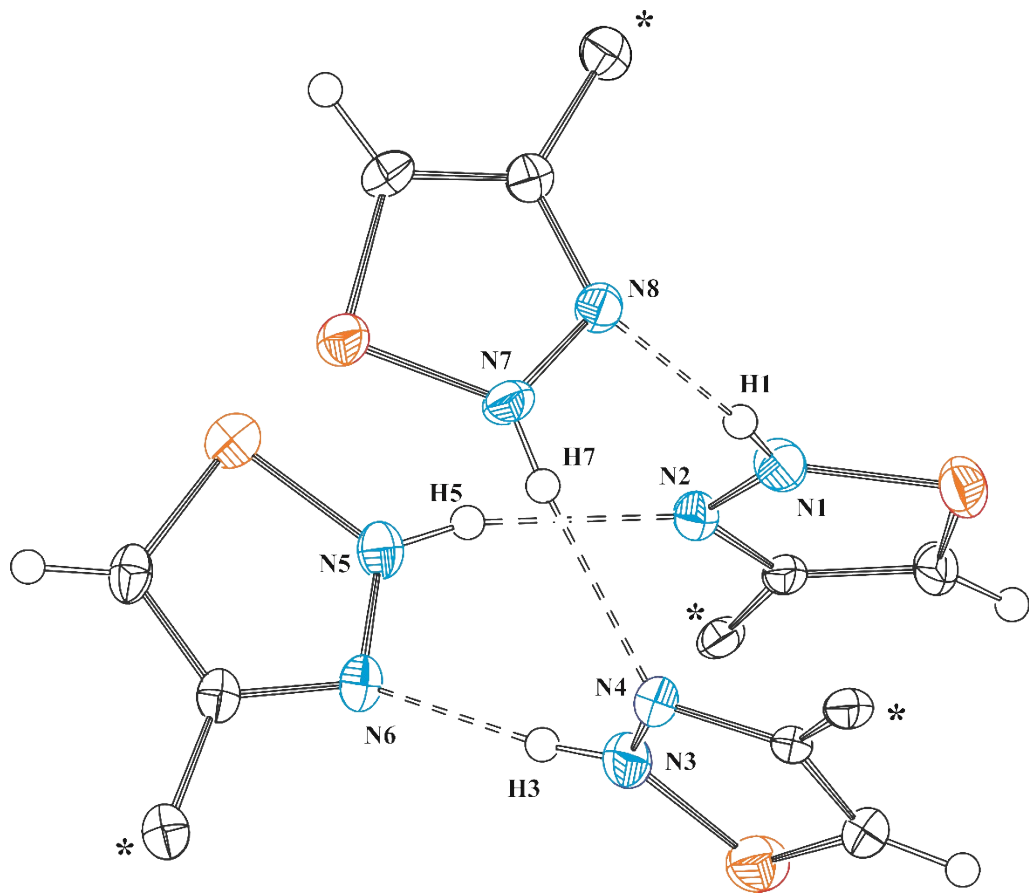


**Figure S65.** Hydrogen bonding scheme found in tetrameric **2a**. Each ferrocenyl group is represented by corresponding *ipso*-carbons of substituted cyclopentadienyl ring (denoted by asterisks).

**Table S2.** Hydrogen-bond geometry for **2a** ( $\text{\AA}$ ,  $^\circ$ ).

D—H…A	D—H	H…A	D…A	D—H…A
<b>N1—H1…N8</b>	0.88	2.10	2.960 (3)	165
<b>N3—H3…N6</b>	0.88	1.99	2.867 (3)	172
<b>N5—H5…N2</b>	0.88	2.10	2.942 (2)	161
<b>N7—H7…N4</b>	0.82	2.21	3.026 (3)	170

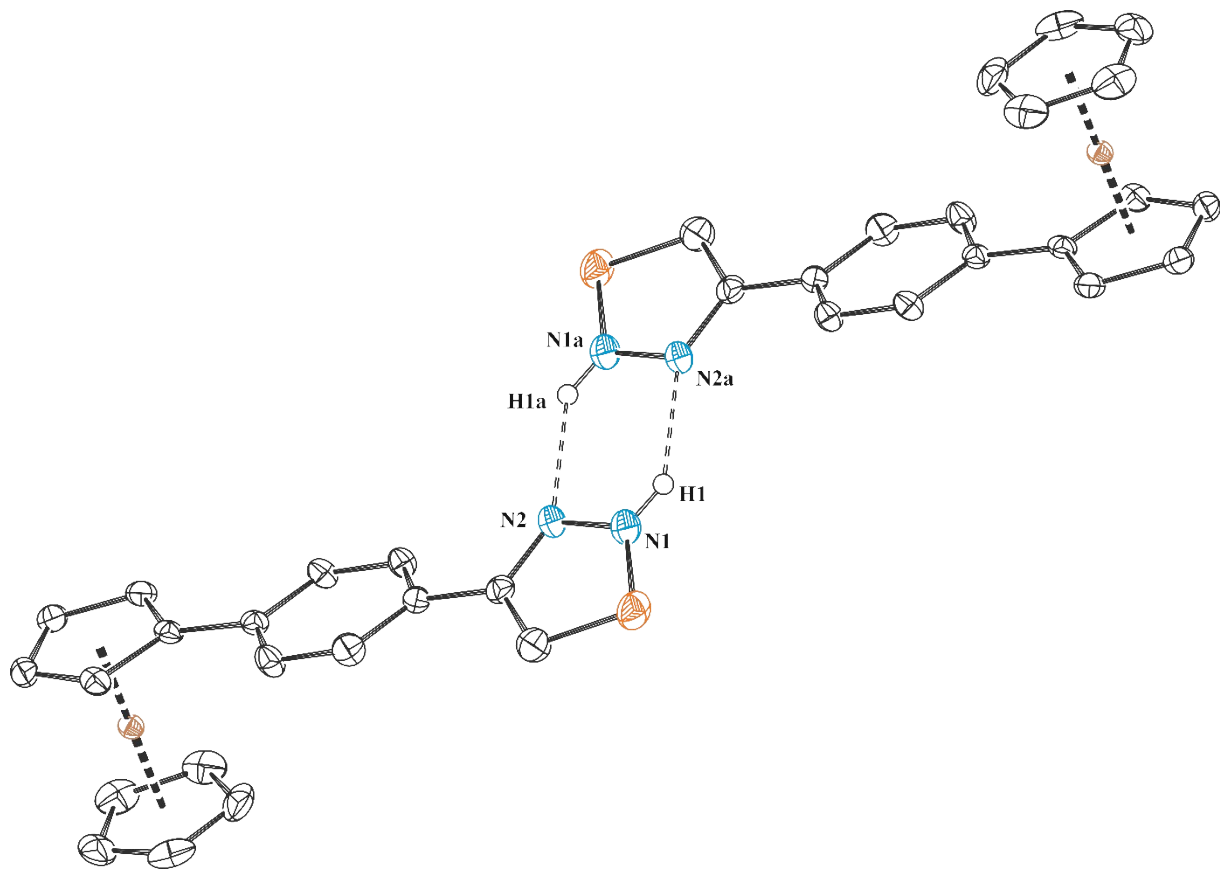


**Figure S66.** Hydrogen bonding scheme found in crystalline **2b**. Hydrogen atoms not involved in hydrogen bond are omitted. Hydrogen-bond geometry ( $\text{\AA}$ ,  $^\circ$ ): N1 $\cdots$ N2a 2.895(4), N1–H1 $\cdots$ N2a 143. Symmetry code: (a) 1 - x, 1 - y, 2 - z.

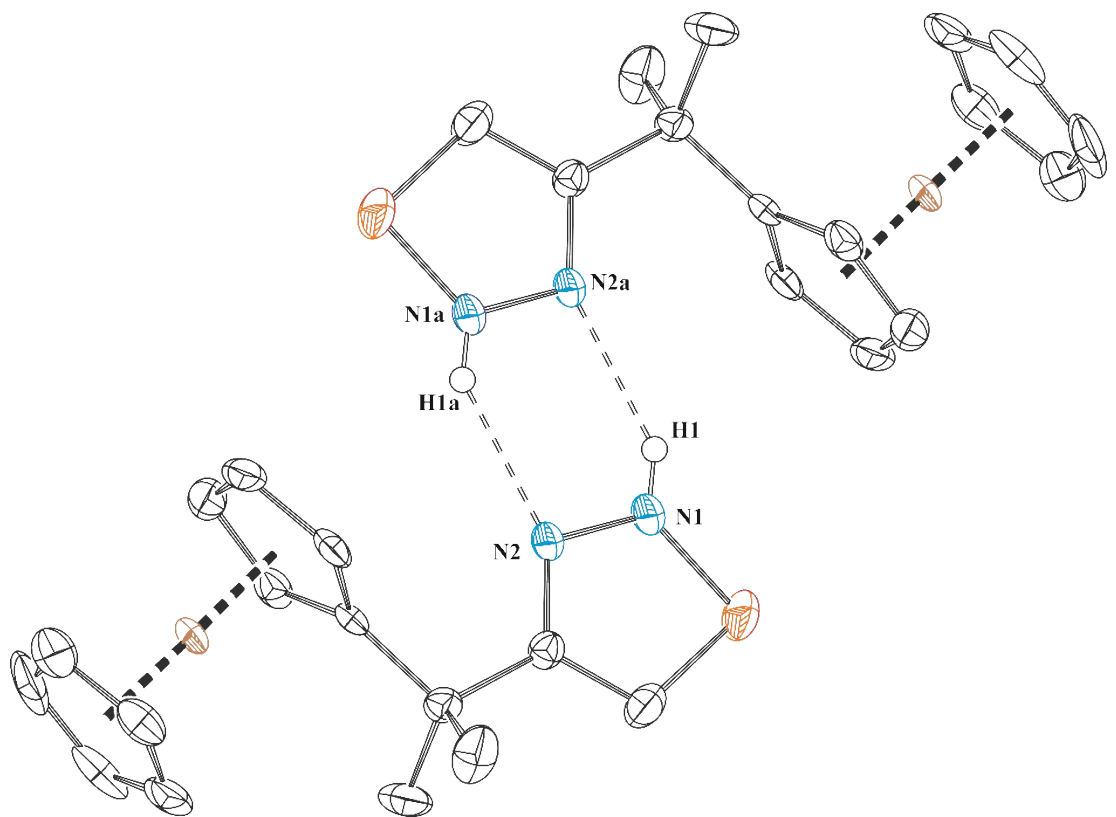


**Figure S67.** Hydrogen bonding scheme found in **2c**. Hydrogen-bond geometry ( $\text{\AA}$ ,  $^\circ$ ): N1 $\cdots$ N2a 2.897(3), N1–H1 $\cdots$ N2a 146. Symmetry code: (a) -x, 1 -y, 1 -z.

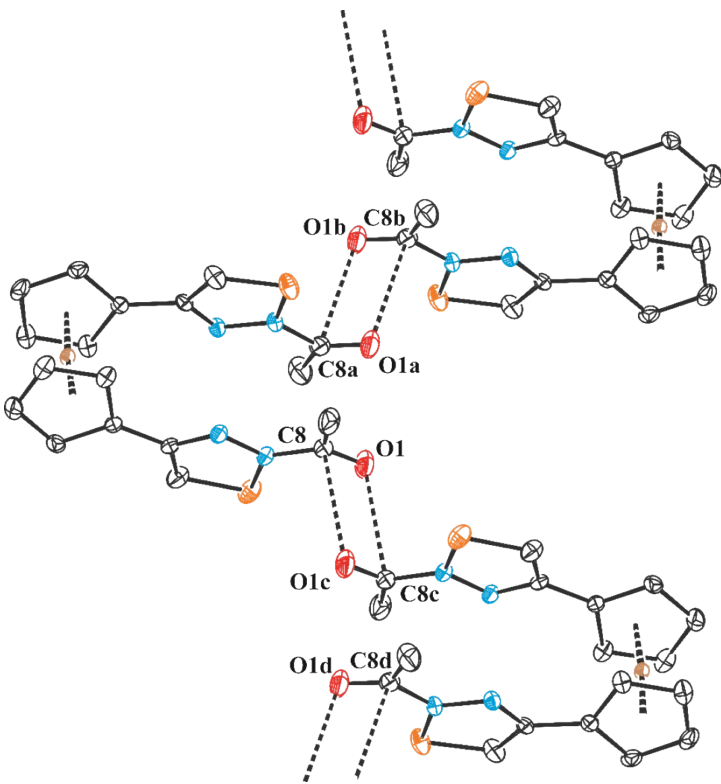


**Figure S68.** Partial packing diagram of **8** showing intermolecular dipole-dipole interactions, hydrogen atoms are omitted for clarity. Observed interatomic distance  $O1 \cdots C8c$  is of  $3.044(3)$  Å and dihedral angle  $C8-O1 \cdots O1c-C8c$  of  $180.0(2)^\circ$ , respectively. Symmetry codes: (a)  $\frac{3}{2} - x, \frac{3}{2} - y, z$ ; (b)  $\frac{1}{2} + x, \frac{1}{2} + y, 1 - z$ ; (c)  $1 - x, 1 - y, 1 - z$ ; (d)  $-\frac{1}{2} + x, -\frac{1}{2} + y, 1 - z$ .

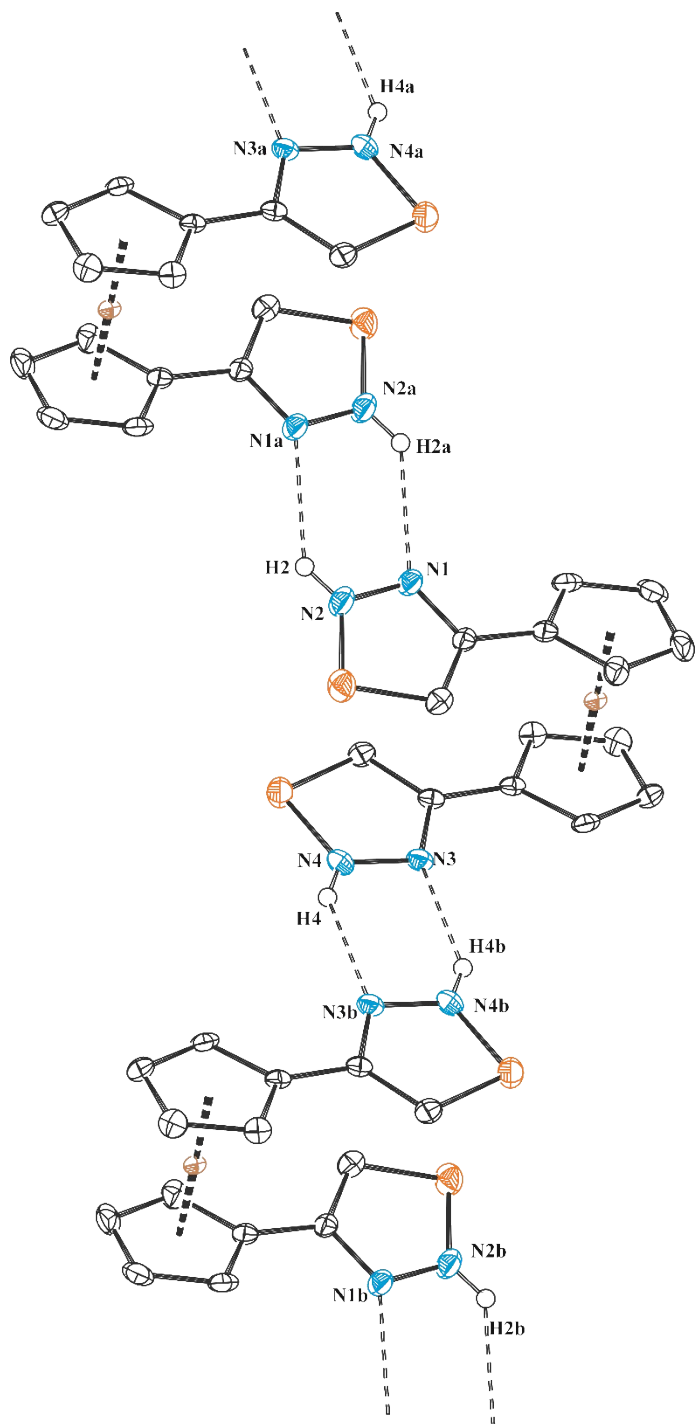


**Figure S69.** Partial packing diagram showing hydrogen-bonding scheme in crystalline **9**, hydrogen atoms not involved in interactions are omitted for clarity. Hydrogen-bond geometry ( $\text{\AA}$ ,  $^\circ$ ): N2 $\cdots$ N1a 2.908(3), N2 $-$ H2 $\cdots$ N1a 144, N4 $\cdots$ N3b 3.017(3), N4 $-$ H4 $\cdots$ N3b 138. Symmetry codes: (a) 2 - x, 1 - y, 1 - z; (b) 2 - x, - y, 2 - z.

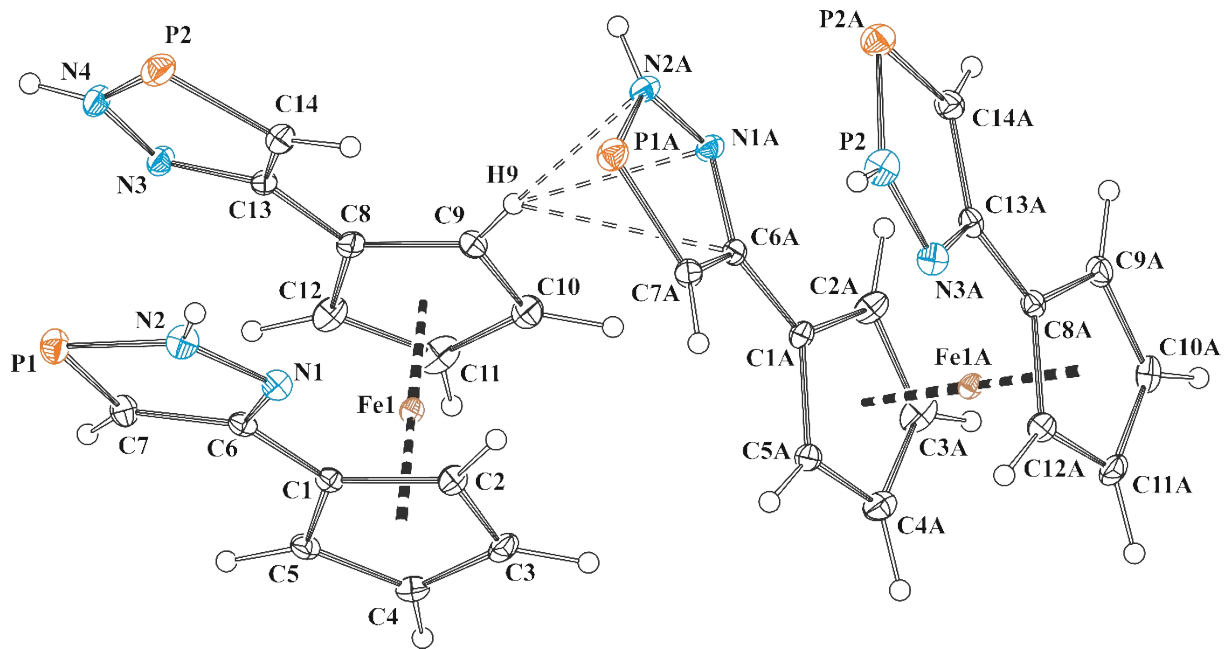


**Figure S70.** The ORTEP view showing two molecules connected *via* C–H... $\pi$  interactions in the asymmetric unit of **9**.

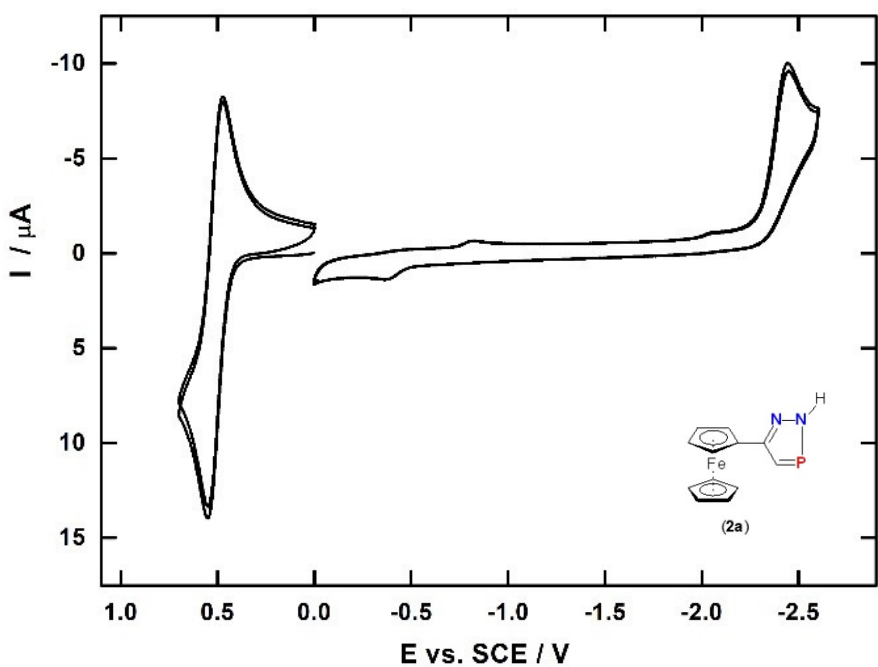


**Figure S71.** Electrochemical behavior of **2a**. Cyclic voltammetry at glassy carbon electrode in DMF,  $c \sim 5.10^{-4}\text{mol.l}^{-1}$ ; scan rate 100 mV/s.

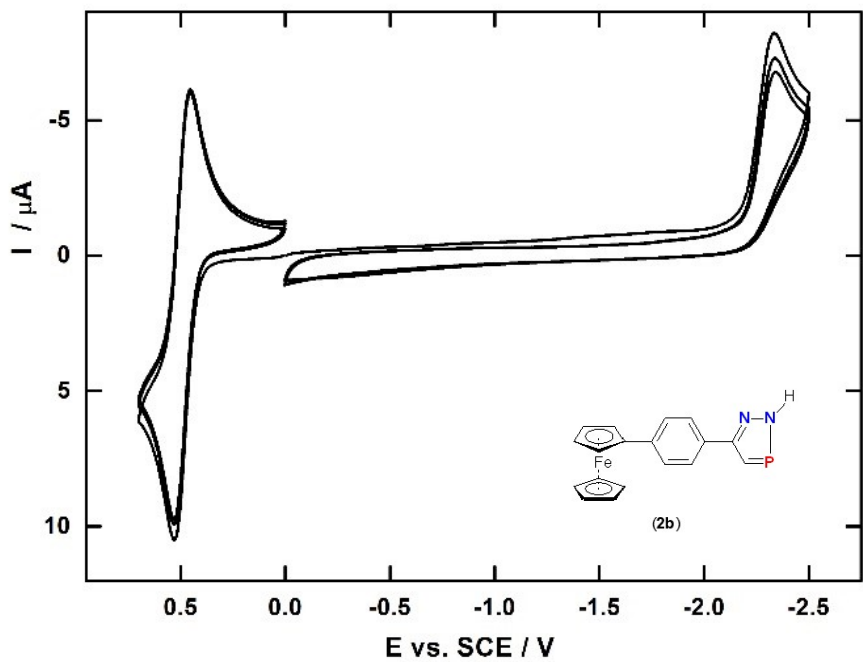


**Figure S72.** Electrochemical behavior of compound **2b**. Cyclic voltammetry at glassy carbon electrode in DMF,  $c \sim 5.10^{-4}\text{mol.l}^{-1}$ ; scan rate 100 mV/s.

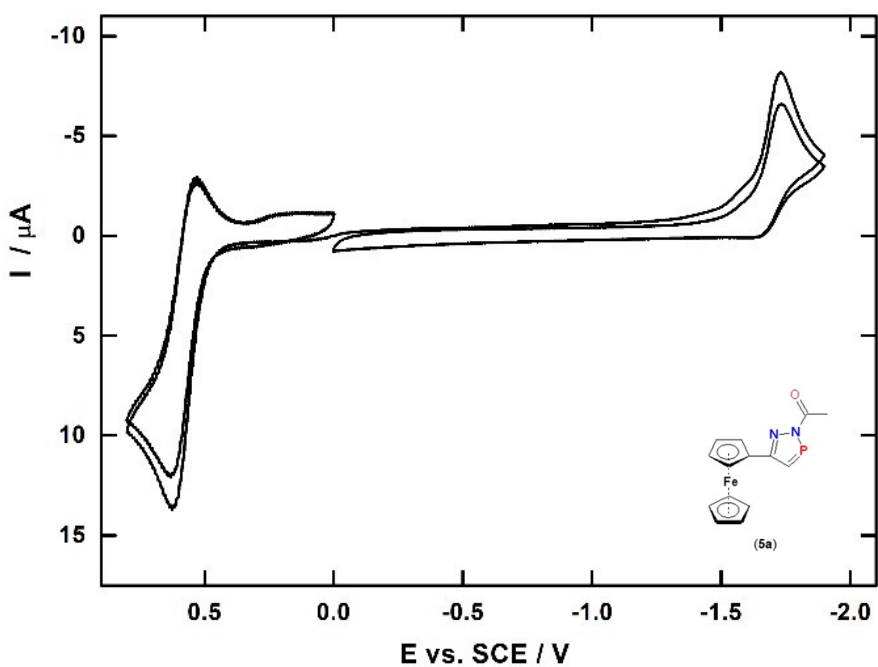


**Figure S73.** Electrochemical behavior of **5a**. Cyclic voltammetry at glassy carbon electrode in DMF,  $c \sim 5 \cdot 10^{-4} \text{ mol.l}^{-1}$ ; scan rate 100 mV/s.

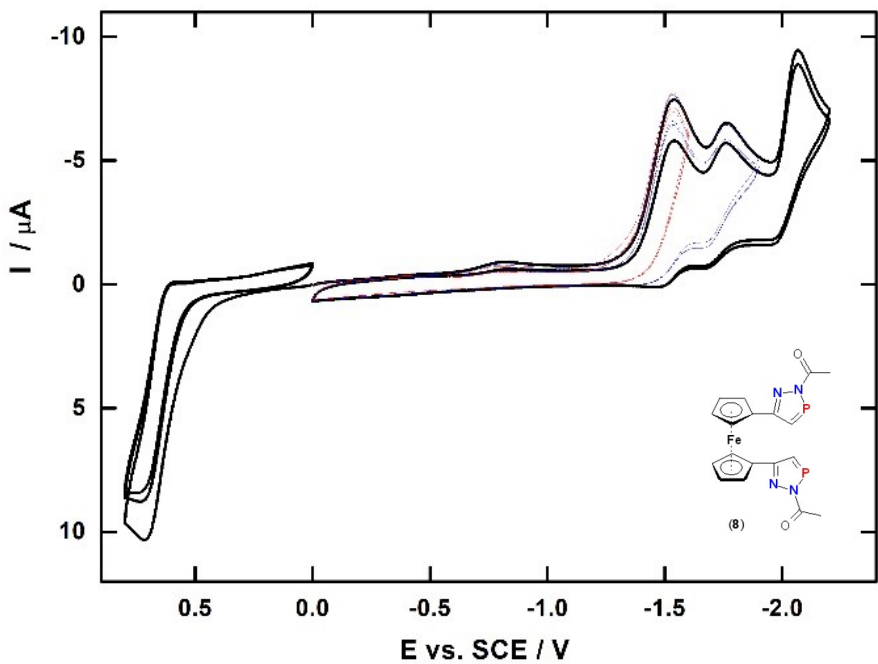


**Figure S74.** Electrochemical behavior of **8**. Cyclic voltammetry at glassy carbon electrode in DMF,  $c \sim 5 \cdot 10^{-4} \text{ mol.l}^{-1}$ ; scan rate 100 mV/s.

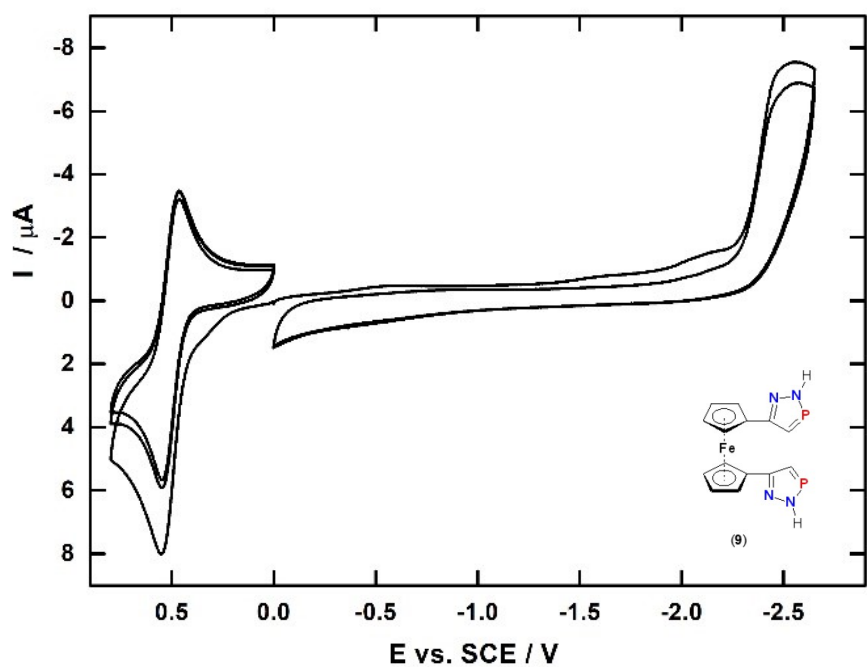


**Figure S75.** Electrochemical behavior of **9**. Cyclic voltammetry at glassy carbon electrode in DMF,  $c \sim 5 \cdot 10^{-4} \text{ mol.l}^{-1}$ ; scan rate 100 mV/s.

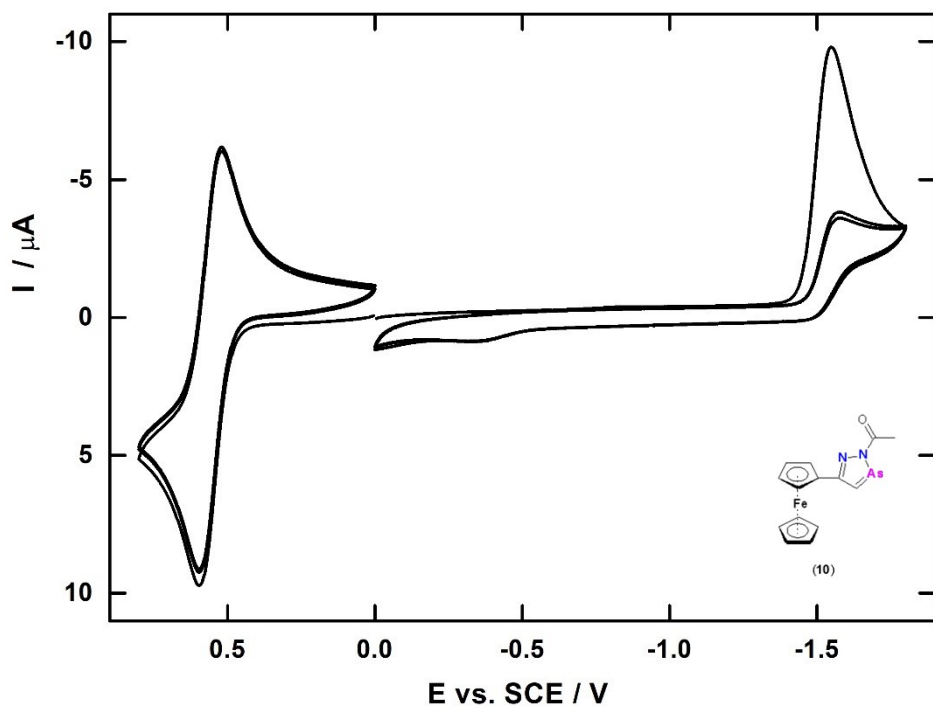


**Figure S76.** Electrochemical behavior of **10**. Cyclic voltammetry at glassy carbon electrode in DMF,  $c \sim 5 \cdot 10^{-4} \text{ mol.l}^{-1}$ ; scan rate 100 mV/s.

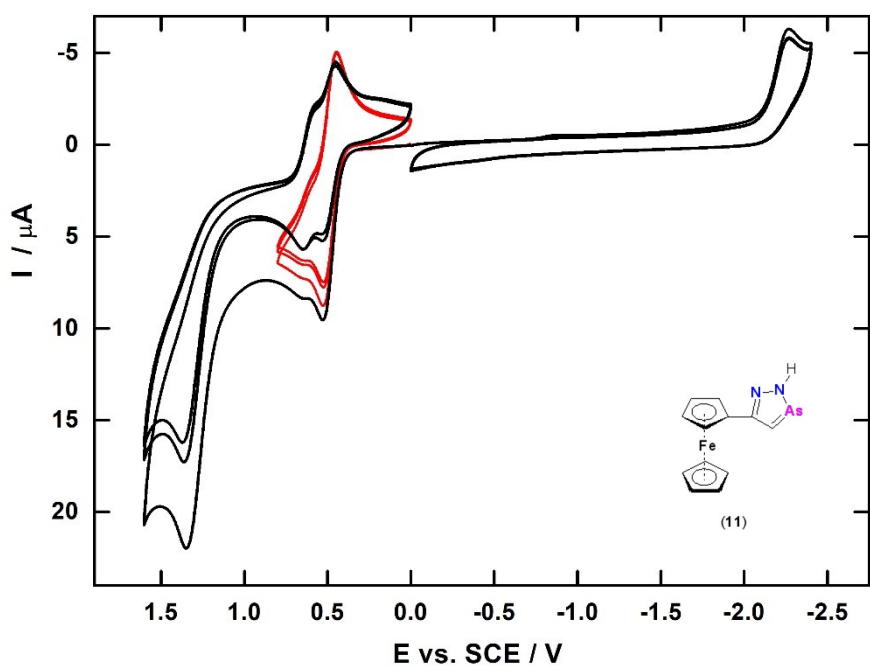


**Figure S77.** Electrochemical behavior of **11**. Cyclic voltammetry at glassy carbon electrode in DMF,  $c \sim 5 \cdot 10^{-4} \text{ mol.l}^{-1}$ ; scan rate 100 mV/s.

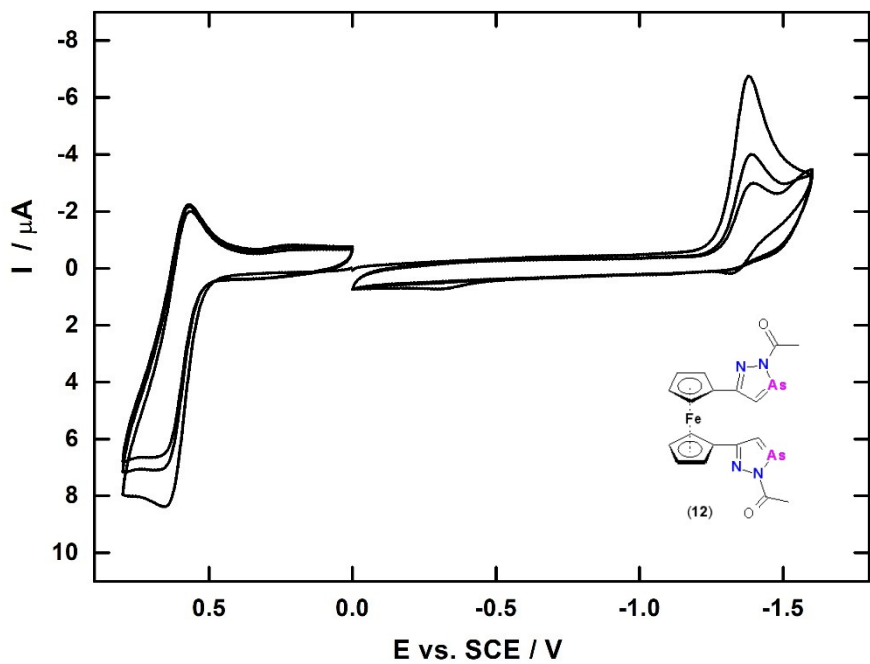


**Figure S78.** Electrochemical behavior of **12**. Cyclic voltammetry at glassy carbon electrode in DMF,  $c \sim 5 \cdot 10^{-4} \text{ mol.l}^{-1}$ ; scan rate 100 mV/s.



**Figure S79.** Electrochemical behavior of **13**. Cyclic voltammetry at glassy carbon electrode in DMF,  $c \sim 5 \cdot 10^{-4} \text{ mol.l}^{-1}$ ; scan rate 100 mV/s.

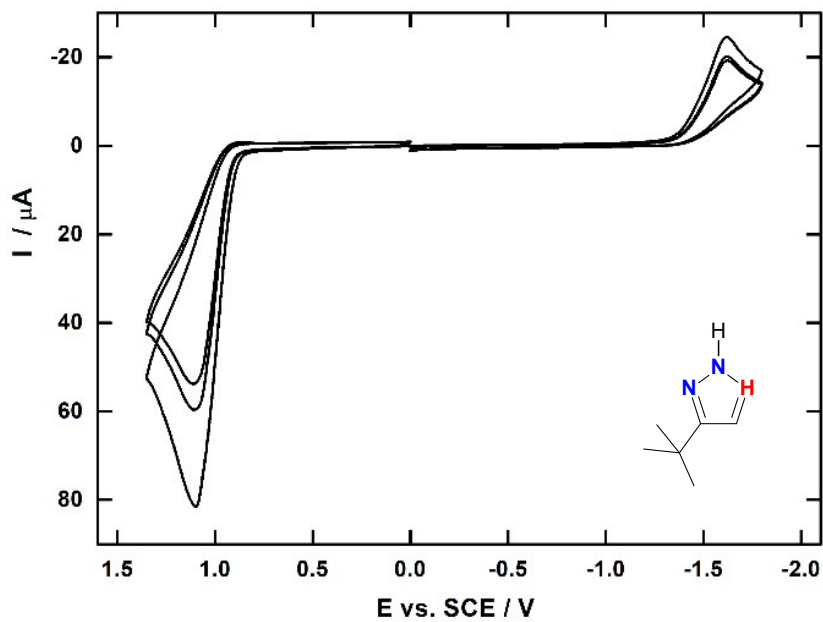


**Figure S80.** Electrochemical behavior of 2H-5-t-butyl-[1,2,3]-diazaphosphole (**2H-5Bu<sup>t</sup>-dap**). Cyclic voltammetry at glassy carbon electrode in DMF; scan rate 100 mV/s.

## References

- S1. Groom, C. R.; Bruno, I. J.; Lightfoot, M. P.; Ward, S. C., The Cambridge Structural Database. *Acta Crystallographica Section B-Structural Science Crystal Engineering and Materials* **2016**, *72*, 171-179.
- S2. Gómez, J.; Hugo Klahn, A.; Fuentealba, M.; Sierra, D.; Olea-Azar, C.; Medina, M. E., Unsymmetrical cyrhetrenyl and ferrocenyl azines derived from 5-nitrofuran: Synthesis, structural characterization and electrochemistry. *Inorganic Chemistry Communications* **2015**, *61*, 204-206.
- S3. Gómez, J.; Sierra, D.; Fuentealba, M.; Artigas, V.; Klahn, A. H., Homo- and heterobimetallic azines derived from ferrocene and cyrhetrene: Synthesis, structural characterization and electrochemical studies. *Journal of Organometallic Chemistry* **2019**, *883*, 65-70.